Adv Polym Sci (2006) 195: 101–176
DOI 10.1007/12_050

Published online: 11 January 2006

Folding and Formation of Mesoglobules in Dilute Copolymer Solutions

Guangzhao Zhang[1,2] · Chi Wu[3] (✉)

[1]Laboratory of Macromolecular Colloids and Solutions,
The Hefei National Laboratory for Physical Sciences at Micro-scale, Hefei,
230026 Anhui, China

[2]Department of Chemical Physics, University of Science and Technology of China,
Hefei, 230026 Anhui, China

[3]Department of Chemistry, The Chinese University of Hong Kong, Shatin,
N.T., Hongkong, China
chiwu@cuhk.edu.hk

Abstract It is known that linear homopolymer chains can undergo a coil-to-globule-to-precipitation transition when the solvent quality gradually changes from good to poor. It is also known that the observation of the coil-to-globule transition without any interchain association is extremely difficult if not impossible. On the other hand, the folding of individual amphiphilic copolymer chains, such as protein chains, in an extremely dilute solution is much easier. As the copolymer concentration increases, inevitable interchain association accompanied by intrachain folding can result in a stable mesoglobular phase (the aggregation of a limited number of chains), existing between single-chain globules and macroscopic phase separation (precipitation). In this article, we mainly review what we have accomplished in the last ten years by starting with a brief discussion of the folding of linear poly(*N*-isopropylacrylamide) (PNIPAM) homopolymer chains in water. Our focus is the folding of different hydrophilically or hydrophobically modified PNIPAM copolymer chains in extremely dilute solutions as well as the formation of stable mesoglobules made of amphiphilic copolymer chains in dilute solutions. The discoveries of the molten globular state and the "ordered-coil" state between the random-coil and compacted globular states will be illustrated. The effects of both the comonomer composition and distribution on the folding of individual copolymer chains into some unique core-shell nanostructures as well as the formation of the mesoglobular phase are discussed. The double roles of hydrophobic interaction in the formation and stabilization of stable mesoglobules will be explained in terms of the viscoelastic effect.

Keywords Folding · Aggregation · Mesoglobule · Copolymer

Abbreviations

Section 1

CTAB	hexadecyltriethylammonium bromide
LCST	lower critical solution temperature
LLS	laser light scattering
M_w	weight-average molar mass
M_w/M_n	polydispersity index
NMR	nuclear magnetic resonance
PNIPAM	poly(*N*-isopropyl-acrylamide)
PNIPAM-*g*-PEO	poly(*N*-isopropylacrylamide)-graft- poly(ethylene oxide)
$\langle R_h \rangle$	average hydrodynamic radius
τ_{crum}	relaxation time of polymer chain in the crumpled globular state
τ_{eq}	relaxation time of polymer chain in the compact globular state

Section 2

A	measured base line (Eq. 2)
A_2	second virial coefficient (Eq. 1)
AIBN	2,2′-azobis(isobutyronitrile)
C	concentration
D	translational diffusion coefficient (Eq. 4)
dn/dC	specific refractive index increment
f	constant related to internal and rotational motions (Eq. 4)
$g^{(1)}(t,q)$	first-order electric field time correlation function (Eq. 2)
$G^{(2)}(t,q)$	intensity-intensity time correlation function (Eq. 2)
$G(\Gamma)$	line-width distribution function of Γ (Eq. 3)
GPC	gel permeation chromatography

k_B	Boltzmann constant
k_d	dynamic second-order virial coefficient (Eq. 3)
KPS	potassium persulfate
MACA	2′-methacryloylaminoethylene)-3α,7α,12α-trihydroxy-5β-cholano-amide
MeOK	potassium methoxide
n	refractive index of solvent
N_A	Avogadro constant
NIPAM	*N*-isopropylacrylamide
NIPAM-*co*-VP	*N*-isopropylacrylamide-*co*-vinylpyrrolidone
PNIPAM-*seg*-St	segmented copolymer of *N*-isopropylacrylamide and styrene
PNIPAM-*co*-KAA	*N*-isopropylacrylamide-*co*-potassium acrylic acid
PAM-*co*-NaAA	acrylamide-co-sodium acrylic acid
P(DEA-*co*-DMA)	poly(*N*,*N*-diethylacrylamide-*co*-*N*,*N*-dimethylacrylamide)
PEO	poly(ethylene oxide)
q	scattering vector
$\langle R_g^2 \rangle_z^{1/2}$ (or $\langle R_g \rangle$)	*z*-average root mean square radius of gyration
$R_{vu}(q)$	Rayleigh ratio for unpolarized scattered light
$R_{vv}(q)$	Rayleigh ratio for vertically polarized scattered light
St	styrene
T	absolute temperature
TEMED	*N*,*N*,*N*′,*N*′-tetramethylethylenediamine
THF	tetrahydrofuran
US-DSC	Ultra-sensitive Differential Scanning Calorimeter
VP	1-vinyl-2-pyrrolidone
$\langle \Gamma \rangle$	*z*-average line-width
η	viscosity of solvent
θ	scattering angle
λ_0	wavelength of light in vacuum
Section 3	
AFM	atomic force microscopy
C_p	partial heat capacity
$f(R_h)$	hydrodynamic radius distribution
h_{brush}	thickness of a polymer brush
ΔH	change of enthalpy
$\langle I \rangle$	average scattered light intensity
I_1/I_3	fluorescence intensity ratio
L_{shell}	shell thickness of a core-shell structure
M_c	mass of the core of a core-shell particle (Eq. 5)
M_s	mass of the shell of a core-shell particle (Eq. 5)
R	radius of the core-shell particle (Eq. 5)
R_c	radius of the core of the core-shell particle (Eq. 5)
SMFS	single-molecule force spectroscopy
T_{max}	temperature corresponding to the maximum heat capacity
α	static expansion factor
$\langle \rho \rangle$	average chain density
ρ_c	density of the core of a core-shell particle
$\langle \rho \rangle_{globule}$	average chain density in globule state
ρ_s	density of the shell of a core-shell particle
σ	grafting density

χ	Flory–Huggins interaction parameter
Section 4	
d_f	fractal dimension of a cluster
DLCA	diffusion-limited cluster aggregation
HPAM	partially hydrolyzed poly(acrylamide)
$M_{w,agg}$	weight average molar mass of aggregates
N_{chain}	average number of chains inside an aggregate
RLCA	reaction-limited cluster aggregation
$\langle S \rangle_{ionic}$	average surface area per ionic group
$\langle V \rangle_{chain}$	average hydrodynamic volume of polymer chains
Section 5	
a_m	length of monomer (Eq. 10)
$\langle D \rangle$	transitional diffusion coefficient of aggregates (Eq. 10)
DEA	*N*,*N*-diethylacrylamide
DMA	*N*,*N*-dimethylacrylamide
D_m	diffusion coefficient of monomer (Eq. 10)
ΔG	change of Gibbs free energy
l_o	interaction range (Eq. 10)
N_{chain}	average aggregation number
N_m	number of monomer
ΔS	change of entropy
$T_{aggregation}$	aggregation temperature
$\langle \nu \rangle$	mean thermal velocity (Eq. 10)
α	scaling exponent
τ_c	collision or interaction time (Eq. 10)
τ_e	time for chain entanglement (Eq. 10)
ϕ_p	average polymer concentration in aggregates (Eq. 10)

1 Introduction

Conformation and phase transition of polymer chains in solution is not only a fundamental problem in polymer research, but also directly linked to the property of a polymeric material. In the long development of polymer science, the research into properties of a polymer solution has always been an important part. Polymer researchers had been puzzled for many years by the simple question whether the conformation of a flexible linear homopolymer chain can change from a random "coil" to a thermodynamically stable single-chain "globule" when the solvent quality gradually changes from good to poor, but still remain in the one phase region. On the other hand, everyday in nature protein chains fold into stable globules though how they fold with no or only a very few mistakes still remains a mystery.

Protein chains generally contain hydrophobic, hydrophilic and/or charged amino acid residues, which can be regarded as amphiphilic copolymers in a broad definition. The coordinate and cooperative interactions, such as

intra- and inter-chain hydrogen bonding, hydrophobic attraction and electrostatic interaction lead to some complicated bio-active structures [1]. Different theories were proposed to explain various properties of proteins from a biological point of view [2–5]. Recently, computer simulation was also used to construct different copolymers with hydrophobic and hydrophilic units to imitate proteins. Particularly, the coil-to-globule transition of different types of copolymer chains was simulated to demonstrate how the comonomer distribution, i.e., the sequence difference in structure, could greatly influence the folding of a single copolymer chain in dilute solution [6–8].

Khokhlov et al. [8] simulated three AB copolymer chains with an identical composition and length, but different comonomer distributions on the chain backbone. Their results showed that for the chain with a globular protein-like structure in which soluble comonomer B was incorporated on the periphery of a collapsed A chain backbone, the chain folding would be easier than that of a random copolymer without a designed sequence. Moreover, the resultant globule was stable and its chain density was higher. The simulation suggested that such a chain could "memorize" or "inherit" some special functional properties of the parent collapsed state. Timoshenko et al. [9] also showed that for a given degree of amphiphilicity, the folding of an AB copolymer chain with a segmented comonomer distribution was easier and the resultant mesoglobular phase was more stable in comparison with a random copolymer chain under the same condition.

However, it is a rather difficult experimental challenge, if not impossible, to prepare a pair of AB copolymers with a similar composition and a similar chain length, but different comonomer distributions on the chain backbone. It is known that poly(*N*-isopropyl-acrylamide) (PNIPAM) is a thermally sensitive polymer with a lower critical solution temperature (LCST $\sim 32\,^{\circ}C$) [10–14]. This interesting thermal property has made PNIPAM a simple model for the simulation of protein de-naturation in aqueous solution even though real protein chains are much more complicated [15]. Recently, using two grafted copolymers, PNIPAM-*g*-PEO, respectively, prepared at temperatures below and near the LCST of PNIPAM, Tenhu et al. [16] studied the comonomer distribution dependence of the chain aggregation. Their interesting results showed that the copolymer chains prepared at different temperatures had different LCSTs, supporting the computer simulation in a general sense. However, we should not forget that chain aggregation is a complicated process, which involves intrachain contraction and interchain association. Therefore, the ultimate test and experimental challenge would be the study of the effect of comonomer distribution on the coil-to-globule transition (folding) of individual amphiphilic copolymer chains without involving any interchain association in dilute solution.

Before discussing the folding of amphiphilic copolymer chains, let us first briefly examine the past studies of the coil-to-globule transition of homopolymer chains in dilute solutions. More than three decades ago, Stockmayer [17]

suggested that in dilute solutions, a flexible linear homopolymer chain can change its conformation from an expanded coil to a collapsed globule if the solvent quality gradually changes from good to poor, but still remain in the one-phase region, on the basis of Flory's mean-field theory [18]. This prediction has been extensively studied both theoretically and experimentally [19–28]. Note that most of the past studies were concentrated on polystyrene solutions because such a study requires a very high molar mass ($> 10^7$ g/mol) homopolymer with a narrow molar mass distribution ($M_w/M_n < 1.1$). Useful experimental results were obtained using static and dynamic laser light scattering (LLS) and interpreted by the existing theory. However, success was limited and no one had observed the thermodynamically stable single-chain globules in such polystyrene solutions. This was because polymer chains always started to undergo an interchain association before each chain has a chance to fully collapse into a globule.

The interchain association had frustrated researchers in this field for many years. In 1993, Grosberg et al. [29] stated that the true equilibrium single chain collapse had not yet been observed experimentally for simple uncharged homopolymers without mesogenic groups. They predicted a two-stage kinetics for the collapse of a single chain, a fast crumpling of the unknotted chain followed by a slow knotting of the collapsed polymer chain. Such two-stage kinetics were roughly observed by Chu et al. [30, 31] in the study of the folding of single polystyrene chains before macroscopic precipitation. In this study, dynamic laser light scattering (LLS) was used to monitor the change of the average hydrodynamic radius ($\langle R_h \rangle$) of individual polystyrene chains in cyclohexane after an abrupt temperature change from 35 (the Θ-temperature) to 29 °C. It was found that the hydrodynamic radius distribution contained two different species, which were attributed to single polystyrene chains and aggregates of the polystyrene chains. From the time dependence of $\langle R_h \rangle$ after the abrupt temperature change, two relaxation times τ_{crum} and τ_{eq}, respectively, for the crumpled globular state and the compact globular state, were reported.

As for thermodynamically stable single-chain globules, Grosberg et al. [29] even claimed in the same 1993 article that "Practically, it cannot be observed with modern instrumentation and the sample preparation technique at this time". Actually, we noted by that time that nearly all the past studies had been conducted in organic solvents. Considering protein folding in water, we proposed to study such a "coil-to-globule" transition by using thermally sensitive water-soluble homopolymer. This is because in water hydrophobic interaction and hydrogen bonding are much stronger than the Van der Waals interaction in organic solvents. Therefore, PNIPAM as a well-known system in the study of intelligent hydrogels became a natural choice. It has been proven that such a proposal is in the right direction. Note that PNIPAM is a wonderful thermally sensitive polymer with the following chemical structure (Scheme 1).

Its isopropyl and carbon-carbon chain backbone groups are hydrophobic, but its acrylamide group is hydrophilic. A proper balance among interac-

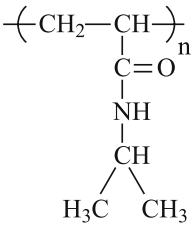

Scheme 1 Poly(*N*-isopropylacrylamide) (PNIPAM)

tion between these opposite groups and water leads PNIPAM to a convenient lower LCST of $\sim 32\,^{\circ}\mathrm{C}$. Namely, it is soluble in water at lower temperatures, but precipitates out at temperatures higher than $32\,^{\circ}\mathrm{C}$. Qualitatively, this delicate balance between hydrophilic and hydrophobic interaction is gradually broken as the solution temperature increases. This is because the dissolution of PNIPAM in water has a negative overall entropy change (the effect on water clusters) that is unusual, but typical for water-soluble polymers. Our recent NMR studies showed that at temperatures below the LCST, some water molecules are associated with the amide group; and during the transition, the associated water molecules dissociate.

It is well known that for a broadly distributed sample, longer chains will normally undergo the phase transition first, leading the entire solution into a thermodynamically unstable two-phase region. After overcoming some difficulties encountered in the sample preparation, we successfully prepared some narrowly distributed ($M_w/M_n < 1.1$) high-molar mass ($M_w > 10^7$ g/mol) linear PNIPAM homopolymers. Armed with these special PNIPAM samples, we were able to study the coil-to-globule transition of single PNIPAM chains in extremely dilute solutions (~ 5 mg/mL) by using a combination of static and dynamic LLS. Finally, stable single-homopolymer-chain globules were, for the first time, observed in 1994 and the results were published in 1995 [32]. After that, a systematic study on a number fundamental problems associated with such a folding transition of homopolymer chains in water was carried out, such as the internal motions of linear coiled chains [33], the discovery of the molten globular state of a collapsed chain during the coil-to-globule transition [34], the coil-to-globule transition of linear chains grafted on a surface [35, 36], the first observation of the reversible globule-to-coil transition of linear homopolymer chains in solution [37, 38], the difference between the coil-to-globule transition of PNIPAM in normal water and in deuterated water [39], and the solvent composition induced coil-to-globule transition of PNIPAM in a mixture of methanol and water [40, 41].

After accumulating sufficient experience in the preparation of narrowly distributed long homopolymer chains and in the study of individual homopolymer chains in dilute solutions, we gradually moved into the direction of the folding and formation of the mesoglobular phase of amphiphilic

copolymer chains in dilute solutions. Various copolymers with different comonomers, such as ionic or nonionic and hydrophilic or hydrophobic, were inserted or attached to the PNIPAM chain backbone with different comonomer compositions and distributions. It should be noted that there were many other research groups who studied the effects of comonomer, especially comonomer composition, on the association of amphiphilic copolymer chains in dilute solutions. However, it is our intention in this article to mainly review what has been done in our laboratory by using a combination of static and dynamic LLS to observe the folding and formation of mesoglobular phase of copolymer chains in dilute solutions. Other authors in this volume will review other theoretical and experimental studies of the association of copolymer chains. This review starts from a brief discussion of the folding of long homopolymer chains in dilute solution. Further discussion of copolymer chains will be divided according to the nature of the comonomers used in the preparation of PNIPAM copolymers. In order to facilitate our discussion, we will outline some details of our experiments in the following section.

2
Experimental Section

2.1
Preparation of Amphiphilic Copolymers

In this review, hydrophilically and hydrophobically modified poly(*N*-isopropylacrylamide) (PNIPAM) copolymers are mainly used to illustrate how amphiphilic copolymer chains can fold from an extended random coil to a collapsed globule in extremely dilute solutions and associate to form a stable mesoglobular phase which exists between single-chain globules and macroscopic precipitation. The copolymers used can be prepared by free-radical reaction.

2.1.1
Poly(*N*-isopropylacrylamide) (PNIPAM) Homopolymer

N-isopropylacrylamide (NIPAM) monomer (courtesy of Kohjin Ltd) can be purified by re-crystallization in a benzene/*n*-hexane mixture and azobisisobutyronitrile (AIBN) (from Aldrich, analytical grade) can also be purified by re-crystallization. In a typical free-radical polymerization, 18 g NIPAM monomer was first dissolved in 150 mL benzene with 1 mol % of AIBN added as the initiator. The solution mixture was then degassed through three cycles of freezing and thawing. Polymerization was carried out in an oil bath at 56 °C for 30 h under a positive nitrogen pressure. The solvent was removed

by evaporation after the polymerization. The resultant crude polymer was further dried and then dissolved in acetone. The polymer was recovered by adding the acetone solution dropwise into *n*-hexane. Upon filtering and drying, a white fabric-like polymer can be obtained. The yield is normally higher than $\sim 70\%$. Details of the polymerization can be found elsewhere [42]. The resultant PNIPAM can be fractionated several times by precipitation from an extremely carefully dried acetone solution to *n*-hexane at $\sim 25\,^{\circ}\mathrm{C}$. It should be emphasized that the use of the dried solvents is one of the key factors for success in the preparation of a narrowly distributed PNIPAM sample. A careful combination of both the fractionation and filtration can lead to some narrowly distributed ($M_w/M_n < 1.1$) high molar mass PNIPAM samples ($M_w > 10^7$ g/mol). The extremely dilute solution ($\sim 10^{-6}$ g/mL) of PNIPAM in water at lower temperatures can be clarified with 0.5-μm filters. The chemical structure of PNIPAM has been listed before.

2.1.2 Linear NIPAM-*co*-VP Copolymers

Comonomer 1-vinyl-2-pyrrolidone (VP) comonomer can be purified by distillation at reduced pressure prior to use. Potassium persulfate (KPS) can be purified in a mixture of water and methanol. NIPAM-*co*-VP copolymers with different amounts of VP can be prepared at temperatures lower or higher than the LCST of PNIPAM by free radical polymerization in water with an initiator of KPS/*N*,*N*,*N*′,*N*′-tetramethylethylenediamine (TEMED) redox. The resultant copolymer can be harvested by precipitation, i.e., pouring the reaction mixture into an equal volume of methanol. Each resultant copolymer can be further purified by several cycles of re-dissolution in water and precipitation in methanol to ensure a complete removal of residual monomers. The final product can be dried under reduced pressure at $40\,^{\circ}\mathrm{C}$.

The copolymer can be further fractionated by precipitation from acetone solution to *n*-hexane at room temperature. In each case, only the first fraction should be used to obtain narrowly distributed high molar mass copolymer chains for LLS measurement. ^{1}H NMR can be used to characterize the copolymer composition. The ratio of the peak areas of the methine proton of the isopropyl group in NIPAM and the two protons neighboring the carbonyl group in VP can be used to determine the VP content. The composition of each NIPAM-*co*-VP copolymer was found to be close to the feeding monomer ratio prior to the copolymerization. The nomenclature used hereafter for these copolymers is NIPAM-*co*-VP/*x*/*y*, where *x* and *y* are the copolymerization temperature (°C) and the VP content (mol%), respectively. The solution with a concentration of as low as 3.0×10^{-6} g/mL can be clarified with a 0.45 μm Millipore Millex-LCR filter to remove dust before the LLS measurement. The resistivity of deionized water used should be close to 18 MΩ cm. The chemical structure of poly(NIPAM-*co*-VP) is as follows (Scheme 2).

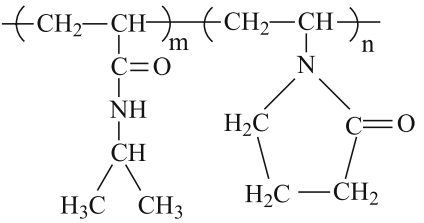

Scheme 2 Poly(*N*-isopropylacrylamide-*co*-1-vinyl-2-pyrrolidone) (Poly(NIPAM-*co*-VP))

2.1.3 Grafted PNIPAM-*g*-PEO Copolymers

Poly(ethylene oxide) (PEO) macromonomers end capped with a reactive methacrylate group can be synthesized by anionic ring-opening polymerization of ethylene oxide in tetrahydro-furan (THF) using potassium methoxide (MeOK) as the initiator. The weight average molar mass and polydispersity of the PEO macromonomers can be determined by gel permeation chromatography (GPC) using chloroform as the eluent and PEO standards. The molar mass of PEO macromonomer is in the range 3000–10 000 g/mol with a polydispersity index (M_w/M_n) less than 1.2. The PNIPAM grafted with PEO macromonomers can be prepared by free-radical copolymerization of different amounts of the PEO macromonomers into the PNIPAM chain backbone in water at temperatures either lower or higher than the LCST of PNIPAM. In a typical reaction, a 250-mL two-neck flask equipped with a nitrogen inlet tube and a magnetic stirrer is used. 0.03 mol NIPAM and different amounts of PEO can be added to a proper amount of deionized water to obtain 1–5 wt % solutions. The KPS/TEMED redox is normally used as the initiator. The molar ratio of KPS/TEMED is 1 : 1. The KPS and TEMED are respectively dissolved in water with concentrations of 0.009 M and 0.045 M. A few mL KPS solution is normally added into the reaction mixture. The solution should be repeatedly degassed at 20 °C and then purged with nitrogen for half an hour before the reaction. After heating the reaction mixture to 45 °C, a few mL TEMED solution is added and the reaction is carried out at this temperature for a certain time in a water bath to control the monomer conversion less than 50%. The PNIPAM-*g*-PEO copolymers can be purified by dialysis in a large amount of water. The final product should be dried under a reduced pressure at 40 °C. The copolymer can be further purified by several cycles of precipitation/fractionation from an acetone solution to *n*-hexane at 35 °C. The apparent weight average molar mass (M_w) of PNIPAM-*g*-PEO can be determined by laser light scattering. The copolymer composition can be estimated by ^{1}H-NMR. The chemical structure of PNIPAM-*g*-PEO is as follows (Scheme 3).

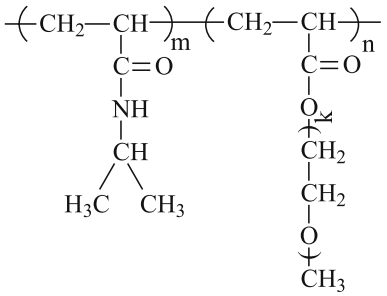

Scheme 3 Poly(*N*-isopropylacrylamide-*graft*-poly(ethylene oxide) (PNIPAM-*g*-PEO))

2.1.4 Segmented PNIPAM-*seg*-St Copolymers

Hydrophobically modified PNIPAM-*seg*-St segmented copolymers can be prepared by evenly inserting short styrene segments (stickers) into a PNIPAM chain backbone using the micellar polymerization. In this method, hydrophobic styrene (St) monomers is first solubilized inside small micelles made of surfactant, hexadecyltriethylammonium bromide (CTAB). KPS and TMED can be used to initiate the polymerization of hydrophilic NIPAM monomers dissolved in the continuous aqueous medium. When the free radical end of a growing PNIPAM chain enters a micelle, styrene monomers entrapped inside start to react to form a short hydrophobic segment (sticker). In this way, the coming-in-and-out of different micelles of each free-radical chain end can "connect" short styrene blocks on a PNIPAM chain.

In a typical reaction, initial concentrations of NIPAM, styrene, CTAB, KPS, and TMEDA are 0.16 M, 5.24 mM, 17.3 mM, 0.34 mM, 0.67 mM, respectively. The styrene content (3.9 mol %) of the resultant segmented PNIPAM-*seg*-St copolymer can be determined by pyrolysis gas chromatography. The average degree of polymerization between two styrene segments can be over a wide range, mainly depending on the initial NIPAM/styrene ratio. The resultant copolymer can be purified and fractionated by a number of successive dissolution-and- precipitation cycles in a mixture of extremely dried

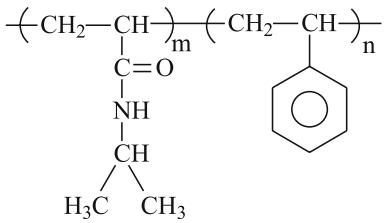

Scheme 4 Poly(*N*-isopropylacrylamide-*seg*-styrene) (PNIPAM-*seg*-St)

acetone and *n*-hexane at 25 °C. In each cycle, only the very first fraction obtained should be used in the next cycle. This combination of fractionation and filtration can result in narrowly distributed PNIPAM-*seg*-St chains with a high weight-average molar mass ($> 10^7$ g/mol) and a low polydispersity index ($M_w/M_n < 1.1$). The chemical structure of PNIPAM-*seg*-St is as shown in Scheme 4.

2.1.5 PNIPAM-*co*-KAA and PAM-*co*-NaAA Ionomers

PNIPAM containing a few molar percent of ionic groups on its chain backbone, ionomers, can be prepared by a free-radical copolymerization of NIPAM and other ionic comonomers, such as acrylic acid (AA), at 60 °C using AIBN as the initiator and a benzene/ethanol mixture as the reaction medium. In a typical synthesis, the reaction is conducted in a 250-mL two-neck flask equipped with a nitrogen inlet tube and a magnetic stirrer. 0.5 mmol NIPAM, proper amount of AA and 0.5 mol % AIBN are added to 50 mL solvent. The total monomer concentration is kept close to 0.5 M. After 30-min nitrogen purging, the mixture can be heated to and react at 60 °C for 1 hr in an oil bath. The monomer conversion should be controlled to be no more than 50%. After terminating the reaction, one can remove the solvent by evaporation at $T < 40$ °C under a reduced pressure. Each product of such prepared ionomers can be purified through three cycles of the acetone-to-hexane reprecipitation.

The selection of this solvent mixture is based on the following consideration: It is known that the preparation of PNIPAM homopolymer in benzene can result in higher molar mass samples than in other solvents. On the other hand, it is also known that alcohol is a relatively moderate chain transfer agent for free radical polymerization. Therefore, it is possible to control the molar mass by using a benzene/ethanol mixture with a varied composition. The average ionic content of each PNIPAM ionomer can be determined by titration using a 0.01-M potassium hydroxide solution with phenolphthalein as the indicator. A distinct color change from colorless to red can be used as an indication of the end point. Hereafter, PNIPAM ionomers neutralized with KOH are labeled as PNIPAM-*m*KAA, where "*m*" represents the average molar content of AA in the ionomer chain. On the other hand, poly(acrylamide) (PAM) ionomers can be prepared from PAM homopolymer. Acrylamide can be purified by re-crystallization. There is nothing special in such a synthesis so we will omit the details of the polymerization. The resultant PAM homopolymer can be fractionated and then hydrolyzed in NaOH and $NaCO_3$ aqueous solution. The hydrolysis is controlled by the reaction time. The hydrolysis degree can be determined by titration. The molecular parameters of these ionomer chains, such as M_w and $\langle R_g \rangle$, can be determined by LLS. Hereafter, these copolymers are denoted as PAM-*co*-*x*NaAA, where "*x*" shows the

molar percent of acrylic acid groups (from the hydrolysis) on the PAM chain backbone. The chemical structure of PNIPAM-*co*-KAA and PAM-*co*-NaAA are as follows (Scheme 5).

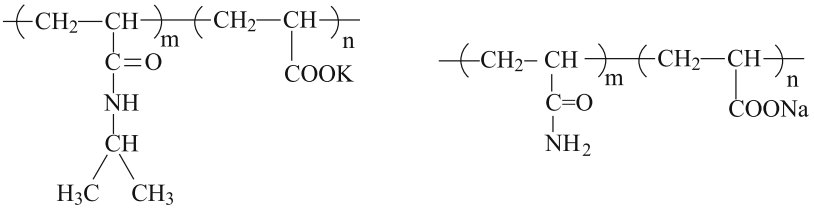

Scheme 5 Poly(*N*-isopropylacrylamide-*co*-potassium acrylate) (PNIPAM-*co*-KAA) and poly(*N*-isopropylacrylamide-*co*-sodium acrylate) (PAM-*co*-NaAA)

2.1.6 P(DEA-*co*-DMA) Copolymers

Poly(*N*,*N*-diethylacrylamide-*co*-*N*,*N*-dimethylacrylamide) P(DEA-*co*-DMA) copolymers with different amounts of DMA can be synthesized by free radical polymerization in THF with AIBN as the initiator (1 mol %). In a typical reaction, the solution mixture is bubbled with dry nitrogen for 30 min prior to polymerization. The temperature is then gradually raised to 68 °C in a period of 2 h and maintained for ~ 18 h. Each reaction mixture was precipitated in ether or hexane after the polymerization. The copolymer composition determined by ^{1}H NMR spectra is normally close to the feed ratio of monomers prior to polymerization. The nomenclature used hereafter for these copolymers is P(DEA-*co*-DMA/*x*), where *x* denotes the mol % content of DMA. The chemical structure of P(DEA-*co*-DMA) is as shown in Scheme 6.

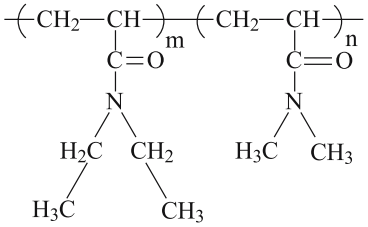

Scheme 6 Poly(*N*,*N*-diethylacrylamide-*co*-*N*-dimethylacrylamide) (P(DEA-*co*-DMA))

2.1.7 PNIPAM-*co*-MACA Copolymers

MACA is 2′-methacryloylaminoethylene)-3α,7α,12α-trihydroxy-5β-cholanoamide, a cholic acid derivative of natural bioactive amphiphilic compound. The synthetic detail of MACA is not what we would like to discuss here.

MACA as a hydrophobic comonomer can be used to modify PNIPAM. Copolymers, PNIPAM-*co*-MACA with different amounts of MACA can be synthesized by free-radical copolymerization of NIPAM and MACA in a mixture of methanol and chloroform with AIBN as the initiator. The resulting copolymers after purification can be dried in vacuum at 40 °C for 24 h. Hereafter, these copolymers are denoted as PNIPAM-*co*-*x*-MACA, where *x* denotes the molar percent of MACA. As expected, their solubility in water decreases as the MACA content or the solution temperature increases. It is also expected that the copolymer chains with a higher MACA content would have a lower LCST in comparison with PNIPAM homopolymer chains. In order to prepare a true solution, one has to dissolve these copolymers in water at low temperatures. The chemical structure of PNIPAM-*co*-MACA is as follows (Scheme 7).

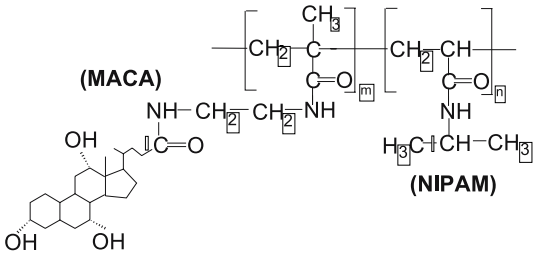

Scheme 7

2.2
Laser Light Scattering (LLS)

Laser light scattering has become a routine instrument in polymer laboratories around the world. We have used two slightly modified commercial LLS spectrometers (ALV, Germany) equipped with a multi-τ digital time correlator (ALV-5000). In our earlier experiments, we used an ALV/SP-150 spectrometer equipped with a solid-state 400-mW laser (ADLAS DPY425II, 400 mW at $\lambda_0 = 532$ nm) as the light source. Since 2002, we have used a newer version (ALV/DLS/SLS-5022F) equipped with a cylindrical 22-mW UNIPHASE He–Ne Laser ($\lambda_0 = 632$ nm) and a sensitive APD detector, in which the 22-mW red laser has the same affect as the 400-mW green laser. The incident light beam was vertically polarized with respect to the scattering plane and the intensity was regulated with a beam attenuator (Newport M-925B) so as to avoid localized heating in the light-scattering cuvette.

In static LLS [43], the angular dependence of the excess absolute time-averaged scattering intensity, known as the Rayleigh ratio $R_{vv}(q)$, is measured. For a dilute solution measured at a relatively small angle (θ), $R_{vv}(q)$ can be related to the weight average molar mass (M_w), the root mean square

radius of gyration ($\langle R_g^2 \rangle_z^{1/2}$) (or simply as $\langle R_g \rangle$), the second virial coefficient (A_2), and the scattering vector (q) as:

$$\frac{KC}{R_{vv}(q)} \approx \frac{1}{M_w}(1 + \frac{1}{3}R_g^2 q^2) + 2A_2 C \tag{1}$$

where $K = 4\pi n^2 (dn/dC)^2/(N_A \lambda_o^4)$ and $q = (4\pi n/\lambda_0)\sin(\theta/2)$ with N_A, n, dn/dC, and λ_o being the Avogadro constant, the solvent refractive index, the specific refractive index increment, and the wavelength of light in vacuum, respectively. Strictly speaking, $R_{vv}(q)$ should be $R_{vu}(q)$ because there was no analyzer in front of the detector. However, in the study of linear flexible polymer chains, depolarization is not a serious problem. Therefore, we can replace $R_{vu}(q)$ with $R_{vv}(q)$. The value of dn/dC is 0.167 mL/g in water at 25 °C, which was determined by using a special novel and precise differential refractometer [44].

In dynamic LLS [45, 46], the intensity-intensity time correlation function $G^{(2)}(t, q)$ in the self-beating mode was measured. For a Poisson distribution of the number of photons, $G^{(2)}(t, q)$ can be related to the normalized first-order electric field time correlation function $g^{(1)}(t, q)$ as [46]

$$G^{(2)}(t, q) = \langle I(0, q) I(t, q) \rangle = A \left[1 + \beta |g^{(1)}(t, q)|^2 \right], \tag{2}$$

where A is the measured base line, $0 < \beta < 1$ is a parameter depending on the coherence of the detection, and t is the delay time. For a broadly distributed sample, $|g^{(1)}(t, q)|$ is related to the line-width distribution $G(\Gamma)$ by

$$|g^{(1)}(t, q)| = \langle E(t, q) E^*(0, q) \rangle = \int_0^\infty G(\Gamma) e^{-\Gamma t} d\Gamma, \tag{3}$$

Using the Laplace inversion program, CONTIN, in the correlator, we were able to calculate $G(\Gamma)$ from $G^{(2)}(t, q)$ on the basis of Eqs. 3 and 4. For a pure diffusive relaxation, Γ is related to the translational diffusion coefficient D as [47]

$$\Gamma = Dq^2(1 + k_d C)(1 + f R_q^2 q^2), \tag{4}$$

where k_d is the dynamic second-order virial coefficient, containing both thermodynamic and hydrodynamic contributions, and f is a constant related to internal and rotational motions of scattering objects. $D = \Gamma/q^2$ if the polymer solution is sufficiently dilute and $qR_g \ll 1$. D can be further converted into the hydrodynamic radius R_h using the Stokes–Einstein equation: $D = k_B T/6\pi\eta R_h$, where k_B, T, and η are the Boltzmann constant, the absolute temperature, and the solvent viscosity, respectively. For narrowly distributed samples, the cumulant analysis of $G^{(2)}(t)$ can result in an accurate average line-width $\langle \Gamma \rangle$.

It should be note that the coherent factor β in dynamic LLS should be as high as possible. The ALV instrument can reach ~ 0.95, a rather high value

for a LLS spectrometer to be used for both static and dynamic LLS simultaneously. This is one of the reasons why we are able to carry out dynamic LLS in an extremely dilute solution, but still have a sufficient signal-to-noise ratio. In addition, with some modifications, one can remove straight lights from the incident bean to make a LLS spectrometer capable of measuring both static and dynamic LLS continuously in the small angle range that is particularly useful in the measurement of ultra-long polymer chains. This is because in static LLS the condition of $qR_g < 1$ is essentially required to determine the precise value of R_g; whereas in dynamic LLS the extrapolation of $q \to 0$ and the interference of the internal motions associated with the long polymer chain in dynamic LLS can be avoided. In addition, in this accessible small angle range the scattered intensity of long polymer chains is much stronger than that at high scattering angles, so that we are able to study an extremely dilute solution. The typical long-term temperature stability inside our LLS sample holder was less than $\pm 0.02\ ^\circ C$.

2.3
Ultra-Sensitive Differential Scanning Calorimeter (US-DSC)

The energy involved in the folding and association of copolymer chains in solutions can be measured by a micro-calorimeter (MicroCal Inc). We used US-DSC at an external pressure of ~ 180 kPa. The cell volume is only 0.157 mL. The heating rate can be varied and the instrument response time is normally a few seconds. All the DSC data should be corrected for instrument response time and can be analyzed using the software in the calorimeter. Note that the concentration used in DSC is normally not lower than 10^{-3} g/mL, much higher than that used in LLS (10^{-6}–10^{-4} g/mL).

3
Folding of Neutral Chains in Extremely Dilute Solutions

In comparison with copolymers, linear homopolymer chains are much simpler because there is no complication of comonomer composition, configuration and distribution on the chain backbone. However, the folding of linear homopolymer chains has been an extremely difficult problem in polymer science. Whether linear homopolymer chains can fold from an expanded random coil conformation in good solvents to a collapsed tiny globule had puzzled polymer researchers for many years and became a classic question since the 1960s. In 1995, Zhou et al. [32] finally showed, for the first time, that linear PNIPAM homopolymer chains can undergo the predicted coil-to-globule transition to form stable single-chain globules in water in the one-phase region without any interference of interchain association.

3.1
Coil-to-Globule Transition of Linear PNIPAM Homopolymer Chains

Figure 1 shows the typical angular dependence of $KC/R_{vv}(q)$ of PNIPAM homopolymer chains in the coiled and the fully collapsed globular states, respectively. The decrease of $\langle R_g \rangle$ from 127 nm to $\sim$ 18 nm, i.e., the decreases of the slope of the lines in Fig. 1 on the basis of Eq. 1, clearly indicates the chain collapse. The transition from the coil state to the globule state can also be directly viewed from the change of the hydrodynamic radius distribution $f(R_h)$ in the inset of Fig. 1. It is worth noting that the respective extrapolations of $[KC/R_{vv}(q)]_{q\to 0}$ lead to the same intercept, indicating that there is no change in M_w on the basis of Eq. 1. The narrowly distributed $f(R_h)$ in the globule state also indicates no interchain aggregation. Moreover, the average scattered light intensity ($\langle I \rangle$) in the globule state (not shown) was independent of time over three days, which indicates the globules were stable, because $\langle I \rangle \propto M_w \propto nM^2$ on the basis of Eq. 1, very sensitive to interchain association.

The plot in Fig. 1 should be the most important and ultimate test whether the folding of individual polymer chains is free of interchain association. Unfortunately, many past studies of the coil-to-globule transition did not present such a plot. It is always questionable whether the solutions studied were truly in the "one-phase" region or in the meta-stable "two-phase" region. Note that in the one-phase region, solvents can be further divided as "good", "theta" and "poor" solvents, depending on the relative strength of the solvent-polymer and solvent-solvent interaction. While in the "two-phase" region, polymer solution forms, in principle, a concentrated layer and a dilute

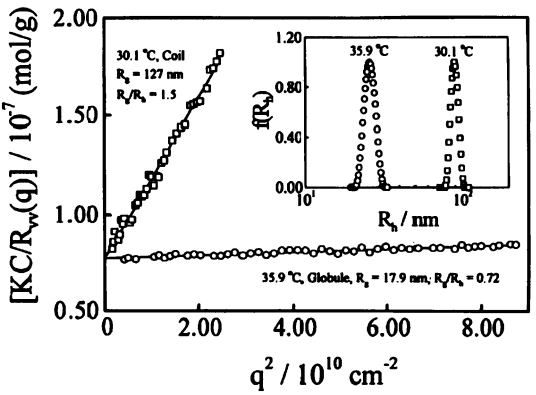

Fig. 1 Typical angular dependence of $KC/R_{vv}(q)$ of PNIPAM in water at two different temperatures, where the weight-average molar mass (M_w) and concentration (C) of PNIPAM are 1.3×10^7 g/mol and 6.7×10^{-7} g/mL, respectively. The *insert* shows the corresponding hydrodynamic radius distributions $f(R_h)$ of the PNIPAM chains respectively in the coiled and the globular states [38]

layer. In real experiments, two macroscopic layers might not be observable, especially in aqueous polymer solutions, because similar densities of polymer chains and water prevent macroscopic phase separation. Instead, only microphase separation, i.e., the formation of the mesoglobular phase, is observed, in which a limited number of polymer chains come together to form stable polymeric colloidal particles floating inside the solution. Within a reasonable experimental time scale, these particles or mesoglobules would not be able to further aggregate to form macroscopic precipitation because there is no sufficient sedimentation force to drag them down.

The earlier results concerning the folding of homopolymer chains have already been reviewed [48], which is schematically summarized in Fig. 2. The essential message of Fig. 2 is that when the solvent quality changes from good to poor, a linear and coiled homopolymer chain first shrink into a crumpet state without some additional knotting and then it passes through a molten globule state before it finally reaches its collapsed globular state. The reverse process (the dissolution or the "globule-to-coil" transition) of the collapsed chain follows a different route; namely, there exists a hysteresis between the folding and unfolding processes.

First, let us look at indirect evidence that the collapsed chain is in a crumpet state instead of a highly knotted state. Figure 3 shows the dissolving kinetics (in terms of the change of $\langle R_h \rangle$) of fully collapsed single PNIPAM chain globules, where t is the standing time after the solution temperature was quenched from 33.02 °C to 30.02 °C. Experimentally, the PNIPAM solution was prepared at 30.02 °C and its $\langle R_h \rangle$ was measured. The solution temperature was then increased to 33.02 °C and aged for more than $\sim 10^3$ s

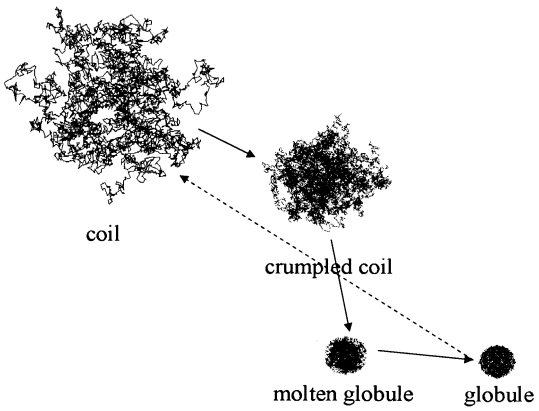

Fig. 2 Schematic of four thermodynamically stable states (random coil, crumpet coil, molten globule and collapsed globule) of a homopolymer chain in the coil-to-globule and the globule-to-coil transitions. There exists a hysteresis between the two transitions around the Θ-temperature ($\sim$ 30.6 °C) of the PNIPAM solution [37]

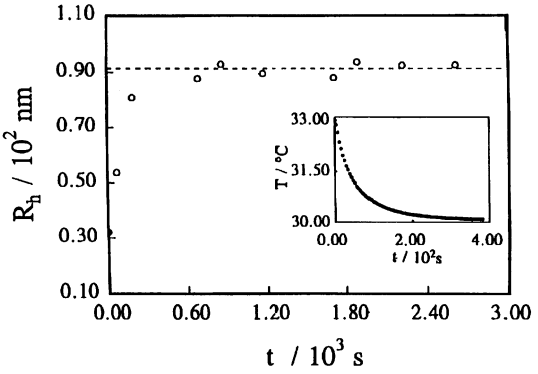

Fig. 3 Dissolving kinetics (in terms of average hydrodynamic radius R_h) of collapsed single-chain PNIPAM globules, where t is the standing time after the solution temperature was quenched from 33.02 to 30.02 °C and the *dashed line* represents a stable average value of R_h of individual PNIPAM random coils at 30.02 °C. The weight-average molar mass (M_w) of the PNIPAM sample used is 1.08×10^7 g/mol with a polydispersity index (M_w/M_n) less than 1.1 [32]

so that individual PNIPAM chains have a sufficient time to collapse into individual single-chain globules. Note that the longest aging time was 3 days and there was no change in $\langle R_h \rangle$ after $\sim$ 800 s. The solution temperature was suddenly cooled down back to 30.02 °C and both $\langle R_h \rangle$ and t were immediately recorded after the temperature change.

The inset in Fig. 3 shows how fast the solution temperature could reach its equilibrium value, wherein a very special LLS cuvette made of a thin wall ($\sim$ 0.4 mm) glass tube was used for all kinetic studies. Figure 3 shows that the change from the globular state to the extended random-coiled state, i.e., the dissolving kinetics, was too fast to be detected in our LLS setup. In other words, before the solution reached its temperature equilibrium at 30.02 °C, individual collapsed PNIPAM globules already expanded into individual extended random coil chains. This fast dissolving time ($< \sim$ 300 s) indicates that there should be no additional and extensive chain knotting inside these highly collapsed single-chain globules because it has been known that it takes one week to dissolve such a long-chain polymer (chains are entangled in bulk) even in a good solvent.

Figure 4 shows a plot of the static expansion factor (α) as a function of the relative temperature Θ/T, where α is defined as $R_g(T)/R_g(\Theta)$ and r is the number of residues that may be one monomer unit or a number of repeat units. When $T < \Theta$ (water is a good solvent for PNIPAM), the data points are reasonably fitted by the line with $r = 10^5$ calculated on the basis of Flory–Huggins theory [15]. Similar results have also been observed for linear polystyrene in cyclohexane [25, 49]. The theory works well in the good-solvent region wherein the interaction parameter (χ) is expected to be

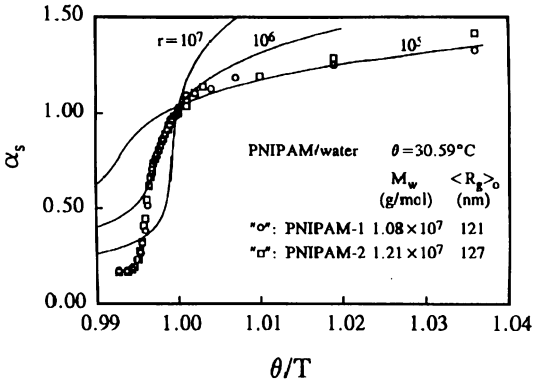

Fig. 4 Plot of static expansion factor (α_s) as a function of relative temperature Θ/T, where α is defined as $R_g(T)/R_g(\Theta)$; symbols are our measured results; and the *lines* are calculated data with three different values of r. If choosing $M = 113$ (molar mass of monomer NIPAM), we have $r \sim 10^5$ for both the PNIPAM samples used [32]

a weak function of temperature [15]. On the other hand, for temperatures higher than Θ, the measured α drops much faster than the line with $r = 10^5$. Up to now, we still do not have a clear understanding of this discrepancy. Apparently, the results can be partially fitted by the line with $r = 10^6$. The remarkable point is that α decreases to a much lower plateau than the predicted value [50, 51]. However, this does indicate that for PNIPAM in water, χ might be a function of temperature or concentration because the local concentration within the volume occupied by the chain increases $\sim$ 500 times during the chain contraction.

Recently, Tanaka et al. [52] suggested that PNIPAM in water can be treated as a "copolymer" because they think that the PNIPAM chain backbone is hydrolyzed in a segmental fashion. They also suggested that the hydrolyzing degree or extent would dramatically decrease when temperatures are higher than the LCST. This suggestion seems to agree well with the two-state theory (hydrolysis and nonhydrolysis) used by Halperin et al. [53] In any case, the short-coming of the concentration-independent χ is obvious. Our results also showed that the average chain density $\langle\rho\rangle$ estimated from $M_w/[N_A(4/3)\pi\langle R_h\rangle^3]$ increases from 0.0025 g/cm^3 (coil) to 0.34 g/cm^3 (globule), close to $\sim$ 0.4 g/cm^3 predicted on the basis of a space-filling model [54]. This means that the inside of single-chain PNIPAM globules is not as dry as what we originally thought and each globule still contains $\sim$ 70–80% of water inside its hydrodynamic volume.

It has been known that $\langle R_g\rangle/\langle R_h\rangle$ can better reflect the chain conformation. Figure 5 shows the temperature dependence of $\langle R_g\rangle/\langle R_h\rangle$ in both the heating and cooling processes. During the heating, in the range 20–30.6 °C (Θ-temperature), $\langle R_g\rangle/\langle R_h\rangle$ remains nearly a constant ($\sim$ 1.5), revealing that the PNIPAM chains keep the random coil conformation as long as $T < \Theta$. The

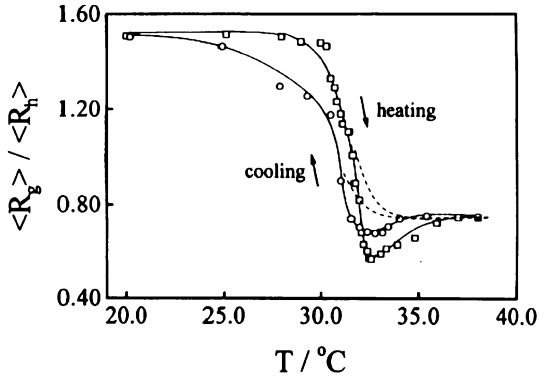

Fig. 5 Temperature dependence of the ratio of average radius of gyration to average hydrodynamic radius ($\langle R_g \rangle / \langle R_h \rangle$) in both heating and the cooling processes, where $M_w = 1.3 \times 10^7$ g/mol and $M_w/M_n < 1.05$ [38]

change of $\langle R_g \rangle / \langle R_h \rangle$ between ~ 1.5 at 20 °C to ~ 0.77 at 38 °C agrees well with the values respectively predicted for a random coil and a solid uniform sphere, clearly indicating the collapse of the PNIPAM chains. In the temperature range 30.6–38 °C, $\langle R_g \rangle / \langle R_h \rangle$ dips into a low value of ~ 0.56 before it comes back to ~ 0.77. This temperature range can be roughly divided into two sub-stages. The first one is from the Θ-temperature to 31.6 °C at which $\langle R_g \rangle = \langle R_h \rangle$; and the second one is from 31.6 to 38 °C in which $\langle R_g \rangle / \langle R_h \rangle$ reaches the minimum value.

The decrease of $\langle R_g \rangle / \langle R_h \rangle$ in the first stage reflects the conformation change from an extended random coil to a *crumpled* coil. If the folding and unfolding were an all-or-none process, the changes of $\langle R_h \rangle / \langle R_g \rangle$ in the second stage would, respectively, follow the two dashed lines in Fig. 5. However, the unexpected minimum, which has later been confirmed by many experiments related to the coil-to-globule transition, reveals that there exists another physical state between the fully collapsed globule and the unfolded random coil. This is identified as the molten globular state. In this molten globular state, the chain density is not evenly distributed inside each single-chain globule. Presumably, the surface of the collapsed single-chain globule contains many small loops (i.e., a rough surface with a lower density) because polymer chains are not infinitely flexible. We can imagine that on the one hand, these small loops are nondraining and they make $\langle R_h \rangle$ larger, and on the other hand, they have much less effect on $\langle R_g \rangle$ because their masses are relatively low. In other words, $\langle R_g \rangle$ decreases relatively faster than $\langle R_h \rangle$. This explains why the ratio of $\langle R_g \rangle / \langle R_h \rangle$ could be smaller than $(3/5)^{1/2}$ predicted for a uniform hard sphere. It is not difficult to imagine that stress must be built up within these small loops when they become smaller and smaller so that the shrinking of these small loops slows down. This is why $\langle R_h \rangle$ decreases slightly, but there is no change in $\langle R_g \rangle$, when $T > 32.4$ °C (not shown).

Figure 5 shows that in the cooling process, $\langle R_g \rangle / \langle R_h \rangle$ reaches ~ 1.5 only after $T < 25\,^{\circ}\mathrm{C}$. There is a clear hysteresis, especially around the Θ-temperature. It reveals that even water becomes a good solvent in the temperature range 25–30.6 °C, individual single-chain globules are still not completely dissolved into the randomly coiled conformation. This hysteresis implies that some additional intrachain interaction (presumably, intrachain hydrogen bonding) is formed when the chain is in its fully collapsed globular state because of a much smaller inter-segment distance and such intrachain interaction persists in the globule-to-coil process until water becomes a very good solvent. The results also revealed that the decrease of $\langle R_g \rangle / \langle R_h \rangle$ in the left side of the minimum point is because the decrease of $\langle R_g \rangle$ is relatively faster, while the increase of $\langle R_g \rangle / \langle R_h \rangle$ at the right side is mainly due to the decrease of $\langle R_h \rangle$.

The transition between a random coil and a crumpet coil can be respectively described by the existing Flory and Birshtein–Pryamitsyn theories [18, 55]. However, a quantitative description of the molten globular state still remains a challenging problem. The deviation of the existing theory from the experimental results could be, at least partially, because the molten and fully collapsed globules have different chain density distributions in comparison with the coils. On the other hand, the Flory–Huggins interaction parameter χ for PNIPAM in water might be a strong function of temperature and/or polymer concentration. The quantitative theory of polymer chain conformation in a poor solvent remains an interesting problem, which is generally related to some basic problems of semi-dilute and concentrated solutions because the local chain density inside the globule is high even though the overall concentration is very low. Moreover, to our knowledge, no one knows the dynamics of a single chain in the crumpet or the collapsed conformation.

3.2 Folding of Amphiphilic Copolymer Chains

The copolymerization of a few molar percent of water-soluble neutral or ionic comonomer on PNIPAM generally makes it more hydrophilic so that its LCST in water decreases. In the synthesis, comonomers can be inserted into or grafted on the PNIPAM chain backbone in a random or a more segmented fashion by using different chain conformations of PNIPAM in water at different temperatures. It was expected that at temperatures higher than its LCST, hydrophilic comonomers would segregate on the periphery of the collapsed PNIPAM chain backbone, while at lower temperatures, the copolymerization would lead to a more random distribution of comonomers on the PNIPAM chain backbone because both of them are hydrophilic. Therefore, by alternating the reaction temperature, we were able to incorporate hydrophilic comonomers into the PNIPAM chain backbone with different comonomer distributions. In the following discussion, we will start with some simpler cases of noncharged neutral copolymer chains and discuss how the comonomer distribution and compo-

sition can affect the folding of individual copolymer chains before moving to charged anionic copolymer chains. This is because long-range electrostatic interaction in water is always troublesome in theory.

3.2.1 Hydrophilically Modified PNIPAM Copolymer Chains

For different applications, water-soluble neutral and ionic comonomers can be incorporated into or attached to the PNIPAM chain backbone to form amphiphilic PNIPAM copolymers via free-radical copolymerization. In this section, we will use the folding of neutral PNIPAM amphiphilic copolymer chains in extremely dilute solutions ($\sim \mu g/mL$) to illustrate a general feature of the folding of hydrophilically modified copolymer chains.

Linear NIPAM-co-VP copolymers: As discussed in the Experimental Section, hydrophilic comonomer, vinyl pyrrolidone (VP), can be purposely copolymerized into PNIPAM at two different temperatures, 30 °C and 60 °C, respectively, below and above the LCST of PNIPAM homopolymer. At each temperature, the copolymers with two different VP/NIPAM ratios (5 and 10 mol %) were prepared. A proper fractionation of resultant copolymers led to narrowly-distributed long NIPAM-*co*-VP copolymer chains with a similar length and VP/NIPAM ratio, but different comonomer distributions.

Figure 6 shows the typical temperature dependence of both $\langle R_g \rangle$ and $\langle R_h \rangle$ of two copolymers synthesized at two different temperatures. As expected,

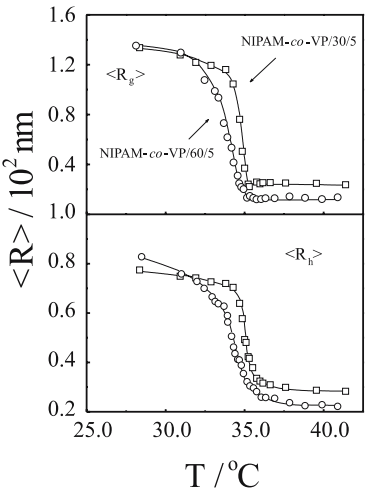

Fig. 6 Temperature dependence of *z*-average root-mean square radius of gyration ($\langle R_g \rangle$) and average hydrodynamic radius ($\langle R_h \rangle$) of copolymers NIPAM-*co*-VP/60/5 and NIPAM-*co*-VP/30/5 in water, where the weight average molar masses are 2.9×10^6 and 4.2×10^6 g/mol, respectively [56]

both $\langle R_g \rangle$ and $\langle R_h \rangle$ decrease sharply during the coil-to-globule transition, revealing the chain collapse at higher temperatures. Note that in each case, the average size of the collapsed chains remains nearly a constant even when the temperature (40 °C) is much higher than the LCST of PNIPAM and water becomes a very poor solvent for PNIPAM, indicating that such formed single-chain globules are very stable. In contrast, previous studies of PNIPAM homopolymer showed that stable single-chain globules could only be observed within a limited temperature range [32]. The formation of such stable single-chain globules can be attributed to the existence of hydrophilic comonomer VP. As expected, the copolymer chains with hydrophilic comonomer VP have a higher transition temperature than PNIPAM homopolymer. The detail values of the coil-to-globule transition temperature and the average hydrodynamic radii in the collapsed state for two pairs of NIPAM-*co*-VP copolymers with different VP contents can be found elsewhere [56].

It is not surprising to see that the chains with a higher hydrophilic comonomer VP content have a higher transition temperature. However, it is rather interesting to see that for each pair of the copolymers with a similar VP content, the copolymer prepared at 60 °C has a lower transition temperature than its counterpart prepared at 30 °C. In order to check this shift in the transition temperature, we also measured the partial heat capacity (C_p) of these copolymers in solution using a micro-calorimeter. Figure 7 shows that for the two copolymers prepared at 60 °C, the temperatures at which the maximum

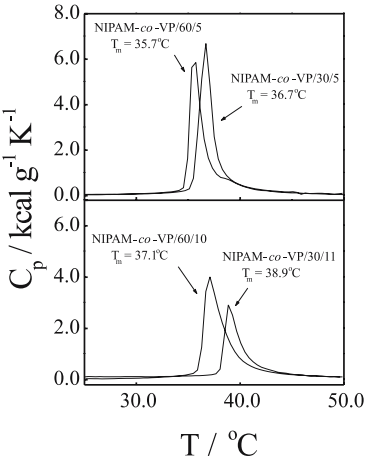

Fig. 7 Temperature dependence of partial heat capacity (C_p) of two pairs of NIPAM-*co*-VP copolymers in water. The weight average molar masses of NIPAM-*co*-VP/60/5, NIPAM-*co*-VP/30/5, NIPAM-*co*-VP/60/10 and NIPAM-*co*-VP/30/10 are 2.9×10^6, 4.2×10^6, 5.6×10^6 and 7.9×10^6 g/mol, respectively. The polymer concentration is 10^{-3} g/mL. The temperature was increased with a rate of 1.5 °C/min and pressure was maintained at 180 kPa [56]

heat capacity (T_{max}) occurs are indeed lower. Such a difference between the transition temperatures can only be attributed to different comonomer distributions on the PNIPAM chain backbone because the copolymers in each pair have a similar chain length and composition.

As we mentioned earlier, at lower temperatures, water is a good solvent for PNIPAM and the PNIPAM segments formed during the copolymerization and that exist as a random coil. In this way, NIPAM and VP are copolymerized in a relatively more random fashion to form a statistical copolymer. In contrast, water at 60 °C becomes such a poor solvent that the PNIPAM chain backbone collapses and the hydrophilic VP comonomer can only be incorporated on its periphery, leading to a segregation of VP, or in other words, a segmented comonomer distribution. Therefore, the average length of the PNIPAM segment between two neighboring VP segments is longer in comparison with a statistical copolymer chain with a similar VP/NIPAM ratio, as schematically shown in Fig. 8.

The lower transition temperature also indicates that the folding of the copolymer chains prepared at higher temperatures is much easier, or in a sense, these chains could "memorize" the parent collapsed globular state in which they were formed. As we discussed earlier, the conformational change can be better viewed in terms of the ratio of $\langle R_g \rangle / \langle R_h \rangle$. For a random coil and a uniform nondraining sphere, $\langle R_g \rangle / \langle R_h \rangle \sim 1.5$ and ~ 0.774, respec-

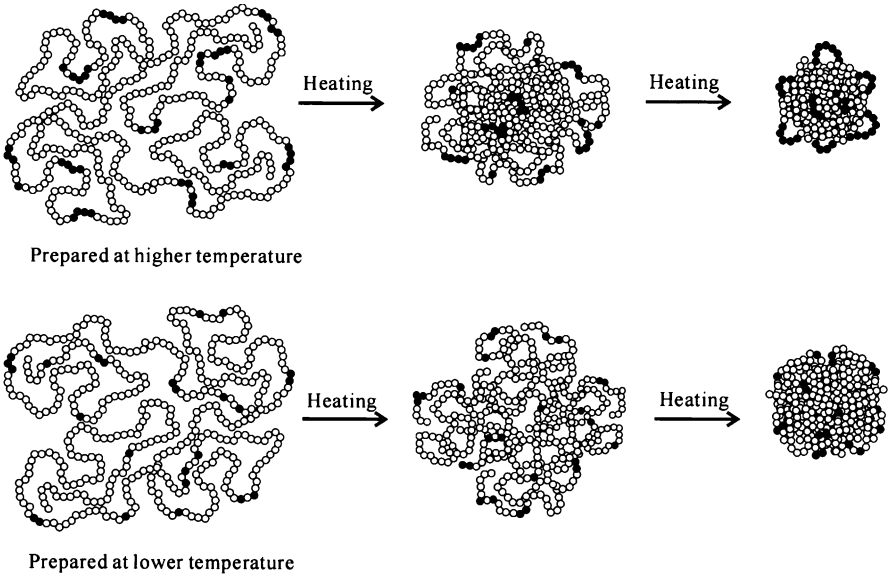

Fig. 8 Schematic of different chain conformations and the coil-to-globule transition of NIPAM-*co*-VP copolymers prepared at two temperatures, respectively, lower and higher than the lower critical solution temperature of PNIPAM homopolymer [56]

tively. In Fig. 9, the decrease of $\langle R_g \rangle / \langle R_h \rangle$ from ~ 1.65 to ~ 0.6–0.8 clearly reveals the coil-to-globule transition of individual copolymer chains. Just like PNIPAM homopolymer in water, before fully collapsing into a uniform globule, the copolymer chains with an extended randomly coiled conformation first collapses into a nonuniform structure with a value of $\langle R_g \rangle / \langle R_h \rangle$ much smaller than 0.774, i.e., the dip of $\langle R_g \rangle / \langle R_h \rangle$ at ~ 35–$36\,^{\circ}\mathrm{C}$. It should be noted that even in the fully collapsed state at higher temperatures, $\langle R_g \rangle / \langle R_h \rangle$ of single-chain globules made of NIPAM-*co*-VP/60/5 is still smaller than 0.774. This suggests that individual single-copolymer chain globules have a nonuniform chain density distribution inside, as previously observed by Khokhlov et al. [8] in a computer simulation. It is also schematically shown in Fig. 8.

As expected, the collapse of longer PNIPAM segments on the copolymer chain prepared at $60\,^{\circ}\mathrm{C}$ forces the hydrophilic VP segments to stay on the periphery, leading to a "core-shell" structure with a denser PNIPAM core and a swollen VP shell presumably made of small VP loops. On the other hand, the copolymer chains prepared at $30\,^{\circ}\mathrm{C}$ should have a more random comonomer distribution and hydrophilic comonomer VP would not be segregated together to form short VP segments, in other words, the average length of the PNIPAM segments is much shorter. The collapse of these shorter PNIPAM segments at high temperatures inevitably pulls hydrophilic comonomer VP inside, resulting in less compact, but more uniform, globules with a ratio of $\langle R_g \rangle / \langle R_h \rangle$ similar to uniform latex particles. The comparison of the coil-to-globule transition of a pair of such copolymer chains is schematically shown in Fig. 8.

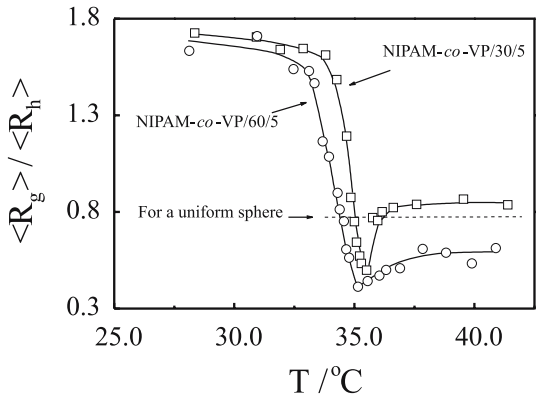

Fig. 9 Temperature dependence of the ratio of average radius of gyration to average hydrodynamic radius ($\langle R_g \rangle / \langle R_h \rangle$) of copolymer NIPAM-*co*-VP chains prepared at two different temperatures, respectively, lower and higher than the lower critical solution temperature of PNIPAM homopolymer. The weight average molar masses of NIPAM-*co*-VP/60/5 and NIPAM-*co*-VP/30/5 are 2.9×10^6 and 4.2×10^6 g/mol, respectively [56]

The structural difference between the collapsed globules made of the chains prepared at different temperatures can also be evidenced in their size and density. Note that in Fig. 6 in the fully collapsed state at $\sim 40\,^{\circ}C$, NIPAM-*co*-VP/60/5 globules have a smaller size than NIPAM-*co*-VP/30/5 globules even though they have a similar $\langle R_g \rangle$ and $\langle R_h \rangle$ in the random coiled state at lower temperatures. Therefore, the former have higher average chain densities ($\langle \rho \rangle_{globule}$). The values of $\langle \rho \rangle_{globule}$ for NIPAM-*co*-VP/60/5 and NIPAM-*co*-VP/30/5 globules are 9.6×10^{-2} and 7.0×10^{-2} g/cm^3, respectively. Such a difference in $\langle \rho \rangle_{globule}$ also indirectly reflects that the copolymer chains prepared at higher temperatures can "memorize" their parental collapsed globule state and fold back to a more compact structure, confirming the computer simulation and prediction [8, 9]. In comparison, $\langle \rho \rangle_{globule}$ of single-chain globules made of amphiphilic copolymer chains is 3–4 times lower than that made of homopolymer chains [32]. This is reasonable because the incorporation of a few percent of hydrophilic comonomer VP into PNIPAM swells the globules and retards the chain packing.

Grafted PNIPAM-g-PEO copolymers: There has been considerable interest in the study of grafted amphiphilic copolymers in selected solvents because they can form stable aggregates with a core-shell structure in solution [57–62]. For example, amphiphilic copolymer chains consisting of the hydrophobic backbone and hydrophilic branches can form stable core-shell colloidal particles in water (a selective solvent) because the hydrophobic chain backbone tends to aggregate to form a hydrophobic core, while the hydrophilic branches grafted on them are forced to stay on the periphery to form a hydrophilic corona (shell) [63–66]. Core-shell particles formed in this way are sterically stabilized and have an average size normally in the range 10–100 nm, depending on the formation condition and the copolymer structure. This has provided a new method to prepare stable surfactant-free polymeric nanoparticles.

By extending the study of the folding of linear PNIPAM homopolymer chains in water, Qiu et al. [67] prepared a series of amphiphilic PNIPAM-*g*-PEO copolymer chains by grafting different amounts of short PEO chains on the PNIPAM chain backbone as described in the Experimental Section. In cold water, both the PNIPAM chain backbone and the grafted PEO branches are hydrophilic so that PNIPAM-*g*-PEO copolymer is soluble in water as individual coiled chains. At temperatures higher than its LCST, the PNIPAM chain backbone becomes hydrophobic, but PEO branches remain hydrophilic. Therefore, a change in the solution temperature about 1–2 degrees can greatly alternate the degree of amphiphilicity of this kind of copolymer to induce the chain folding and to form stable single-chain globules with a hydrophobic PNIPAM core and a soluble hydrophilic PEO shell. Such a core-shell nanostructure can be switched on and off simply by a very small temperature variation.

Figure 10 shows a schematic of the formation of a single chain core-shell nanostructure. It is known that the short grafted PEO chains have an average

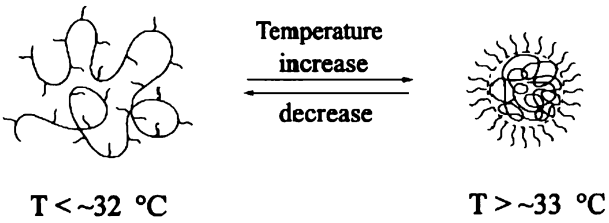

Fig. 10 Schematic of formation of a single chain core-shell nanostructure through the coil-to-globule transition of the PNIPAM-*g*-PEO copolymer chain backbone [67]

hydrodynamic radius of ~ 3 nm. For the PNIPAM-*g*-PEO copolymer chains ($M_w = 7.29 \times 10^6$ g/mol) are grafted, on average, ~ 70 short PEO chains per PNIPAM chain backbone, its $\langle R_g \rangle$ changes from 155 nm to 21 nm and the ratio of $\langle R_g \rangle / \langle R_h \rangle$ decreases from 1.5 to 0.74 during the chain folding. Assuming that these short PEO chains grafted on the periphery have a similar chain conformation as those free in water, one can estimate the shell thickness (L_{shell}) and the radius of the core to be ~ 6 nm and ~ 23 nm, respectively. Further, using the molar mass of the PNIPAM chain backbone, one can also estimate the average chain density of the core to be ~ 0.25 g/cm^3, significantly lower than the average chain density (~ 1 g/cm^3) of conventional polymeric latex particles. In other words, the PNIPAM core still contains $\sim 75\%$ of water even in its fully collapsed state. Therefore, this core-shell nanostructure might be used as a carrier to load a large amount of drugs or catalysts because of its large free volume. Another advantage of using it as a carrier is that such a single-chain core-shell nanostructure can be quickly switched on and off by a small temperature variation of only 1–2 °C.

Figure 11 shows the releasing and encapsulation of pyrene (an imitation of drugs/catalysts) by these PNIPAM-*g*-PEO copolymer chains in water in

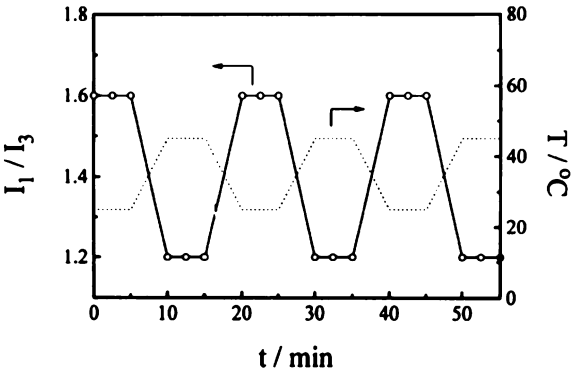

Fig. 11 Temperature dependence of fluorescence intensity ratio (I_1/I_3) of pyrene as an imitated drug/catalyst in deionized water in the presence of PNIPAM-*g*-PEO chains, where the concentration of pyrene is 2×10^{-7} M [67]

terms of its temperature-dependent fluorescence intensity ratio (I_1/I_3), where the pyrene concentration is $\sim 2 \times 10^{-7}$ M. It has been known that I_1/I_3, the highest energy vibrational band I_1 (373 nm) to the third highest energy vibrational band I_3 (385 nm), is sensitive to micro-environmental polarity [17]; namely, in pure water, $I_1/I_3 \sim 1.8$, while in a hydrophobic domain, I_1/I_3 could be as low as 1.2. The change of I_1/I_3 between ~ 1.6 and ~ 1.2 clearly shows that the folding and unfolding of these copolymer chains can release and encapsulate pyrene when the temperature is alternated between 25 to 45 °C. It should be noted that the change of I_1/I_3 would be a much sharper step function if one could change the temperature instantly.

Recently, Tenhu et al. [16, 58] studied the influence of the PEO content on the aggregation of such copolymer chains and found that the chains prepared at different temperatures had different values of LCST. As expected, the PEO content has a great effect on the phase transition. Following their method, Chen et al. [59] synthesized four PNIPAM-*g*-PEO copolymers with different PEO contents, but a similar chain length, at 45 °C. Their objective was to study the effect of the PEO content on the folding and unfolding of such amphiphilic copolymer chains in dilute solutions by using a combination of static and dynamic LLS as well as US-DSC. Surprisingly, they found that the PNIPAM-*g*-PEO copolymer chains with a higher PEO content underwent two transitions. One sharp transition at ~ 33 °C is related to the collapse of the PNIPAM chain backbone. Another broad transition in the range 35–45 °C disappeared when the PEO content was lower, which was attributed to the stretching and collapsing of short PEO chains grafted on the PNIPAM chain backbone.

Figures 12 and 13 summarize the temperature dependence of $\langle R_g \rangle$ and $\langle R_h \rangle$ of PNIPAM-*g*-PEO copolymer chains in water during one heating-and-

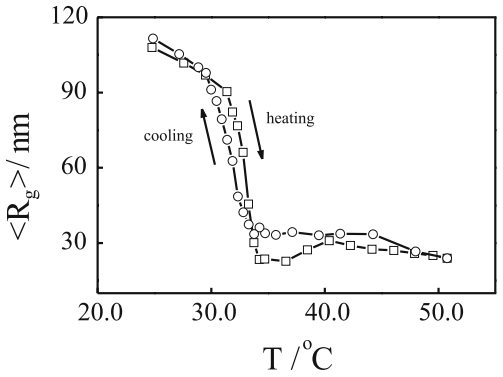

Fig. 12 Temperature dependence of *z*-average root-mean-square radius of gyration ($\langle R_g \rangle$) of copolymer PNIPAM-*g*-PEO chains in water during heating and cooling, where the weight-average molar mass (M_w) is 7.2×10^6 g/mol, the molar number ratio of NIPAM monomers to PEO macromonomers is 111, and on average, there are 392 short PEO chains grafted on each PNIPAM chain [69]

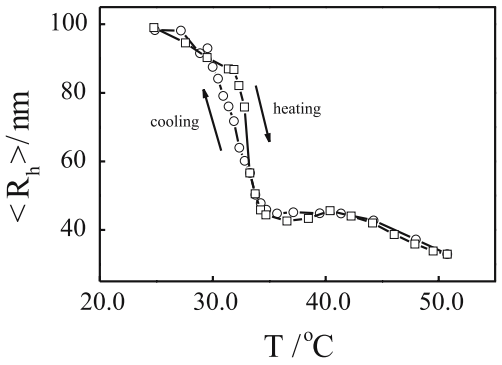

Fig. 13 Temperature dependence of average hydrodynamic radius ($\langle R_h \rangle$) of copolymer PNIPAM-*g*-PEO chains in water during heating and cooling, where the weight-average molar mass (M_w) is 7.2×10^6 g/mol, the molar number ratio of NIPAM monomers to PEO macromonomers is 111, and on average, there are 392 short PEO chains grafted on each PNIPAM chain [69]

cooling cycle. In the heating process, both $\langle R_g \rangle$ and $\langle R_h \rangle$ drop sharply in the range 31–33 °C, reflecting the expected coil-to-globule transition of the PNIPAM chain backbone. Further increase of the temperature first results in slight increases of both $\langle R_g \rangle$ and $\langle R_h \rangle$ and is then followed by a slow decrease over a broad temperature range. In comparison with PNIPAM homopolymer chains, such additional changes of both $\langle R_g \rangle$ and $\langle R_h \rangle$ must be related to short PEO chains grafted on the chain backbone. To explain the results (Figs. 12 and 13) we have to look at what has happened during the shrinking of the chain backbone.

As we discussed earlier, at lower temperatures, each copolymer chain in water exists as an extended random coil. The heating makes the PNIPAM chain backbone insoluble in water so that it undergoes the coil-to-globule transition. In this process, short hydrophilic PEO chains are forced to stay on the periphery of the PNIPAM core to form a core-shell nanostructure, such as schematically shown in Fig. 14a. The estimated average surface area per PEO chain at ~ 33 °C is ~ 10 nm^2. Further shrinking of the PNIPAM core increases the chain density on the periphery. As expected, the repulsion among different PEO chains forces them to stretch, as schematically shown in Fig. 14b. During this stage, the stretching of short PEO chains in the shell and the collapse of the PNIPAM chain backbone in the core have opposite effects on the measured $\langle R_g \rangle$ and $\langle R_h \rangle$ when the PEO content is high. The slight increases of both $\langle R_g \rangle$ and $\langle R_h \rangle$ in the range 35–40 °C indicates that the stretching of short PEO chains dominates slightly. As for the slow decreases of both $\langle R_g \rangle$ and $\langle R_h \rangle$ in the high temperature range ($T > 40$ °C), this could be explained by two possible scenarios as follows.

One is that the shrinking of a long PNIPAM chain backbone in the core overrides the stretching of short PEO chains in the shell. The other is the

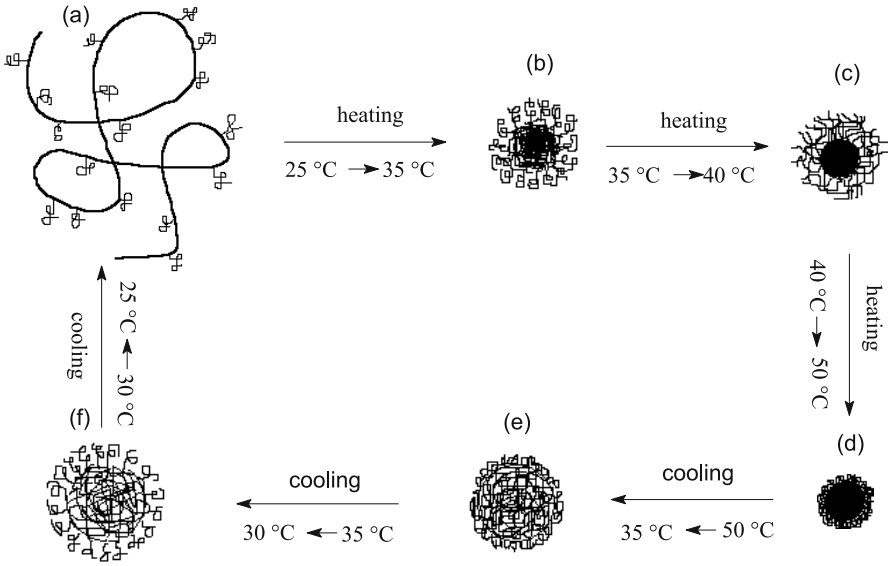

Fig. 14 Schematic of the coil-to-globule-to-coil transition of a copolymer PNIPAM-*g*-PEO chain with a higher PEO content during a heating-and-cooling cycle [69]

n-clustering-induced collapse of short PEO chains because we know that polymer chains in bulk or in a very concentrated solution adopt a random coil conformation, as with the Θ-temperature [70, 71]. In addition, the solvent quality of water for PEO decreases as the solution temperature increases. In order to differentiate these two scenarios, the temperature dependence of $\langle R_g \rangle / \langle R_h \rangle$ is plotted in Fig. 15 to reflect the chain density distribution. The fact that $\langle R_g \rangle / \langle R_h \rangle \sim 1.1$ at lower temperatures, instead of ~ 1.5 (an expected value for linear coil chains), reflects its branching structure because short PEO chains have a length similar to the PNIPAM segments between two neighboring grafting points. The decrease of $\langle R_g \rangle / \langle R_h \rangle$ from ~ 1.0 to ~ 0.5 clearly reveals a change of the chain conformation.

As discussed before, the lower value of $\langle R_g \rangle / \langle R_h \rangle$ confirms that the collapsed chain has a core-shell nanostructure and the collapsed PNIPAM core is denser than the swollen PEO shell. In comparison with a uniform sphere with the same $\langle R_h \rangle$, the denser core leads to a smaller $\langle R_g \rangle$. The increase of $\langle R_g \rangle / \langle R_h \rangle$ in the range 35–40 °C reflects the core-shell structure and becomes more uniform in density because the PEO chains in the shell are forced to overlap each other when the PNIPAM core continues to shrink (Fig. 14c). In Fig. 15, it is the further increase of $\langle R_g \rangle / \langle R_h \rangle$ in the range 40–50 °C that differentiates the two scenarios. Namely, if the first one was correct, $\langle R_g \rangle / \langle R_h \rangle$ should decrease because the core becomes denser. On the other hand, in the second scenario, the collapse of the PEO chains increases the chain density of the shell so that the core-shell nanostructure becomes more uniform, as

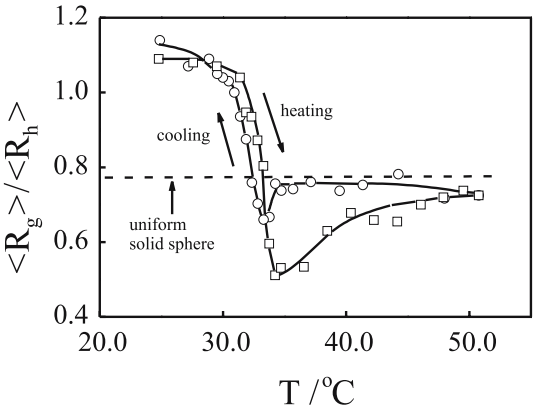

Fig. 15 Temperature dependence of ratio of average radius of gyration ($\langle R_g \rangle$) to average hydrodynamic radius ($\langle R_h \rangle$) of copolymer PNIPAM-*g*-PEO chains in water during heating and cooling. The weight-average molar mass (M_w) is 7.2×10^6 g/mol, the molar number ratio of NIPAM monomers to PEO macromonomers is 111, and there are 392 short PEO chains grafted on each PNIPAM chain [69]

schematically shown in Fig. 14d. This explains why $\langle R_g \rangle / \langle R_h \rangle$ gradually approaches 0.774 as the solution temperature increases.

A combination of Figs. 12–15 shows that the reversible globule-to-coil transition does not follow the coil-to-globule path. There exists a hysteresis between the heating and cooling processes. In the cooling process, both $\langle R_g \rangle$ and $\langle R_h \rangle$ have no peak in the range 35–50 °C and $\langle R_g \rangle / \langle R_h \rangle$ remains nearly a constant, indicating a uniform swelling, as schematically shown in Fig. 5e, very different from the shrinking process. The small dip of $\langle R_g \rangle / \langle R_h \rangle$ at $\sim$ 33 °C indicates that the collapsed PEO chains in the shell are finally swollen back into individual coils on the periphery and the PNIPAM chain backbone in the core has not reached its fully swollen state, as schematically shown in Fig. 14f.

On the other hand, when the PEO content is low, the temperature dependence of $\langle R_g \rangle$, $\langle R_h \rangle$ and $\langle R_g \rangle / \langle R_h \rangle$ has only one transition related to the coil-to-globule transition of the PNIPAM backbone. The transition temperature is close to the LCST ($\sim$ 32 °C) of PNIPAM homopolymer. Moreover, the PEO content has nearly no effect on such a transition. This is expected because when the PEO content is low there is no strong interaction among the PEO chains in the shell. Such a single transition temperature indirectly supports our discussion of the second transition; namely, it is related to the repulsion-induced stretching followed by the clustering-induced collapse of short PEO chains in the shell because the chain density increases as the PNIPAM core shrinks. It was also found that at higher temperatures, the copolymer chains with a low PEO content have a smaller $\langle R_g \rangle$ even though they are longer. The difference further reflects the repulsion-induced stretching of short PEO chains in the shell when the PEO content is higher.

The *n*-clustering-induced stretch and collapse of short PEO chains can be better viewed when they are grafted on a thermally sensitive PNIPAM spherical microgel [34, 70]. In the temperature range 25–35 °C, the microgel can shrink ∼ 3 times in its diameter, i.e., its surface area can decrease ∼ 10 times, providing a convenient way to continuously increase the grafting density because the average number of the PEO chains grafted on each microgel is fixed. The microgels were prepared by dispersion polymerization in aqueous solution at 70 °C, similar to the preparation of amphiphilic PNIPAM-*g*-PEO copolymer chains, but with a proper amount of crosslinking agent, *N*,*N*′-methylenebis(acryl-amide). The core was collapsed and cross-linked at the reaction temperature. The resultant microgels were successively purified by ultra-centrifugation at 40 °C to remove all remaining small molecules. The average grafting density determined by NMR was ∼ 370 PEO chains per microgel, or in other words, each PEO chain occupies ∼ 320 nm^2 at 25 °C.

Figure 16 shows that in the heating-and-cooling cycle, the shrinking-and-swelling of the microgel with short PEO chains grafted on its periphery is completely reversible. It indicates that there was no hysteresis in the process. This is apparently inconsistent with some previous predictions for the grafted PEO chains [71] and also different from the hysteresis observed in the same process for ultra-long PNIPAM homopolymer chains and PNIPAM-*g*-PEO chains [37]. Note that intrachain association of PEO unlikely exists in this case. On the other hand, the collapse of a long chain has a much higher entropy penalty than the shrinking of a microgel. The fact that no hysteresis was observed for the grafted PEO chains can also be attributed to the much shorter chain length (∼ 10^4 g/mol).

As the temperature increases, the PNIPAM core shrinks and the grafting density increases. It is expected that the repulsion would force the PEO-chains on its surface to stretch, i.e., the thickness of the PEO shell (h_{brush})

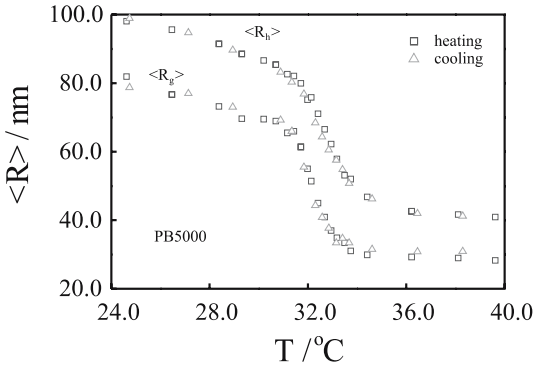

Fig. 16 Temperature dependence of average hydrodynamic radius ($\langle R_h \rangle$) and average radius of gyration ($\langle R_g \rangle$) of PNIPAM microgels grafted with linear PEO chains in the heating-and-cooling cycle, where the dispersion concentration is ∼ 1.0×10^{-5} g/mL [70]

increases, as the grafting density increases. In this way, the PNIPAM core becomes denser, but the PEO shell becomes thicker. Note that the core has ~ 90% of mass so that the shrinking of the core has a more profound effect on $\langle R_g \rangle$, while the stretching of the grafted PEO chains in the shell slows down the decrease of $\langle R_h \rangle$, according to their own definitions. This is why $\langle R_g \rangle / \langle R_h \rangle$ decreases in the range 23–33 °C [34]. When the temperature is higher than ~ 33 °C, $\langle R_g \rangle / \langle R_h \rangle$ starts to increase and finally approaches 0.71 at ~40 °C [71]. As shown in Fig. 16, when $T > \sim 37$ °C, the decrease of $\langle R_g \rangle$ nearly stops, but $\langle R_h \rangle$ still decreases, reflecting that the increase of $\langle R_g \rangle / \langle R_h \rangle$ is attributed to the collapse of the PEO shell. This can be better viewed from the change of the PEO shell thickness.

Figure 17 shows the grafting density dependence of the average thickness of the PEO shell ($\langle h \rangle_{brush}$), i.e., the average height of the grafted PEO chains, where $\langle h \rangle_{brush}$ was obtained by two completely different methods. One is from the difference between the average radii of the microgels with and without the grafted PEO chains; namely, $\langle h \rangle_{brush} = \langle R_h \rangle_{microgel+PEO} - \langle R_h \rangle_{microgel}$. The other is indirectly from the ratio of $\langle R_g \rangle / \langle R_h \rangle$, involving a combination of static and dynamic LLS results. The principle of the second method is outlined as follows. The microgel grafted with the PEO chains can be viewed as a core-shell particle, in which the masses of the core (M_c) and the shell (M_s) are

$$M_c = \frac{4}{3}\pi\rho_c R_c^3 \quad \text{and} \quad M_s = \frac{4}{3}\pi\rho_s \left(R^3 - R_c^3\right) \tag{5}$$

where R_c and R are the radii of the PNIPAM core and the entire microgel; ρ_c and ρ_s are the densities of the core and the shell, respectively. Note that for the first approximation, the shell and the core are assumed to be uniform.

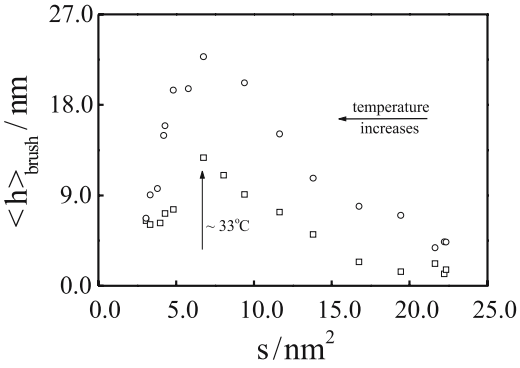

Fig. 17 Dependence of the average PEO brush height ($\langle h \rangle_{brush}$) on the surface area per grafted chain (s), where $\langle h \rangle_{brush}$ was calculated by two different methods. The squares represent $\langle h \rangle_{brush}$ from the difference between the average radii of the PNIPAM microgels with and without the grafted PEO chains; and the circles from the ratio of $\langle R_g \rangle / \langle R_h \rangle$ [70]

In reality, they are not uniform. However, this assumption will not affect our discussion. Also note that no mixing between the grafted PEO layer and the PNIPAM core is assumed. At higher temperatures, the hydrophobic PNIPAM core should not mix with the hydrophilic PEO shell. Even at lower temperatures, it would be more favorable for the PEO chains to stay on the periphery than to penetrate inside the PNIPAM gel network. Substituting Eq. 5 into the definition of R_g leads to

$$R_g^2 = \frac{\int_v \rho(r) r^2 \mathrm{d}v}{\int_v \rho(r) \mathrm{d}v} = \frac{\int_0^{R_c} 4\pi\rho_c r^4 \mathrm{d}r + \int_{R_c}^{R} 4\pi\rho_s r^4 \mathrm{d}r}{\int_0^{R_c} 4\pi\rho_c r^2 \mathrm{d}r + \int_{R_c}^{R} 4\pi\rho_s r^2 \mathrm{d}r}$$

$$= \frac{3\left[M_c R_c^2 R^3 - \left(M_c + M_s\right) R_c^5 + M_s R^5\right]}{5\left(M_c + M_s\right)\left(R^3 - R_c^3\right)}. \quad (6)$$

Letting the mass ratio $M_c/M_s = A$ and the radius ratio $R_c/R = x$, one can rewrite Eq. 2 as:

$$R_g^2 = \frac{3R^2\left[Ax^2 - (1+A)x^5 + 1\right]}{5\left(1 + A/\left(1 - x^3\right)\right.}. \quad (7)$$

Replacing R with R_h, Eq. 7 can be re-arranged as

$$\frac{R_g}{R_h} = \left\{\frac{3\left[Ax^2 - (1+A)x^5 + 1\right]}{5(1+A)\left(1 - x^3\right)}\right\}^{1/2}, \quad (8)$$

where A is a constant for a given PNIPAM microgel grafted with a fixed number of PEO chains. From each measured R_g/R_h in Fig. 16, one can numerically find a corresponding x, and then R_c. In this way, we can determine $\langle h\rangle_{brush}$ from $R - R_c$.

Figure 17 shows that before the temperature reaches its lower critical solution temperature (LCST, $\sim 33\,^{\circ}C$), $\langle h\rangle_{brush}$ increases while the surface area per PEO chain (s) decreases (i.e., the increase of the temperature). The absolute values of $\langle h\rangle_{brush}$ obtained from the two different methods do not quantitatively agree with each other due to experimental uncertainties. Such stretching of the PEO chains is expected because they are forced to approach each other as s decreases. It should be stated that the shell thickness is much smaller than the average radius of the microgels (~ 100 nm) so that the grafted PEO chains can be treated as a quasi-planar brush even if the microgel surface is curved. It is helpful to note that the PEO shell at $23\,^{\circ}C$ is slightly thicker than the hydrodynamic diameter (~ 4 nm) of the PEO macromonomers free in water [72], indicating that the grafted chains are slightly elongated even at the room temperature. One of the possible explanations of the unexpected collapse of the PEO chains in the temperature range

of $T > \sim 33\,^{\circ}\mathrm{C}$ might be related to the formation of an equilibrium between one dilute phase made of stretched chains and one dense phase made of collapsed chains [70, 73].

In general, the hydration has been attributed to the dissolution of PEO in water [74]. It has been shown that the interchain interaction among individual PEO chains is so strong that it is rather difficult to completely dissolve bulk PEO into individual chains in pure water [75, 76]. Nevertheless, water is peculiar due to its structured conformation and could be viewed as a polymeric solvent [77]. A theoretical study of PEO in aqueous solution showed that the pressure could also induce the collapse of the PEO chains [78]. It is known that polymer chains in bulk adopt a random coil conformation. It is our opinion that as the grafting density increases, the grafted chains are pushed together, the PEO chains are gradually dehydrated and most of the water molecules are gradually excluded. Therefore, as the grafted PEO layer becomes "drier" and "drier", it approaches the bulk state, the stretched PEO chains have to collapse at some point. It is similar to the report that in a bad or polymeric solvent, polymer brushes would gradually collapse as more solvent molecules leave the grafted layer and the configuration entropy of the solvent becomes more important [79].

Figure 18 shows that during the stretching, i.e., before reaching $\sim 33\,^{\circ}\mathrm{C}$, the brush height ($\langle h \rangle_{\mathrm{brush}}$) can be scaled to the grafting density (σ) as $\langle h \rangle_{\mathrm{brush}} \propto N\sigma^{1.0\pm0.2}$, where N is the degree of polymerization. The theoretical studies and experimental results in the past showed $\langle h \rangle_{\mathrm{brush}} \propto N\sigma^{\beta}$ with $\beta = 1/3$ for polymer brush in a good solvent [80, 81]. Note that $\sigma^{-1} = s$, which is the average surface area occupied per grafted chain and $\langle h \rangle_{\mathrm{brush}}\sigma^{-1}$ represents the average hydrodynamic volume per grafted PEO chain. Therefore, the scaling of $\langle h \rangle_{\mathrm{brush}} \propto \sigma^{1.0\pm0.2}$ suggests that the average hydrodynamic volume per grafted PEO chain is close to a constant, or in other words, the

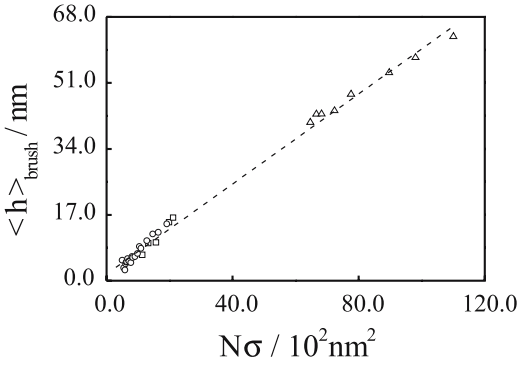

Fig. 18 Grafting density (σ) dependence of average PEO brush height ($\langle h \rangle_{\mathrm{brush}}$) during the PEO chain stretching. The *line* represents a least square fitting of $\langle h \rangle_{\mathrm{brush}} \propto N\sigma^{1.0\pm0.2}$, where N is the degree of polymerization of the grafted chain [70]

average hydrodynamic volume per grafted PEO chain is incompressible during the chain stretching. Further studies of other types of grafted polymer chains are needed to differentiate whether this incompressibility is only related to PEO, or in general, to high grafting chain density.

In order to justify the discussion about the second PEO-related transition in Figs. 12 and 13, the partial heat capacity (C_p) of four PNIPAM-*g*-PEO copolymers with different PEO contents in aqueous solutions was measured using a micro-calorimeter. Figure 19 shows that in the heating process, the peaks located at $\sim 33\,^{\circ}C$ are similar and independent of the PEO content, which can be attributed to the PNIPAM chain backbone. The DSC results agree well with the LLS ones. The second broad peak in the range 40–50 °C gradually disappears when the PEO content becomes lower. Noted that in the US-DSC measurement, both the intra-chain contraction and the inter-chain association are involved because a much higher concentration (10^{-3} g/mL) had to be used to give a sufficiently high signal-to-noise ratio. By investigating both PNIPAM hydrogels and PNIPAM linear chains in water, Laszlo et al. [82] and Ding et al. [83] found two exothermal peaks in the temperature range $\sim$ 30–33 °C in the cooling process when the scanning rate was low and only one endothermic peak in the heating at any scanning rate. They attributed this additional peak to the kinetic effect. In Fig. 19, two peaks, respectively, located at ~ 32 and $\sim 50\,^{\circ}C$ appear in both the heating and cooling.

Around the first transition peak in Fig. 19, the hysteresis is obvious. Such a hysteresis has been attributed to the formation of some additional intra-chain hydrogen bonding in the collapsed state [34]. The second broad peak reveals that the stretching of the grafted PEO chains and further collapse of the PNIPAM chains in the core occur over a wider temperature range. Figure 19 further reveals that the heating and cooling involve a certain amount of endothermic and exothermic heat, respectively. One can define the area

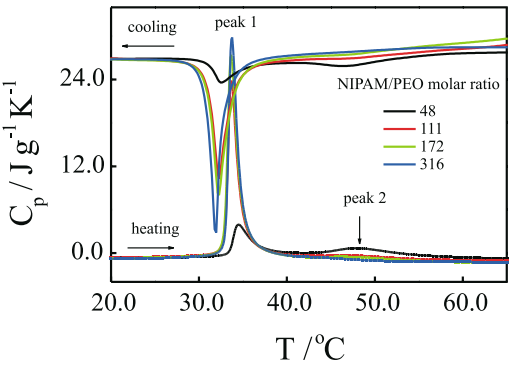

Fig. 19 Temperature dependence of partial heat capacity (C_p) of copolymer chains with different PEO contents in water, where the heating rate is 1.0 °C/min [69]

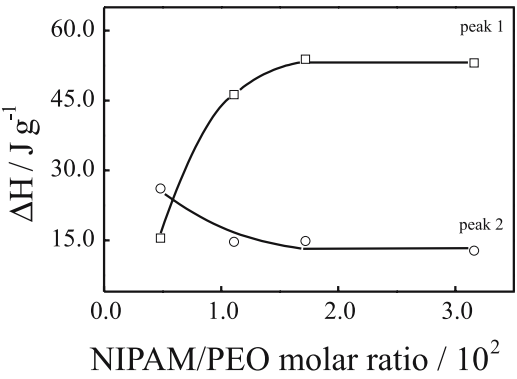

Fig. 20 PEO content dependence of endothermic heats, respectively, for both the transitions in Fig. 19 [69]

under each peak as the total endothermic or exothermic heat (the change of enthalpy ΔH) for each transition.

Figure 20 shows the PEO content dependence of the enthalpy change (ΔH) for the two transitions in Fig. 19. For the copolymer chains with a higher PEO content, the average length of the PNIPAM segment between two grafted neighboring PEO chains is short. This is why the peak at $\sim 33\,^{\circ}C$ related to the PNIPAM segments becomes smaller. On the other hand, when the PEO content decreases, the PNIPAM segments become longer and the PEO shell becomes less crowded so that the peak related to the stretching and collapsing of the grafted PEO chains disappear during the heating process.

3.2.2
Hydrophobically Modified PNIPAM Copolymer Chains

The presence of only a few molar percent of hydrophobic monomer units (stickers) in a hydrophilic polymer chain backbone can sufficiently trigger chain association in water or in a selective solvent to form large insoluble clusters or even a gel, depending on solvency and polymer concentration. The associating copolymers are widely used in industry as viscosity modifiers, colloidal stabilizers and surface-active agents [84–86]. Such copolymer chains can adopt a more complicated conformation in dilute solutions than a corresponding homopolymer. It has been predicted and observed that in a solvent selectively poor for the stickers, the chain can self-fold into a multiflower nanostructure; namely, a number of neighboring stickers undergo intrachain association to form a string of micelle-like flowers along the chain backbone [87–90]. It has also been suggested that the self-folding could lead to a single flower-like core-shell nanostructure with all stickers condensed in the center and short hydrophilic chain segments between stickers swollen like a flower petal (chain loop) [86–88]. It is expected that such a chain fold-

ing may provide a simple model for the study of more complicated problems, such as protein folding and DNA packing.

However, due to experimental difficulties, especially in the sample preparation, few studies have been reported clarifying this point. In most cases, interchain association often occurs with intrachain self-folding, which spoils the study and leads to multi-chain micelles coexisting with single-chain micelles [91, 92]. To our knowledge, only Kikuchi and Nose [93] experimentally studied intrachain micelle formation. They used polystyrene-*g*-poly(methyl methacrylate) to observe the formation of thermodynamically stable single-chain multi-flower structures and revealed that the resultant structure was rigid and on average consisted of ca. five flower-like micelles on each chain, resembling a string of closely packed pearls. Experimentally, the formation of a single flower-like single-chain nanostructure was only reported two years ago by Zhang et al. [94] after successfully preparing long and narrowly distributed PNIPAM-*seg*-St copolymer chains ($M_w = 1.33 \times 10^7$ g/mol and $M_w/M_n < 1.1$) by following the micelle polymerization method developed by Candau et al. [95], and Dowling et al. [96]. On average, each chain had ~ 230 hydrophobic St stickers and each St sticker had ~ 20 styrene monomer units. Note that it is extremely difficult, if not impossible, to characterize the structure (comonomer distribution) of such prepared chains. This still remains a challenging problem in polymer characterization, especially for protein-like amphiphilic chains.

Recently, Cui et al. [97] used single-molecule force spectroscopy (SMFS) developed on the basis of atomic force microscopy (AFM) to measure the length distribution of the PNIPAM segment between two neighboring hydrophobic St stickers. They adsorbed long PNIPAM-*seg*-St copolymer chains on a flat PS surface, as schematically shown in Fig. 21. The flat PS substrate was prepared from a sheet extruder, which was sufficiently smooth for SMFS. The PS segments are so short that the surface can be considered very smooth; i.e., each PS segment was laid flat on the substrate. Before the adsorption, the PS substrate was thoroughly rinsed with ethanol (99.5%) and purified water (> 18 MΩ cm) and then confirmed as a blank sample by SMFS. No obvious force signal was detected during over 1000 cycles of AFM tip's approach and retraction. 0.2 mL PNIPAM-*seg*-PS aqueous solution was then deposited on the PS substrate and left for approximately 12 h to form a thin layer. Afterward, the sample was rinsed with purified water for 1 min to remove loosely adsorbed PNIPAM-*seg*-PS before being measured.

A homemade SMFS with a silicon nitride cantilever (Park, Sunnyvale, CA) was used. Each tip was calibrated by using a standard sample. The spring constants of these cantilevers were in the range 0.010–0.012 N/m. By moving the piezo tube, one could bring the sample into contact with the AFM tip so that some polymer chains were physically adsorbed onto the tip, resulting in a number of "bridges". As the distance between the tip and the substrate increased, the chains were stretched and the elastic force deflected

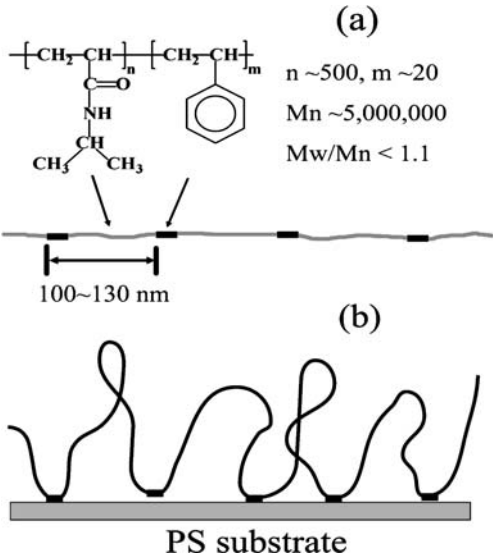

Fig. 21 **a** Schematic of a linear segmented poly(*N*-isopropylacrylamide-*seg*-styrene) (PNIPAM-*seg*-St) coplymer chain prepared by micelle copolymerization, in which short PS segments are relatively evenly distributed on the chain backbone. **b** Schematic of the adsorption of a linear PNIPAM-*seg*-PS chain on a hydrophobic PS substrate in water [97]

the cantilever. A recorded deflection-piezo path curve was converted into a force extension curve. It has been shown that the adhesion force between the tip and the adsorbed chain can be up to a few nano-Newtons in magnitude. Using SMFS, the weak interaction force between the copolymer chain (sticker) and the substrate can be measured. The stretching velocity used by Cui et al. [97] was in the range 520–4600 nm/s. Prior to the force measurement, a drop of purified water, acting as a buffer, was injected between the substrate and the cantilever holder, whereupon both the substrate and the cantilever were immersed in water. The force measurements were performed at 22 °C at which long PNIPAM segments are hydrophilic and soluble in water with a random coil conformation. The details of instrumentation can be found elsewhere [98, 99].

As expected, the adsorption of two insoluble short hydrophobic PS segments onto the PS substrate resulted in many PNIPAM "loops". Figure 22a shows that each force curve exhibits a saw-tooth pattern. To find such a pattern and how it is related to the chain structure, Cui et al. [97] analyzed the distribution of the distance between each two adjacent peaks (teeth) in the force curve, as shown in Fig. 22b. The Gaussian fitting of the histogram led to an average distance of ~ 114 nm. This value is very close to the average length of the "repeat unit" (one long PNIPAM segment plus one short PS segment) in the copolymer chain on the basis of the synthesis condition

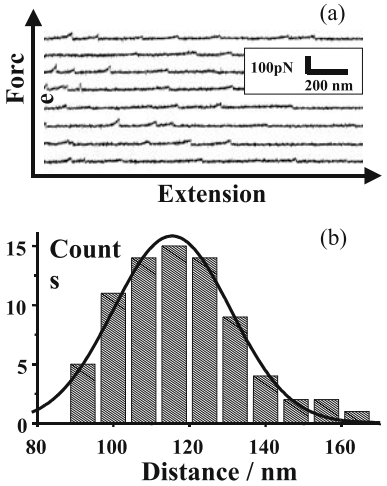

Fig. 22 **a** Measured force curves of linear segmented poly(*N*-isopropylacrylamide-*seg*-styrene) (PNIPAM-*seg*-St) copolymer chains adsorbed on a hydrophobic PS substrate in water. **b** Statistics of the distance between two adjacent peaks in the measured force curves [97]

and NMR characterization. It confirms that styrene comonomer molecules are indeed uniformly distributed on the PNIPAM chain backbone as short segments.

In an LLS study, Zhang et al. [94] dissolved this well-characterized PNIPAM-*seg*-St copolymer in deionized water for 10 days to ensure complete dissolution. The final concentration used was 7.2 E – 7g/mL and it was clarified with a 0.5 μm Millipore Millex-LCR filter to remove dust. Note that in their experiment, the scattering volume ($\sim 10\,\mu$L) still contained 10^5–10^6 copolymer chains so that the number of density fluctuations was not a problem even in such a dilute solution. Their original objective was to determine whether such a copolymer chain could self-fold into the predicted single-flower-like core-shell nanostructure.

Figure 23 shows that the slope of $KC/R_{vv}(q)$ vs. q^2 sharply decreases as the temperature increases. It is known in LLS that the slope of each line is related to $\langle R_g \rangle$ of polymer chains. The decrease of $\langle R_g \rangle$ indicates shrinking of the chains. Such a shrinking can be viewed directly in terms of the shift of the hydrodynamic radius distribution $f(R_h)$ from ~ 124 nm to ~ 31 nm, as shown in the inset of Fig. 23, where $f(R_h)$ was calculated from the digital time correlation function measured in dynamic LLS. On the other hand, the extrapolation to $q \to 0$ leads to M_w since the copolymer concentration is extremely low. The same intercept clearly reveals no change in M_w, i.e., no interchain association. Therefore, the shrinking of the chains with increasing temperature is purely a single chain (intrachain) process. The plot of $qR_{vv}(q)/KC$ versus $q\langle R_g \rangle$ reveals the increase of the chain segment density at higher temperatures.

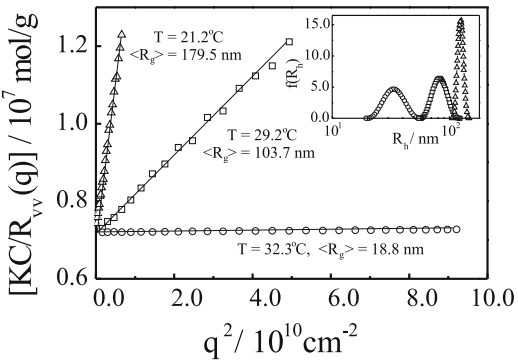

Fig. 23 Angular dependence of Rayleigh ratio ($R_{vv}(q)$) of segmented PNIPAM-*seg*-St copolymer chains in water measured from static LLS, where K is a constant, q is the scattering vector and polymer concentration (C) was 7.2×10^{-7} g/mL. The *inset* shows the temperature dependence of the hydrodynamic radius distribution $f(R_h)$ determined from dynamic LLS [94]

Figure 24 shows that both $\langle R_g \rangle$ and $\langle R_h \rangle$ decrease as the temperature increases. Each data point was obtained only after the solution had reached thermodynamically equilibrium and the measured value was stable. Note that in each curve there exists a small kink at $\sim 29.4\,^{\circ}$C and that $\langle R_g \rangle / \langle R_h \rangle$ remains constant at ~ 1.15 in the range 29–30.6 °C, representing an additional transition prior to the collapse of the PNIPAM chain segments. The decreases of both $\langle R_g \rangle$ and $\langle R_h \rangle$ after the kink become faster. As shown before, the coil-to-globule transition of PNIPAM homopolymer chains do not present such a "kink" [32–34, 37–40]. The sharp decrease of $\langle R_g \rangle / \langle R_h \rangle$ from ~ 1.5 to ~ 0.6 in the inset confirms the coil-to-globule transition of individual copolymer chains. However, a careful examination of Fig. 24 raises a number of questions.

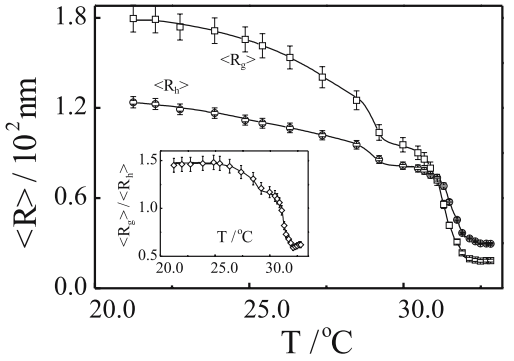

Fig. 24 Temperature dependence of *z*-average root-mean square radius of gyration $\langle R_g \rangle$ and average hydrodynamic radius $\langle R_h \rangle$ of PNIPAM-*seg*-St copolymer chains in water; the *inset* shows the temperature dependence of the ratio of $\langle R_g \rangle / \langle R_h \rangle$ [94]

The first question concerns the association of the stickers: do they associate into a string of micelle-like flowers or as one core-shell-like flower? If a string of flowers were formed, the overall chain structure would become more rigid and, hence, $\langle R_g \rangle / \langle R_h \rangle$ should increase. In addition, these micelle-like flowers would collapse and pack together at higher temperatures to form a uniform globule. In contrast, if only one micelle-like flower was formed, the hydrophobic stickers would condense in the center so that the resultant globule should have a core denser than the shell. According to the definitions of $\langle R_g \rangle$ and $\langle R_h \rangle$, a hard sphere with a denser core has a smaller $\langle R_g \rangle$ than a uniform sphere with the same size, but the density distribution has no effect on $\langle R_h \rangle$. In Fig. 22, the ratio $\langle R_g \rangle / \langle R_h \rangle$ decreases from ~ 1.5 to ~ 1.1 in the range 25–29.8 °C, and at higher temperatures, becomes much smaller than 0.774. As discussed earlier, the lower value of $\langle R_g \rangle / \langle R_h \rangle$ indicates a core-shell structure. They also measured the ratios of $\langle R_g \rangle / \langle R_h \rangle$ for surfactant-free polystyrene nanoparticles before and after grafting a layer of linear polymer chains. The decrease of $\langle R_g \rangle / \langle R_h \rangle$ from ~ 0.8 to ~ 0.6 was due to the hydrodynamic draining of the grafted layer [100]. As discussed before, the lower values of $\langle R_g \rangle / \langle R_h \rangle$ reflects a core-shell structure with a dense core, presumably, made of the hydrophobic styrene stickers.

The second question is related to the existence of an additional transition at ~ 29.4 °C. As expected, hydrophobic styrene stickers tend to associate in water. At lower temperatures, water is such a good solvent for PNIPAM that the copolymer chain adopts a random coil conformation. The movements of the stickers are also random and not correlated to each other because the PNIPAM segments randomly fluctuate in solution. As the temperature increases in the range 25–30.6 °C, the solvency of water for PNIPAM gradually decreases and the hydrophobic stickers tend to gather towards the chain center and to move in a more correlated fashion. Since water is not a poor solvent yet, the PNIPAM chain backbone is still in its swollen and coiled state, reflected in the fact that the decrease of $\langle R \rangle$ in Fig. 24 is only $\sim 30\%$. In order to distinguish such a chain conformation from a normal random coil, it was named an "ordered coil".

Figure 25 schematically shows such a conformation transition from the random coil to the ordered coil. As the temperature approaches ~ 30.6 °C (the Flory Θ-point), the stickers start to gather towards the center and each PNIPAM chain segment between two neighboring stickers forms a flower petal (loop). The overall chain conformation becomes flower-like. Further increase of the temperature leads to the condensation of all the stickers to form a core and the shrinking of the PNIPAM loops in the shell, resulting in a collapsed core-shell nanostructure. To confirm the existence of two such different transitions, Zhang et al. [94] carried out a thermal analysis of the copolymer aqueous solution using a Micro-calorimeter (MicroCal Inc, USA) with a heating rate of 0.5 °C/min and a response time of 5.6 s.

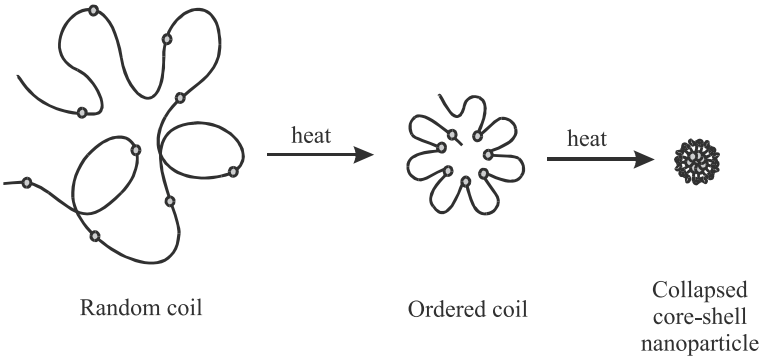

Fig. 25 Schematic of transitions of chain conformation of a segmented copolymer chain with stickers in dilute solution from a random coil to an "ordered coil" and then from an "ordered coil" to a collapsed core-shell globule as the solvency of water for the PNIPAM chain backbone decreases [94]

Figure 26 shows that for the PNIPAM homopolymer, the endotherm of the transition is slightly skewed towards the high temperature side, whereas the endotherm of a solution of PNIPAM-*seg*-St is abnormally skewed towards the low temperature side, and surprisingly, the transition occurs at a higher temperature. This is because copolymerizing hydrophobic comonomers into PNIPAM should decrease its shrinking temperature. Figure 26 shows that for a random NIPAM and styrene copolymer with a comonomer composition similar to the PNIPAM-*seg*-St copolymer used, the endotherm of the PNIPAM-*co*-St solution has the normal skew and is indeed shifted to lower temperatures in comparison with the PNIPAM homopolymer solution. Considering the kink in Fig. 26, one has to attribute the abnormal skew to a transition, which involves a small amount of energy, prior to the shrinking of PNIPAM.

The inset in Fig. 26 shows that the endotherm related to the collapse of the segmented copolymer can indeed be de-convoluted into two peaks. A small peak appears $\sim 1.2\,^{\circ}\mathrm{C}$ before the homopolymer peak. It is ascribed to the transition from the random coil to the ordered coil, while the large peak is related to the collapse of the PNIPAM chain backbone. Note that in comparison with the transition temperatures obtained in LLS, all the peak temperatures in DSC were ca. $1\,^{\circ}\mathrm{C}$ higher. This is because the transitions in DSC were slightly behind the temperature scanning, while the measurement in LLS could be considered as an infinitely slow scanning. Therefore, the small peak in DSC corresponds well with the kink in LLS. Also note that the collapse temperature of the short PNIPAM chain segments, the flower petals, is $\sim 0.6\,^{\circ}\mathrm{C}$ higher than that of long PNIPAM homopolymer chains. This could be ascribed to the chain length dependence of the phase transition temperature and also to the fact that the collapse of those small PNIPAM petals (loops) has to overcome an additional internal stress.

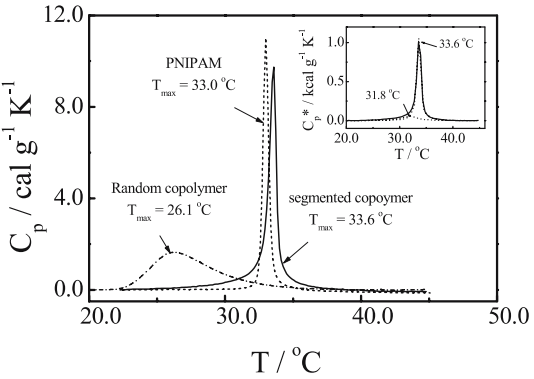

Fig. 26 Temperature dependence of partial heat capacity (C_p) of PNIPAM homopolymer, PNIPAM-*co*-St (4.1 mol %) random copolymer and NIPAM-*seg*-St (3.9 mol %) segmented copolymer in water; the polymer concentration was 1.0 g/L and the heating rate was 0.5 °C/min. The *inset* shows the de-convolution of stand partial heat capacity (C_p^*) of PNIPAM-*seg*-St [94]

4
Ionomers—From Intrachain Folding to Interchain Association

By definition, ionomers are copolymers with a few molar percent ionic groups inserted on their chain backbones. The solubility of ionomers in water mainly depends on the chemical nature of the chain backbone. For example, polystyrene ionomers are insoluble in water and poly(acrylamide) ionomers are completely soluble in water in the temperature range 0–100 °C. Water-insoluble ionomers have been extensively studied and reviewed and these reviews can be easily found in the literature. Hereafter we will discuss only ionomers soluble in water.

4.1
PNIPAM-*co*-KAA Copolymer Chains

PNIPAM has been anionically and cationically modified for different applications. Normally, such prepared copolymers are still thermally sensitive, just like PNIPAM, in water as long as its ionic content is not too high. PNIPAM ionomers generally have a higher LCST than PNIPAM homopolymers. In principle, they could be considered as one special example of hydrophilically modified PNIPAM chains as we described in Sect. 3.2.1. However, we like to review it as a special group of amphiphilic copolymers. This is because hydrophilic ionic groups have a much longer electrostatic interaction range in pure water than hydrophilic neutral groups. In other words, each ionic group can stabilize a larger surface area and play a stronger stabilization role when the PNIPAM chain backbone becomes hydrophobic at higher temperatures.

Using PNIPAM ionomers as a bridge, we will shift our discussion from the folding of individual copolymer chains in extremely dilute solutions to the formation of the mesoglobular phase of hydrophilically and hydrophobically modified copolymer chains in dilute solutions. The synthesis of PNIPAM-*co*-*x*KAA ionomers has been described before.

Figure 27 shows that for four different PNIPAM-*co*-0.8KAA concentrations, $R_{vv}(\theta)/KC$ of each solution remains nearly a constant ($\sim 4–5 \times 10^6$ g/mol) in the range 25–32 °C, very close to the average molar mass of individual PNIPAM-0.8KAA chains, indicating that there was no interchain aggregation [101]. When the temperature is raised to $\sim$ 32.5–33 °C, slightly higher than the LCST of PNIPAM, $R_{vv}(\theta)/KC$ abruptly increases when the solution concentration is higher than $\sim 10^{-5}$ g/mL, clearly indicating interchain association. Further increase of the solution temperature to $\sim$ 34–35 °C, leads $R_{vv}(\theta)/KC$ to a plateau, indicating that interchain association stops. From the ratio of $[R_{vv}(\theta)/KC]_{T=45\,^\circ C}/[R_{vv}(\theta)/KC]_{T=25\,^\circ C}$, the average number of the chains inside each aggregate (N_{chain}) can be estimated. The values of N_{chain} are $\sim$ 17, $\sim$ 8 and $\sim$ 4, respectively, for $C = 5.0 \times 10^{-4}$, 1.0×10^{-4} and 9.5×10^{-6} g/mL. For the lowest concentration (4.7×10^{-6} g/mL), $R_{vv}(q)/KC$ is independent of temperature. Note that $R_{vv}(q)$ is proportional to the square of the molar mass of the scattering objects, i.e., a dimer scatters four times more light than an unimer. A trace amount of interchain association can lead to a large increase in $R_{vv}(\theta)/KC$. The temperature independence of $Rvv(q)/KC$ indicates no interchain association in such an extremely dilute solution even at temperatures as high as 45 °C. This is very different from the folding of individual PNIPAM homopolymer chains. First, single-homopolymer chain globules are not stable at very high temperature. Second, it is much more difficult to induce the coil-

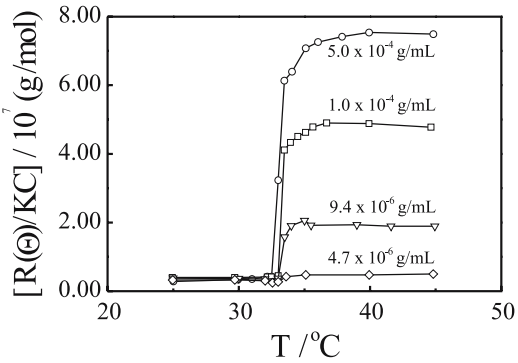

Fig. 27 Temperature and concentration dependence of the excess scattering intensity $R_{vv}(\theta)/KC$ of PNIPAM-0.8KAA in deionized water, where K is a constant, and $R_{vv}(\theta)/KC$ approximately equals the weight-average molar mass (M_w) because the solution is very dilute [101]

to-globule transition of homopolymer chains in a real experiment without any interchain association. We will come back to discuss this point later.

Figure 28 shows that in the most dilute solution, $\langle R_h \rangle$ decreases as the solution temperature increases, reflecting the intrachain coil-to-globule transition because we know from Fig. 27 that in this solution there is no interchain association in the heating process. This is similar to the collapsing process observed for a neutral PNIPAM homopolymer chain in an extremely dilute solution [32–34, 37–41]. However, we have to note that the ionomer chains used here are broadly distributed with a polydispersity index of $M_w/M_n = 1.6–1.7$ in comparison with those ($M_w/M_n < 1.1$) used in the study of the folding of individual PNIPAM homopolymer chains, which makes the experiment much easier. This is due to the stabilization role of ionic groups. The decrease of $\langle R_h \rangle$ can be divided into three stages. In the low temperature range (25–32 °C), water progressively changes from a good solvent to a poor solvent, resulting in slight contraction of the PNIPAM chain with a slightly smaller $\langle R_h \rangle$. Around the phase transition temperature (32–35 °C), the PNIPAM chain backbone undergoes the coil-to-globule transition so that $\langle R_h \rangle$ rapidly decreases. Finally, at temperatures higher than $\sim$ 35 °C, the PNIPAM chain backbone reaches its fully collapsed globule state so that further increase of the solution temperature has little effect on $\langle R_h \rangle$.

In the solution with a higher concentration, interchain association accompanies intrachain contraction. When interchain association is dominant, $\langle R_h \rangle$ increases as the temperature increases, leading to a peak in the temperature range of 32–35 °C. At higher temperatures, $R_{vv}(q)/KC$ stops to increase at $\sim$ 34 °C, as shown in Fig. 27, and reflects the end of interchain association. Therefore, the decrease of $\langle R_h \rangle$ at temperatures higher than $\sim$ 34 °C is related to further collapse of the PNIPAM chain backbones inside each aggregate. Besides $\langle R_g \rangle$ and $\langle R_h \rangle$, a combination of static and dynamic LLS results can also lead to other microscopic parameters of these stable interchain aggre-

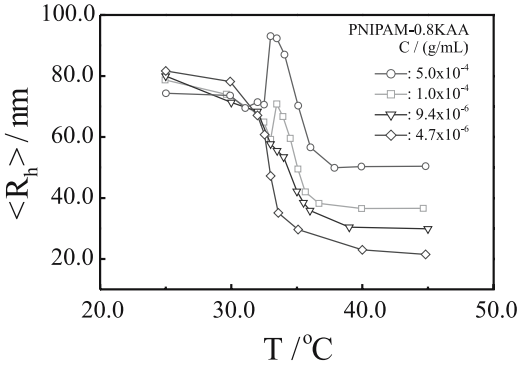

Fig. 28 Temperature and concentration dependence of the average hydrodynamic radius $\langle R_h \rangle$ of PNIPAM-0.8KAA in deionized water [101]

gates at $\sim 34\,^{\circ}$C, such as the weight average molar mass ($M_{w,\,\mathrm{agg}}$), the average number of copolymer chains inside each aggregate ($\langle N\rangle_{\mathrm{agg}}$), the average surface area per ionic group ($\langle S\rangle_{\mathrm{ionic}}$), the average hydrodynamic volume of each polymer chain inside ($\langle V\rangle_{\mathrm{chain}}$) and the average chain density ($\langle\rho\rangle$) defined as $M_{w,\,\mathrm{agg}}/(4\pi\langle R_{\mathrm{h}}\rangle^3 N_{\mathrm{A}}/3)$. Table 1 summarizes these microscopic parameters.

It is worth noting that at 34 °C the aggregates formed in different solutions have a similar $\langle V\rangle_{\mathrm{chain}}$ and $\langle\rho\rangle$. It indicates that at a given temperature the average degree of the shrinking of the polymer chains is similar in spite of the fact that each interchain aggregate contains different numbers of chains, in other words, interchain association has nearly no effect on intrachain contraction. Conventional wisdom tells us that interchain association should retard intrachain contraction. However, the results in the table above clearly reveal that intrachain contraction (the coil-to-globule transition) and interchain association are two *independent* and *competing* processes. This is important information.

In the fully collapsed state (45 °C), $\langle R_{\mathrm{g}}\rangle/\langle R_{\mathrm{h}}\rangle$ is in the range 0.73–0.84, indicating that the aggregates behave like uniform solid spheres without any draining. Note that this is different from single-chain core-shell structures made of PNIPAM-*g*-PEO copolymers. The average density $\langle\rho\rangle$ of the aggregates decreases as the aggregation number $\langle N\rangle_{\mathrm{agg}}$ decreases. It can be attributed to the imperfect packing of the copolymer chains inside each aggregate when only a few chains are packed inside each aggregate because the chain backbone is not infinitely flexible and the intrachain wrapping inside each aggregate results in a larger free volume in comparison with interchain wrapping [102]. When $\langle N\rangle_{\mathrm{agg}} > 8$, $\langle\rho\rangle \sim 0.34\,\mathrm{g/cm^3}$, similar to the value of the aggregates made of neutral PNIPAM homopolymer chains [103, 104]. For single-chain globules formed in the extremely dilute solution, $\langle\rho\rangle \sim 0.2\,\mathrm{g/cm^3}$, slightly lower than that made of a single PNIPAM homopolymer chain [32, 33], indicating that the ionic groups are on the periphery of the aggregate and have nearly no effect on the coil-to-globule transition of the PNIPAM chain backbone. The slightly lower density can be attributed to the ionic groups on the periphery, which leads to a slightly larger $\langle R_{\mathrm{h}}\rangle$ because of the hydration of ionic groups.

Table 1 Light-scattering results of PNIPAM-0.8KAA aggregates, respectively, formed at 34 and 45 °C

			34 °C				45 °C		
C g/mol	$M_{w,\mathrm{agg}}$ 10^7 g/mol	$\langle N\rangle$	$\langle R_{\mathrm{h}}\rangle$ nm	$\langle S\rangle_{\mathrm{ionic}}$ nm^2	$\langle V\rangle_{\mathrm{chain}}$ 10^5 nm^3	$\langle N\rangle_{\mathrm{agg}}$	$\langle R_{\mathrm{h}}\rangle$ nm	$\langle R_{\mathrm{g}}\rangle/\langle R_{\mathrm{h}}\rangle$	$\langle\rho\rangle$ g/mol^3
5.0×10^{-4}	7.68	17	87	17.8	1.62	17	87	0.78	0.34
1.0×10^{-4}	3.88	8	68	20.9	1.64	8	68	0.73	0.34
9.4×10^{-6}	1.86	4	54	26.3	1.64	4	54	0.75	0.28
4.7×10^{-6}	4.97	1	35	49.1	1.80	1	35	0.84	0.20

We can reasonably paint the following picture. During the coil-to-globule transition, the PNIPAM chain backbone, more precisely, the segments between two neighboring ionic groups, collapse and associate with each other, while all the ionic groups stay on the periphery of each resultant aggregate to act as stabilizers. As the chain association proceeds, the average number of ionic groups on each resultant particle should be proportional to the mass of the aggregate (M_{agg}) or the cubic of the size ($\langle R_h \rangle^3$) if we assume that the aggregates have a uniform chain density. On the other hand, the average surface area of the aggregate is only proportional to the square of the size ($\langle R_h \rangle^2$) or $M_{agg}^{2/3}$. Therefore, the surface area per ionic group is reversibly proportional to $\langle R_h \rangle$, i.e., $\langle R_h \rangle^{-1}$ or $M_{agg}^{-1/3}$. This means that $\langle S \rangle_{ionic}$ should decrease as the chain association proceeds. At the same time, the intrachain coil-to-globule transition also leads to the decrease of $\langle S \rangle_{ionic}$.

Figure 29 shows a sharp decrease of $\langle S \rangle_{ionic}$ in the temperature range of 32.5–33 °C, which exactly corresponds to the interchain association (the increase of $R_{vv}(\theta)/KC$) in Fig. 25 and the peak position of $\langle R_h \rangle$ in Fig. 26). Logically, there is a minimum value of $\langle S \rangle_{ionic}$, at which the surface of each aggregate is "fully covered" by ionic groups so that further chain association becomes impossible because of long-range electrostatic repulsion. However, the intrachain coil-to-globule transition inside the aggregates continues. This is exactly why $\langle R_h \rangle$ in Fig. 26 first increases and then decreases, but $\langle S \rangle_{ionic}$ in Fig. 29 only decreases. It is worth noting that for aggregates with different sizes formed in different solutions, $\langle S \rangle_{ionic}$ approaches a similar value at high temperatures. This is reasonable because for a given colloidal system, or more precisely, an interface (here this is water/collapsed PNIPAM), the surface area occupied per stabilizer should be a constant, independent of the particle size, if we consider that the process is thermodynamically controlled. This point has already been experimentally demonstrated with different systems, such as micro-emulsion [105–107] and the formation of various surfactant-free

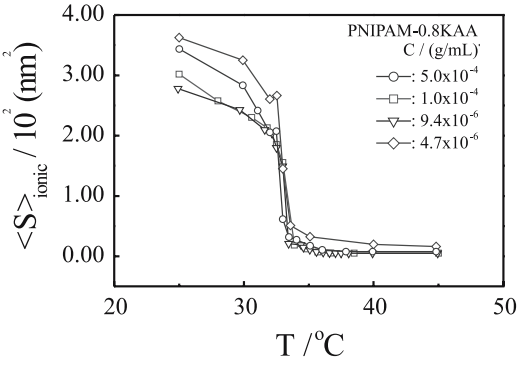

Fig. 29 Temperature dependence of the average surface area $\langle S \rangle_{ionic}$ per ionic group on the PNIPAM-0.8KAA aggregates, where $\langle S \rangle_{ionic}$ is defined as $4\pi \langle R_h \rangle^2 / \langle N \rangle_{ionic}$ [101]

polymeric nanoparticles [108–112]. Therefore, $\langle S \rangle_{\text{ionic}}$ is a fundamental parameter governing the final size of the chain aggregates.

As expected, increasing the ionic content generally resulted in smaller aggregates [101], but the competition between intrachain contraction and interchain association have a similar effect in this aspect, because for PNIPAM ionomers with a higher ionic content, it requires a much lower degree of aggregation to reach the same minimum value of $\langle S \rangle_{\text{ionic}}$. For PNIPAM-4.5KAA in an extremely dilute solution ($C = 5.0 \times 10^{-6}$ g/mL), only intrachain contraction (the coil-to-globule transition) occurs. Figure 30 shows that $\langle R_h \rangle$ returns to the starting point when the solution was cooled to 25 °C, indicating that the solution returns to its initial state in which only individual ionomer chains exist. On the other hand, the heating rate independence of $\langle R_h \rangle$ at 45 °C implies that the solution at 45 °C reaches a thermodynamic equilibrium state. However, near the coil-to-globule transition temperature (32–34 °C), the values of $\langle R_h \rangle$ in the heating and cooling processes are different at the same temperature. The hysteresis is similar to the folding of PNIPAM homopolymer chains. It can be attributed to some intrachain hydrogen bonding formed in the collapsed globular state, which persists around the Θ-temperature in the cooling process because water is still a very good solvent. This is why $\langle R_h \rangle$ is smaller. When the temperature is lower than 25 °C, water becomes such a good solvent that all intrachain association is destroyed and $\langle R_h \rangle$ returns to its initial value before the heating.

In principle, intrachain contraction should occur before interchain association as long as the solution is sufficiently dilute. The limitation is the sensitivity of our detection in laser light scattering. Note that in Fig. 27,

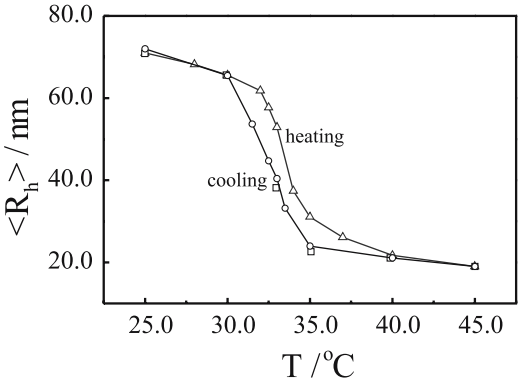

Fig. 30 Temperature dependence of $\langle R_h \rangle$ of a dilute PNIPAM-4.5KAA solution ($C = 5.0 \times 10^{-6}$ g/mL) respectively in slow heating and cooling processes, □ represents that the solution was jumped from 25 to 45 °C by a single step and then slowly cooled to each measurement temperature; △ and ○ represent that the solution was slowly heated to each measurement temperature from 25 °C to 45 °C and then slowly cooled to each measurement temperature. Every data point was obtained after the system reached its equilibrium [101]

temperature-induced intrachain contraction and interchain association simultaneously occurs when the concentration is slightly higher. However, the processes are so fast that one cannot distinguish the two processes even in dilute solutions. In the lowest concentration, only intrachain contraction occurs and ionic groups on the periphery stabilize single-chain collapsed globules. It would be ideal to find a system where under proper experimental conditions the evolution from intrachain contraction to interchain association could be observed. The following is an example.

4.2 PAM-*co*-NaAA Copolymer Chains

It is known that certain metal ions like Ca^{++} can specifically interact with carboxylic groups. If carboxylic groups are attached to a polymer chain backbone, such as partially hydrolyzed poly(acrylamide) (HPAM), the COO^-/Ca^{++} interaction could lead to intrachain contraction and interchain association through the polyion/metal "complexation" [113]. Flory and Osterheld [114] showed, as early as 1954, that Ca^{++} ions could change the chain conformation. Ohmine et al. [115] and Ben Jar et al. [116] studied the effects of monovalent and divalent cations on the collapsing of HPAM. Moreover, a few mechanistic models have been used to describe the aggregation of polyelectrolyte chains [117–119]. Michaeli [120] interpreted the aggregation as a function of the ionization degree and of the inert monovalent electrolyte concentration in terms of a stoichiomeric complex between divalent cations and anionic groups.

The aggregation kinetics have also been extensively studied [121]. The recent observation of fractal structures of the polymer clusters has sparked a renewed interest in aggregation kinetics [122]. Two distinct aggregation kinetic processes have been proposed and investigated. One is the diffusion-limited cluster aggregation (DLCA) controlled by the time taken for two clusters to collide via Brownian diffusion [123, 124]; and the other is the reaction-limited cluster aggregation (RLCA) in which the probability of forming a bond upon collision of two clusters is so high that the aggregation rate is chemically limited by its reaction rate. The RLCA has been observed in several colloid systems and modeled by computer simulation [125–128]. In general, the fractal dimension d_f is defined as: $M \sim R^{d_f}$, where M is the molar mass and R is the cluster size [124]. In RLCA, $d_f \sim 1.55$ and ~ 2, respectively, in 2-dimensional and hierarchical 3-dimensional simulations. The experimental values of d_f for the clusters formed in RLCA were $\sim 2.1 \pm 0.1$. Ball et al. [129] pointed out that in RLCA, the slightly larger experimental d_f values were due to the cluster's polydispersity.

Peng et al. [130] used the complexation of the HPAM chains in $CaCl_2$ aqueous solution to investigate the complexation-induced transition from intrachain contraction to interchain association over a wide range of the hydrolysis degrees and Ca^{++} concentrations as well as the structure of the HPAM/Ca^{++}

complexes. They hydrolyzed PAM homopolymer in an aqueous solution (10% NaOH + 10% $NaCO_3$) at 60 °C [131]. The hydrolysis degree (HD%) is controlled by the reaction time. The hydrolysis degree can be determined by titration with a 0.10 N HCl standard solution [132]. The complexation was induced by adding dropwise a proper amount of dust-free $CaCl_2$ aqueous solution into ~ 2 mL of dust-free HPAM aqueous solution. The initial concentration of the HPAM solution was kept at 1.00×10^{-5} g/mL. All the HPAM solutions used in LLS were clarified with a 0.5 μm Millipore filter and the $CaCl_2$ aqueous solution was clarified with a 0.1 μm Whatman filter (Anotop 25) to remove dust.

Figure 31 shows the kinetics of the complexation between HPAM/Ca^{++} in terms of the change of $\langle R_h \rangle$ for five different HPAM samples in a given $CaCl_2$ aqueous solution. For each HPAM sample, $\langle R_h \rangle$ approaches a plateau $\langle R_h \rangle_{max}$. As expected, $\langle R_h \rangle_{max}$ decreases with the hydrolysis degree. Note that there exists an initial stage in which $\langle R_h \rangle$ decreases, that reveals intrachain complexation in which individual chains contract before interchain association. For HPAM5, interchain complexation is dominant and initial intrachain contraction is too short to be observed, while for HPAM1, intrachain complexation becomes so dominant that there is no increase of $\langle R_h \rangle$. As for HPAM2, HPAM3 and HPAM4, the transition from *intrachain* to *interchain* is fairly clear. Figure 31 also reveals that for a given Ca^{++} concentration, the complexation-induced interchain association is directly related to the hydrolysis degree. This is because the carboxylic groups on the chain backbone act as "stickers" to "glue" different chains together, similar to the results of the PMA/Ca^{++} system reported by Yuko et al. [133].

Figure 32 shows the Ca^{++} concentration dependence of $\langle R_h \rangle_{max}$ for five different HPAM samples. The inset shows an enlargement of the low [Ca^{++}] range in which $\langle R_h \rangle_{max}$ first decreases as [Ca^{++}] increases, indicating the complexation-induced intrachain contraction. Further increase of Ca^{++} con-

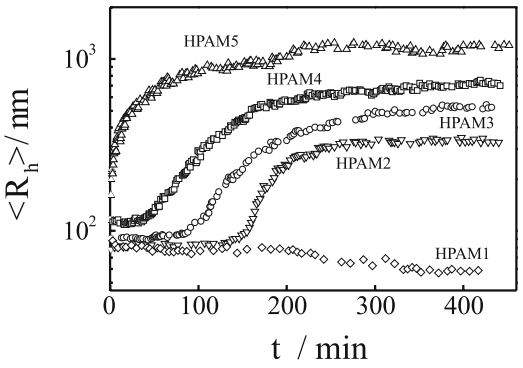

Fig. 31 Time dependence of average hydrodynamic radius ($\langle R_h \rangle$) of the HPAM/Ca^{++} complexes for complexation of HPAM chains in 0.08 M $CaCl_2$ aqueous solution [130]

centrations leads to a sharp increase of $\langle R_h \rangle$, revealing the complexation-induced transition from intrachain contraction to interchain association. The results in Figs. 31 and 32 reveal that the complexation between the HPAM chains in $CaCl_2$ aqueous solution can be dominated by either intrachain or interchain interaction, depending on both the hydrolysis degree and Ca^{++} concentration. The complexation can be viewed as follows. Each HPAM is a long coil chain with hundreds of "stickers" ($-COO^-$). Two "stickers" and one Ca^{++} ion can be driven thermodynamically together to form one $(-COO)_2Ca$ complex point. These interchain "points" result in the clustering of the HPAM chains and they further collide with each other or with individual HPAM chains, leading to larger clusters. Finally, when either Ca^{++} ions or $-COO^-$ groups are consumed, the complexation stops. In the process, clusters with different sizes were formed. Note that the *intrachain* $-COO^-$ groups are closer than those *interchain* $-COO^-$ groups in a dilute solution. For the HPAM chains with a low hydrolysis degree in a low Ca^{++} concentration, intrachain complexation is expected to be easier; while for a higher hydrolysis degree and a higher Ca^{++} concentration, interchain complexation becomes dominant. In the middle range of $[Ca^{++}]$ and $[-COO^-]$, individual HPAM chains first undergo intrachain complexation through the neighboring carboxylic acid groups on the same chain before interchain complexation becomes apparent.

Figure 33 shows double logarithmic plots of M_w versus $\langle R_h \rangle$ of HPAM/Ca^{++} complexes for a given HPAM sample but different Ca^{++} concentrations. Figure 34 shows double logarithmic plots of M_w versus $\langle R_h \rangle$ for a given Ca^{++} concentration but different HPAM samples, where the values of M_w were calculated from the measured Rayleigh ratio on the basis of Eq. 1. Note that the ratio of $\langle R_g \rangle / \langle R_h \rangle$ nearly remains a constant of ~ 1.35 in the measurable range of $\langle R_g \rangle$. Figures 33 and 34 clearly reveal that M_w can be scaled to $\langle R_h \rangle$ as $M_w \propto \langle R \rangle^{2.11 \pm 0.04}$ for different Ca^{++} concentrations and different HPAM

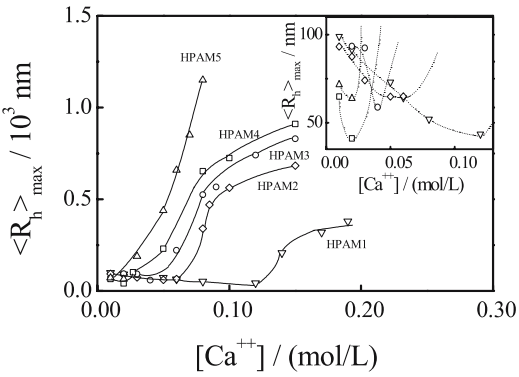

Fig. 32 Ca^{++} concentration dependence of the maximum average hydrodynamic radius $\langle R_h \rangle_{max}$, where $\langle R_h \rangle_{max}$ is the plateau value as shown in Fig. 31 [130]

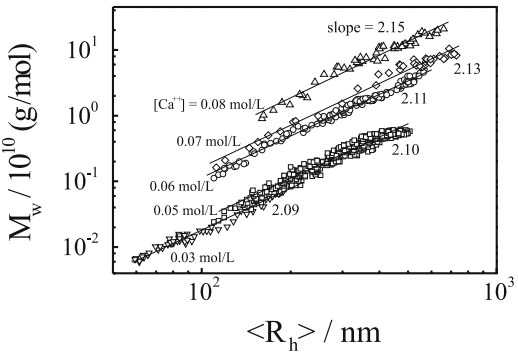

Fig. 33 Double logarithmic plots of weight average molar mass (M_w) vs. average hydrodynamic radius $\langle R_h \rangle$ for the HPAM5 chains in the presence of different amounts of Ca^{++} ions [130]

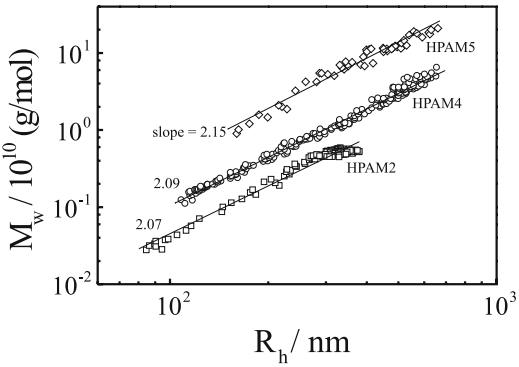

Fig. 34 Double logarithmic plots of weight average molar mass (M_w) vs. hydrodynamic radius $\langle R_h \rangle$ for different HPAM samples in 0.08 M $CaCl_2$ aqueous solution [130]

samples. This suggests that the HPAM/Ca^{++} complexes have a fractal structure with a dimension of $d_f = 2.11 \pm 0.04$, which is in good agreement with the value predicated for RLCA [134, 135].

5
Formation of a Stable Mesoglobular Phase in Dilute Solutions

The above discussion clearly shows that the increase of anionic copolymer concentration or the strength of chain interaction can lead to a transition from intrachain contraction to interchain association. It can result in a mesoglobular phase in which a limited number of copolymer chains are associated together to form polymeric colloidal particles stable between microscopic single-chain globular phase and macroscopic phase separation (precipitation). It is not a surprise to see the formation of such stable mesoglob-

ules because ionic groups on the periphery have strong electrostatic repulsion to prevent further aggregation. Note that such long-range electrostatic interaction is difficult to handle in theory. In literature, the formation of stable mesoglobules made of neutral copolymer chains without any stabilizer has also been predicted [136–138]. It also should be noted that the effect of comonomer composition on chain association has not been systematically investigated. This is partially because it requires some challenging synthesis to control the comonomer composition.

5.1 Effect of Comonomer Composition

Recently, Siu et al. [139] studied the effect of comonomer composition on the formation of the mesoglobular phase of amphiphilic copolymer chains in dilute solutions. The copolymer used was made of monomers, *N*,*N*-diethylacrylamide (DEA) and *N*,*N*-dimethylacrylamide (DMA). Like PNIPAM, PDEA is also a thermally sensitive polymer with a similar LCST, but PDMA remains water-soluble in the temperature range (< 60 °C) studied. At room temperature, copolymers made of DMA and DEA are hydrophilic, but become amphiphilic at temperatures higher than ~ 32 °C. Before the association study, each P(DEA-*co*-DMA) copolymer was characterized by laser light scattering to determine its weight average molar mass (M_w) and its chain size ($\langle R_g \rangle$ and $\langle R_h \rangle$). The copolymer solutions (6.0×10^{-4} g/mL) were clarified with a 0.45 μm Millipore Millex-LCR filter to remove dust before the LLS measurement.

Figures 35 and 36 reveal that for each copolymer studied, the average aggregation number (N_{agg}) and average hydrodynamic radius ($\langle R_h \rangle$) of polymer clusters made of collapsed and associated P(DEA-*co*-DMA/*x*) chains increase and approach corresponding constants after a certain time, indicating the for-

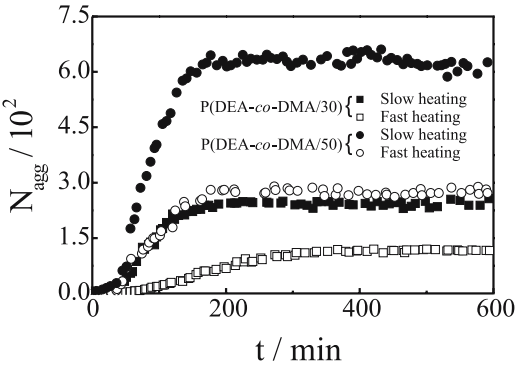

Fig. 35 Time dependence of average aggregation number (N_{agg}) of P(DEA-*co*-DMA) mesoglobules formed under different heating rates [139]

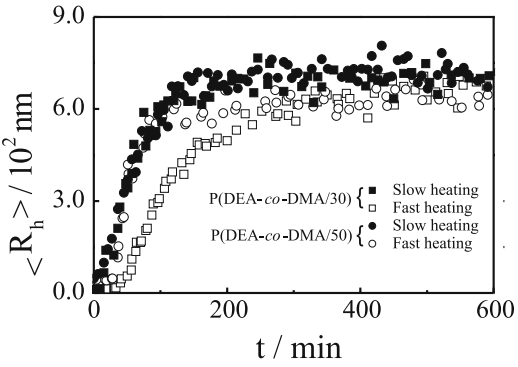

Fig. 36 Time dependence of average hydrodynamic radius ($\langle R_h \rangle$) of P(DEA-*co*-DMA) mesoglobules formed under different heating rates [139]

mation of stable mesoglobules, where N_{agg} was calculated from the ratio of the weight-average molar masses of the interchain aggregates and individual copolymer chains measured in static LLS. Note that for larger particles, the following Guinier plot instead of the Zimm plot (Eq. 1) has to be used.

$$\left(\frac{KC}{R_{vv}(q)}\right)_{C\to 0} \cong \frac{1}{M_w}\exp(-\frac{1}{3}R_g^2 q^2) \quad \text{for} \quad R_g q > 1\,. \tag{9}$$

It should be stated that aggregates formed in this way were so stable that no change in the scattering intensity was observed over months. It is also helpful to note that the stabilization in water was reached without the addition of any ion or surfactant. The stabilization is due to the concentration of hydrophilic DMA segments on the periphery of the aggregates during the microphase separation. It has been found that $\langle R_h \rangle$ is nearly independent of q in the low scattering angle range. The resultant stable mesoglobules are narrowly distributed with a relative width less than 0.05, as shown in Fig. 37. This is understandable because the association is an average process.

A combination of Figs. 35 and 36 shows that for a given heating process, N_{agg} increases with the DMA content. On the other hand, for a given copolymer, the fast heating results in a much smaller N_{agg} with a slightly larger size with $\langle R_g \rangle / \langle R_h \rangle \sim 1$, indicating that they must have a loose structure. In comparison, the aggregates formed in the slow heating have a ratio of $\langle R_g \rangle / \langle R_h \rangle \sim 0.8$. Further, it shows that at the very initial stage of the microphase transition, N_{agg} remains a constant, but $\langle R_h \rangle$ slightly decreases (not so obvious in Fig. 36) in the fast heating process, reflecting that intrachain contraction appears before interchain association. As expected, intrachain contraction must force the hydrophilic DMA segments to stay on the periphery to minimize the surface energy and slow down interchain association, resulting in a slower kinetics and smaller mesoglobules presumably consisting of many loosely packed small single- or pauci-chain collapsed globules. It

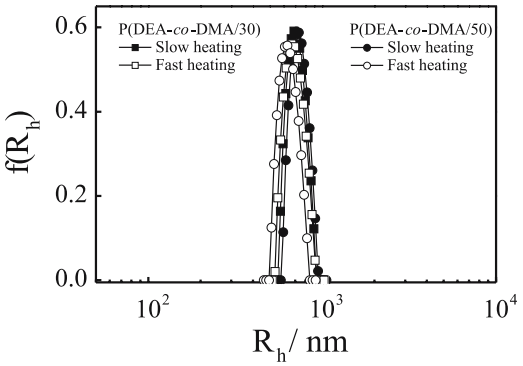

Fig. 37 Typical hydrodynamic radius distributions ($f(R_h)$) of resultant P(DEA-*co*-DMA) mesoglobules formed under different heating rates [139]

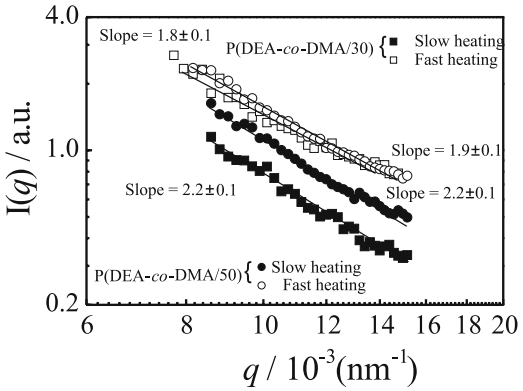

Fig. 38 Scattering vector (q) dependence of scattered light intensity (I) of resultant P(DEA-*co*-DMA) mesoglobules formed under different heating rates [139]

should be noted (not straight forward) that intrachain contraction ("folding") can lead to a chain density lower than interchain aggregation (interchain penetration) because no chain is infinitely flexible. This partially explains why the mesoglobules formed in the fast heating have a lower chain density.

Such a lower chain density can also be viewed from the scaling between the scattered light intensity (I) and the scattering vector (q) for resultant stable mesoglobules formed in different heating processes (Fig. 38). It is known that the scaling exponent α in $I \propto q^{-\alpha}$ is the fractal dimension in the scaling between molar mass and size, i.e., $M \propto R^{\alpha}$. The increase of α from 1.8–1.9 to 2.2 indicates that the association changes from a diffusion-limited process to a reaction-limited process [140]. In a reaction-limited process, many collisions only results in a sticking (association), while in a diffusion-limited process, each collision leads to a sticking. Therefore, in a reaction-limited process, each particle or cluster has a much higher chance to penetrate

into the "fiords" of the existing aggregates before they stick together [140], which results in a higher chain density. This explains why α is higher for the mesoglobules formed in the slow heating process.

5.2 Effect of Comonomer Distribution

After investigating the effect of comonomer composition on the chain association as well as the effect of comonomer distribution on the chain folding, Siu et al. [141] extended their study to the effect of comonomer distribution on the chain association. They copolymerized NIPAM and vinyl pyrrolidone (VP) at temperatures, respectively, higher and lower than the LCST, which resulted in segmented and random VP distributions on the PNIPAM chain backbone. The synthesis characterization of these PNIPAM-*co*-VP amphiphilic copolymers with a similar chain length and comonomer composition, but different comonomer distributions, were described in previous sections.

The results showed that after the solution temperature is raised to a temperature higher than the LCST, both M_w and $\langle R_h \rangle$ increase as the time elapses and approach corresponding constants after a certain time, similar to Figs. 35 and 36. Mesoglobules formed in this way were stable for a long time, indicating that the interchain association stopped at a certain stage. It was also found that the average hydrodynamic radius of such resultant stable mesoglobules ($\langle R_h \rangle_{t\to\infty}$) decreases as the aggregation temperature ($T_{aggregation}$) increases, while their weight average molar mass ($(M_w)_{t\to\infty}$) increases when $T_{aggregation} < \sim 37\,^{\circ}C$, but decreases when $T_{aggregation}$ is higher than 37 °C. The fact that stable aggregates formed at 36 °C have a smaller M_w, but a larger $\langle R_h \rangle$, clearly indicates that they have a loose structure. This is because the copolymer chains are only partially collapsed at 36 °C. The stable mesoglobules are narrowly distributed, similar to those in Fig. 37. No precipitation was observed even after a long time, reflecting no change in the scattering intensity.

$\langle R_g \rangle / \langle R_h \rangle$, as shown in Fig. 39, reveals the structural information of these mesoglobules. The date points are scattered due to experimental uncertainties, especially in the measurement of $\langle R_g \rangle$ for large aggregates. However, the decrease of $\langle R_g \rangle / \langle R_h \rangle$ from $\sim$ 1.5–1.7 to $\sim$ 0.8 reveals a change from extended random-coil chains to uniform spherical aggregates, i.e., mesoglobules. The mesoglobules made of the NIPAM-*co*-VP/30/11 chains have the highest ratio of $\langle R_g \rangle / \langle R_h \rangle$. This is because NIPAM-*co*-VP/30/11 has the highest hydrophobic VP content and a random distribution of VP on the chain backbone so that its contraction is hindered. The formation of such stable mesoglobules is analogous to that described by Timoshenko et al. [136–138].

Figure 40 shows the temperature dependence of the average aggregation number (N_{chain}) of stable mesoglobules made of four different P(NIPAM-

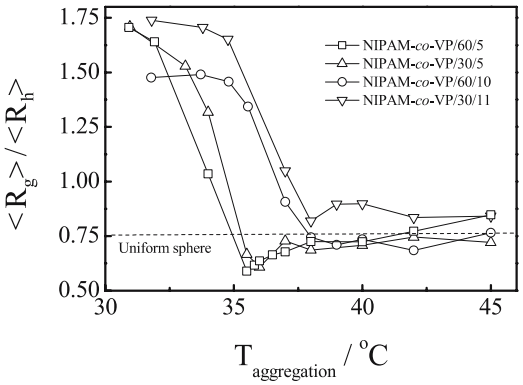

Fig. 39 Aggregation temperature dependence of ratio of average radius of gyration to average hydrodynamic radius ($\langle R_g \rangle / \langle R_h \rangle$) of resultant stable mesoglobules made of different copolymers [141]

co-VP) copolymers, where N_{chain} was obtained from the ratio of the weight average molar masses of the mesoglobules and chains. Note that for the copolymers with 10 mol % VP, N_{chain} reaches its maximum at a higher temperature because they are more hydrophilic. For each pair of copolymers with a similar VP content, the mesoglobules made of the copolymer chains prepared at 60 °C have a higher N_{chain}. On the other hand, for each pair of copolymers prepared at the same temperature, the copolymer with a higher VP content has an expected smaller N_{chain} because the average length of the PNIPAM segments is shorter and the copolymers are more hydrophilic.

It is a hypothesis that the copolymer chains prepared at higher temperatures would have a more segmented structure because it is expected that most of the VP monomers would be copolymerized on the periphery of collapsed PNIPAM segments. In other words, the chains prepared at 60 °C would have a more segmented structure in comparison with those prepared at 30 °C. In this way, for a given VP content, the average length of the PNIPAM segments between two neighboring VP segments should be longer than that of a statistically random copolymer prepared at 30 °C. It is expected that at high temperatures NIPAM-*co*-VP/60/*x* copolymers with longer PNIPAM and PVP segments can provide a stronger hydrophobic interaction as well as a stronger hydrophilic stabilization force, which have the opposite effect on the formation of the mesoglobular phase. However, the effect of hydrophobic interaction should be larger because PNIPAM is a major component and the length increase of the PNIPAM segment is much faster when the VP monomers start to group together as short segments. This explains why the copolymer chains prepared at 60 °C result in larger aggregates.

Another feature of Fig. 40 is the initial sharp increase of N_{chain} followed by a gradual decrease. Note that for each copolymer, the temperature at which N_{chain} reaches its maximum roughly corresponds to the temperature at which

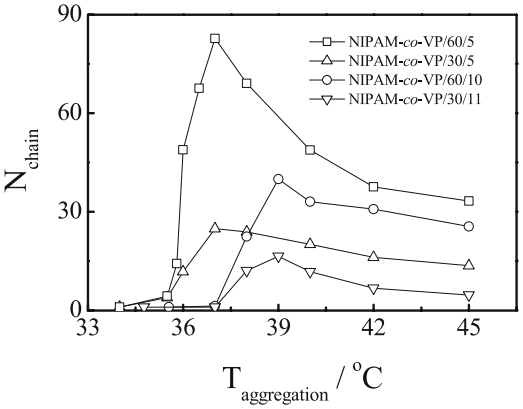

Fig. 40 Aggregation temperature dependence of average aggregation number (N_{chain}) of resultant stable mesoglobules made of different copolymers, where N_{chain} is defined as $M_{w,\,mesoglobule}/M_{w,\,chain}$ [141]

individual copolymer chains reach their fully collapsed states. The increase of N_{chain} with the aggregation temperature is understandable because long PNIPAM segments become more and more hydrophobic. Before reaching the collapse temperature, less compact chains can interpenetrate with each other so that the interchain association dominates. At higher aggregation temperatures, intrachain contraction becomes dominant and short hydrophilic VP segments tend to stay on the periphery to minimize the interfacial energy. In this way, the interchain association is retarded, which explains why N_{chain} decreases in the high aggregation temperature range.

Thermodynamically, the formation of stable mesoglobules instead of macroscopic phase separation requires a delicate balance between enthalpic and entropic contributions. In comparison with macroscopic precipitation, the existence of many small mesoglobules must gain in the translational entropy ($\Delta S > 0$) as well as in the interfacial energy ($\Delta H > 0$). For a homopolymer in a poor solvent, the gain of ΔH is larger than $T\Delta S$, i.e., $\Delta G = \Delta H - T\Delta S > 0$. Therefore, the equilibrium moves towards the direction of forming macroscopic precipitation. For amphiphilic copolymers in a selective solvent (often water), a microphase separation can occur, in which the association of hydrophobic segments leads to intrachain contraction and interchain aggregation, but hydrophilic segments tend to stay on the periphery. Under a proper condition, $T\Delta S$ can offset that of ΔH, i.e., $\Delta G = \Delta H - T\Delta S < 0$, so that further interchain aggregation stops. It is expected that more hydrophilic groups on the periphery would lead to smaller mesoglobules. However, due to the chain connectivity, a perfect arrangement to expose all hydrophilic VP components on the periphery is impossible. For a given type of copolymers with a similar composition, longer hydrophobic (shorter hydrophilic) segments should make the arrangement easier. As

discussed before, the copolymer synthesized at 60 °C has longer PNIPAM segments than its counterpart prepared at 30 °C for a given comonomer composition. Longer PNIPAM segments provide a stronger hydrophobic attraction at high temperatures so that the copolymer chains prepared at 60 °C have a lower LCST and a higher N_{chain} than its counterpart prepared at 30 °C.

The competition between intrachain contraction and interchain association can be better viewed from the temperature dependence of $\langle R_h \rangle$, as shown in Fig. 41. A comparison of Figs. 40 and 41 shows that such a temperature dependence can be roughly divided into three regions. In the lower temperature range, where N_{chain} remains constant (~ 1), $\langle R_h \rangle$ decreases as the solution temperature increases, reflecting the contraction of individual chains. In the middle temperature range, N_{chain} and $\langle R_h \rangle$ increase before reaching their maximum values, showing that interchain association becomes dominant. In the higher temperature range, both N_{chain} and $\langle R_h \rangle$ decrease as the aggregation temperature increases. It should be noted that the decrease of $\langle R_h \rangle$ in the lower and higher temperature ranges is caused by completely different reasons. In the higher aggregation temperature range, intrachain contraction happens prior to interchain association. The higher the aggregation temperature the faster the contraction rate. Therefore, individual collapsed copolymer chains have much less chance to undergo interchain association. This is why both N_{chain} and $\langle R_h \rangle$ decrease in this region.

Figure 42 shows the temperature dependence of the average chain density ($\langle \rho \rangle$) of stable mesoglobules, where $\langle \rho \rangle$ is defined as $M_w/(4\pi \langle R_h \rangle^3 N_A/3)$. For all the copolymers studied, $\langle \rho \rangle$ always increases with the aggregation temperature. As discussed before, intrachain folding normally results in a lower chain density than interchain penetration because the chains are not infinitely flexible. For the copolymer pair, NIPAM-*co*-VP/60/10 and NIPAM-

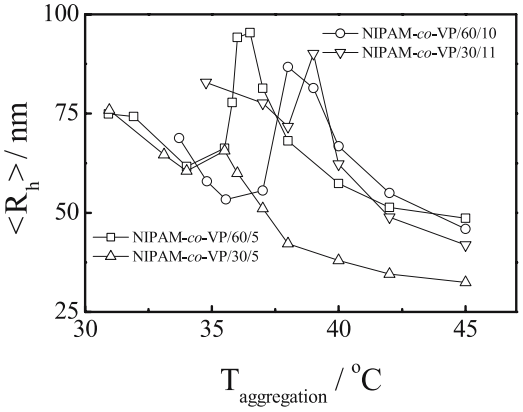

Fig. 41 Aggregation temperature dependence of average hydrodynamic radius ($\langle R_h \rangle$) of resultant stable mesoglobules made of different copolymers [141]

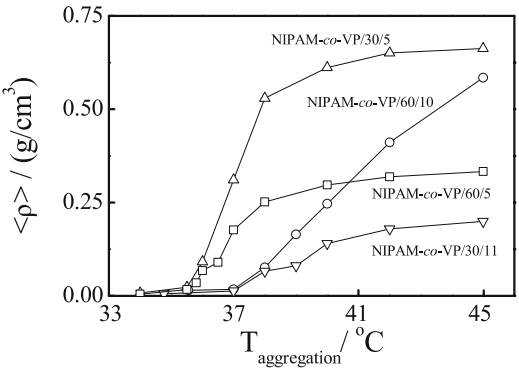

Fig. 42 Aggregation temperature dependence of average chain density ($\langle\rho\rangle$) of resultant stable mesoglobules made of different copolymers, where $\langle\rho\rangle$ is defined as $M_w/(4\pi\langle R_h\rangle^3 N_A/3)$ [141]

co-VP/30/11, the NIPAM-*co*-VP/60/10 mesoglobules have a higher average chain density because the copolymers prepared at 60 °C have longer PNIPAM segments and tend to form stronger interchain association as discussed earlier. However, for the pair of copolymers with a lower VP content, the NIPAM-*co*-VP/60/5 mesoglobules have a lower $\langle\rho\rangle$. The study of the chain folding showed that the coil-to-globule transition of individual NIPAM-*co*-VP/60/5 chains is easier [56]. The lower chain density reflects that NIPAM-*co*-VP/60/5 mesoglobules consist of many small collapsed single-chain globules, i.e., intrachain contraction is dominant in the formation of the mesoglobular phase.

5.3 Viscoelastic Effect on Formation and Stabilization of Mesoglobules

It is understandable, if not straightforward, that the copolymerization of some hydrophilic comonomers into a hydrophobic chain backbone can prevent macroscopic phase separation (precipitation) in aqueous solutions and result in stable mesoglobules because these water-soluble comonomers have a tendency to stay on the periphery and reduce the surface energy. On the other hand, hydrophobically modified water-soluble chains are known as associating polymers because hydrophobic comonomers in the chain backbone act as "stickers" in water. In a semi-dilute or concentrated solution, such copolymer chains can associate with each other to form insoluble large clusters or even form a hydrogel. Due to such strong interchain association, it would be difficult to imagine that they could form small stable mesoglobules.

Recently, we surprisingly found that even hydrophobically modified PNIPAM-*co*-MACA comonomer chains can form stable mesoglobules at higher temperatures [142]. Moreover, opposite to our expectation, the PNIPAM copolymer with a higher content of hydrophobic comonomer could

form smaller aggregates in water under an identical experimental condition. Note that MACA homopolymer is insoluble in water at room temperature.

Three copolymers, PNIPAM-*co*-1.0-MACA, PNIPAM-*co*-2.9-MACA and PNIPAM-*co*-4.9-MACA were used. Their weight-average molar masses (M_w) are 9.4×10^5, 8.3×10^5 and 6.5×10^5 g/mol, respectively. In order to avoid possible interchain association, we kept each dilute solution in a refrigerator for at least one day to ensure a complete dissolution. The solution was clarified by a 0.45 Millipore (Hydrophlic Millex-LCR, PTFE) filter and then kept in a refrigerator again for a few days before LLS measurements.

Figure 43 shows an expected decrease of the LCST with an increasing hydrophobic MACA content. For PNIPAM-*co*-1.0-MACA, a gradual heating of the solution from 10 °C to 50 °C leads to large mesoglobules with $N_{agg} \sim 4000$, while for PNIPAM-*co*-4.8-MACA, the same heating results in much smaller aggregates only with $N_{agg} \sim 10$, which clearly shows that N_{agg} decreases with an increasing MACA content. On the other hand, the initial decrease of $\langle R_h \rangle$ in the range $T <$ LCST, as shown in Fig. 44, reflects intrachain contraction because $N_{agg} = 1$ in the same temperature range. For PNIPAM-*co*-1.0-MACA, the increases of both N_{agg} and $\langle R_h \rangle$ in the range $T >$ LCST reflect that interchain association becomes dominant. For PNIPAM-*co*-4.8-MACA, Fig. 44 shows a continuous decrease of $\langle R_h \rangle$ before its leveling-off at ~ 32 °C, similar to the coil-to-globule transition of individual single chains [13]. However, the increase of N_{agg} in Fig. 43 reveals that there still exists interchain association even though intrachain contraction is dominant here. For PNIPAM-*co*-2.9-MACA, the transition from intrachain-contraction dominant to interchain-association dominant is fairly clear. The leveling-off of N_{agg} and $\langle R_h \rangle$ for

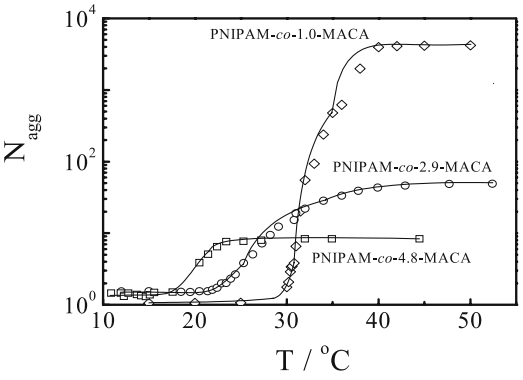

Fig. 43 Temperature dependence of average aggregation number (N_{agg}) of PNIAPM-*co*-MACA mesoglobules formed in a gradual heating process, where $N_{agg} = M_{w,agg}/M_{w,chain}$ with $M_{w,agg}$ and $M_{w,chain}$, the weight-average molar masses of the copolymer aggregates and of the chains, respectively; and copolymer concentration is $\sim 10^{-5}$ g/mL. Note that each data point was obtained after the temperature equilibrium was reached [142]

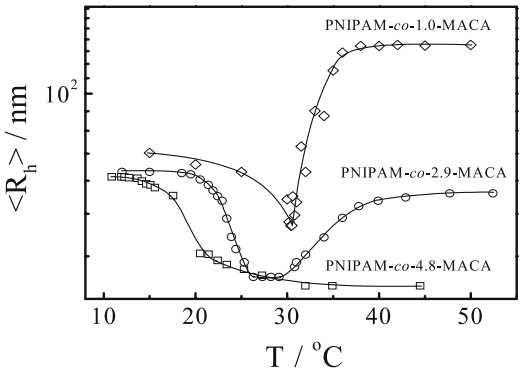

Fig. 44 Temperature dependence of average hydrodynamic radius ($\langle R_h \rangle$) of PNIAPM-*co*-MACA mesoglobules formed in a gradual heating process, where each data point was obtained after the temperature equilibrium was reached and copolymer concentration is $\sim 10^{-5}$ g/mL [142]

all the samples at higher temperatures indicates the formation of stable mesoglobules.

Now, let us discuss why those chains with a high content of hydrophobic MACA form smaller aggregates. Picarra and Martinho [143] showed that in the phase separation of a thin-layer dilute *homopolymer* solution on the surface, the collision would not be effective as long as the collision (or contact) time (τ_c) is shorter than the time (τ_e) needed to establish a permanent chain entanglement between two approaching aggregates. Quantitatively, Tanaka [144] showed that τ_c and τ_e could be roughly characterized as

$$\frac{l_o}{\langle v \rangle} < \tau_c < \frac{l_o^2}{\langle D \rangle} \quad \text{and} \quad \tau_e \sim \frac{a_m^2 N_m^3 \phi_p^{3/2}}{D_m}, \tag{10}$$

where l_o is the interaction range, $\langle v \rangle$ and $\langle D \rangle$ are the mean thermal velocity and transitional diffusion coefficient of aggregates, respectively, ϕ_p is the average polymer concentration inside chain aggregates, and a_m, N_m and D_m are the length, number and diffusion coefficient of monomer, respectively. When $\tau_c \ll \tau_e$, two colliding aggregates have no time to stick together and they behave just like two tiny elastic nonadhesive "glass" balls. Such an effect is a character of the viscoelasticity of long polymer chains. Our previous study showed that ϕ_p in the collapsed state could be as high as 30 wt % even though the overall concentration was very low ($\sim 10^{-6}$ g/mL) [32]. Therefore, the relaxation of long chains inside each aggregate is very slow. Homopolymer aggregates formed in this way are thermodynamically unstable because there is no hydrophilic stabilization group on the periphery to reduce τ_c.

For a given polymer solution under certain experimental conditions, l_o, a_m, N_m and D_m in Eq. 10 are constants. One can only increase $\langle D \rangle$ and ϕ_p to

ensure that $\tau_c \ll \tau_e$ in order to reach a stable mesoglobular phase. Over the years, researchers always tried to make the aggregate's periphery hydrophilic to prevent the aggregation on the basis of thermodynamics, which actually reduces l_o and τ_c, but overlooked the effect of increasing τ_e to keep $\tau_c \ll \tau_e$, i.e., how to use the viscoelasticity to stabilize mesoglobules. As expected, increasing the hydrophobic MACA content promotes both interchain association and intrachain contraction. In dilute solutions, enhancing intrachain contraction increases ϕ_p inside each aggregate even though the overall macroscopic concentration remains. At the same time, τ_c decreases because the strong intrachain contraction reduces the initial size of the aggregates, leading to a higher $\langle D \rangle$. Moreover, hydrophobic association inside each mesoglobule gravely slows down the chain relaxation inside each mesoglobule and increases τ_e. Therefore, in some sense, it is not so crazy to claim that the hydrophobic association plays a partial role in the stabilization.

On the other hand, considering such a competition between intrachain contraction and interchain association as well as the viscoelastic effect, we dilute the copolymer solution to the limit of our LLS detection in order to suppress interchain association. Figure 45 shows that after $\sim$ 10-time dilution, there is no observable change in the time-average scattering intensity $\langle I \rangle$ over the entire temperature range studied. As discussed earlier, $\langle I \rangle$ is extremely sensitive to interchain association; namely, the association of two chains doubles the scattering intensity. The constant value of $\langle I \rangle$ indicates that there is no interchain association. Figure 45 represents a pure intrachain coil-to-globule transition. We must note that due to the help of "hydrophobic stabilization", the experimental realization of the folding of individual MACA modified PNIPAM copolymer chains without interchain association is

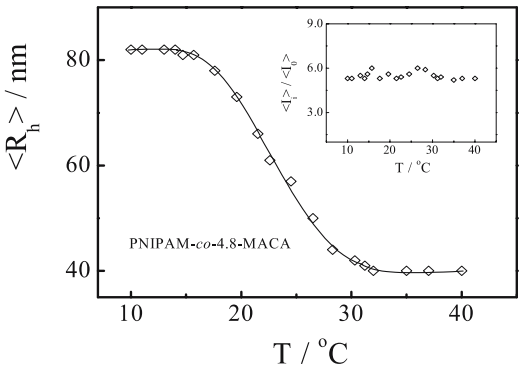

Fig. 45 Temperature dependence of average hydrodynamic radius ($\langle R_h \rangle$) of PNIAPM-*co*-4.8-MACA mesoglobules formed in a gradual heating process, where each data point was obtained after the temperature equilibrium was reached and copolymer concentration is 10x more dilute than that in Figs. 1 and 2. The *inset* shows the temperature dependence of average scattering intensity ($\langle I \rangle / \langle I \rangle_0$), where $\langle I \rangle_0$ is the reference intensity [142]

much easier in comparison with the formation of single PANPM homopolymer chain globules [32]. We also found that intrachain contraction can be promoted if the copolymer solution is quickly quenched to a desired phase separation condition because of sudden increases of ϕ_p and τ_e.

The above discussion has been schematically summarized in Fig. 46. The formation of the mesoglobular phase of amphiphilic copolymer chains in dilute solution during microphase separation inevitably involves competition between intrachain contraction and interchain association. The resultant mesoglobules are stabilized not only by the well-known concentration of hydrophilic components on the periphery, but also by the overlooked hydrophobic association inside each mesoglobule. This can be attributed to the effect of viscoelasticity even in a dilute solution; namely, when the chain entanglement time (t_e) between two colliding mesoglobules is much longer than their interaction time (t_c), each mesoglobule becomes a tiny nonadhesive "glass" ball. Either increasing the rate of microphase separation or diluting the solution can decrease t_c because intrachain contraction becomes so dominant that smaller initial mesoglobules are formed with a larger diffusion coefficient. On the other hand, increasing either the MACA content or the chain length can increase t_e.

On the basis of Eq. 10, using long chains (larger N) should be a very effective way to increase τ_e. Conventionally, one would think that the association of long chains should lead to larger aggregates. However, long copolymer chains can reach the condition of $\tau_e > \tau_c$ much more easily in the earlier stage of the microphase separation than short chains so that further entan-

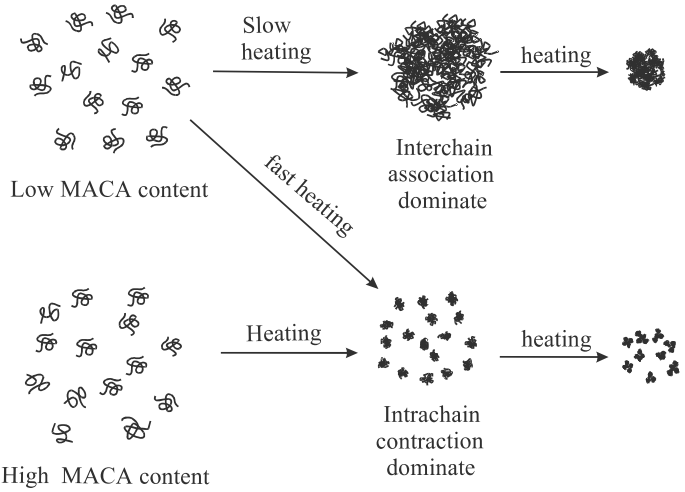

Fig. 46 Schematic of competition between intrachain contraction and interchain association in formation of PNIAPM-*co*-MACA mesoglobules, respectively, made of the chains with low and high hydrophobic MACA contents [142]

glement between longer chains respectively in two different mesoglobules becomes much more difficult, if not impossible, in the experimental time scale. In other words, the viscoelastic effect "overwrites" thermodynamics and leads to a special meta-stable, but very stable, state in dilute solution. Some years ago, Qiu et al. [145] found that longer PNIPAM-*g*-PEO copolymer chains could form smaller stable mesoglobules if other conditions were kept the same, but they did not attribute this to the effect of viscoelasticity at that time. They used two copolymers, PNIPAM-*g*-PEO1 ($M_w = 7.29 \times 10^6$ g/mol) and PNIPAM-*g*-PEO2 ($M_w = 7.85 \times 10^5$ g/mol) copolymers with a similar PEO distribution.

Figures 47 and 48, respectively, show the temperature and concentration dependence of $\langle R_h \rangle$ and $R_{vv}(\theta)/KC$ of PNIPAM-*g*-PEO1 in water. $R_{vv}(\theta)/KC$ is proportional to the weight average molar mass M_w on the basis of Eq. 1.

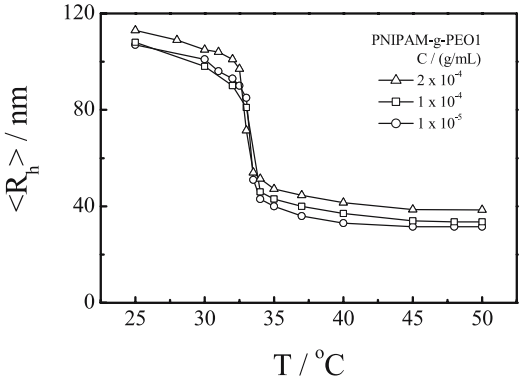

Fig. 47 Temperature and concentration dependence of the average hydrodynamic radius $\langle R_h \rangle$ of PNIPAM-*g*-PEO1 in deionized water [145]

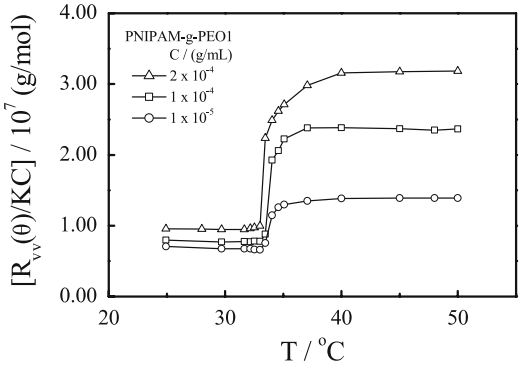

Fig. 48 Temperature and concentration dependence of the excess scattering intensity $R_{vv}(\theta)/KC$ of PNIPAM-*g*-PEO1 in deionized water [145]

Here, the solution temperature was raised step-by-step from 25 to 50 °C, i.e., it was stopped at each measurement temperature and the LLS measurement was conducted only after the equilibrium was reached. The change of $\langle R_h \rangle$ can be divided into three stages. In the first stage, when the solution temperature increases from 25 to 32 °C, water progressively becomes a poor solvent for the PNIPAM chain backbone, resulting in a slight decrease of $\langle R_h \rangle$. In the second stage ($\sim$ 32–34 °C), the PNIPAM chain backbone undergoes the intrachain "coil-to-globule" transition so that $\langle R_h \rangle$ rapidly decreases. In the last stage ($> \sim$ 34 °C), the PNIPAM chain backbone is already in its fully collapsed state so that further increase of the solution temperature has little effect on $\langle R_h \rangle$.

On the other hand, Fig. 48 shows that in the range $\sim$ 25–32 °C, $R_{vv}(\theta)/KC$ nearly remains a constant ($7 - 8 \times 10^6$ g/mol), very close to the weight average molar mass of individual PNIPAM-*g*-PEO1 chains, indicating no interchain aggregation. This is expected since both the PNIPAM chain backbone and PEO branches are hydrophilic and soluble in water in this temperature range. An abrupt increase of $R_{vv}(\theta)/KC$ at $\sim$ 33 °C clearly indicates interchain association. Over a narrow temperature range $\sim$ 33–36 °C, each $R_{vv}(\theta)/KC$ curve reaches a higher plateau, implying the formation of stable mesoglobules. From the value of each plateau and the average molar mass of individual PNIPAM-*g*-PEO1 chains, the average number of the copolymer chains ($N_{\text{PNIPAM-}g\text{-PEO}}$) inside each nanoparticle can be estimated. In Fig. 47, $N_{\text{PNIPAM-}g\text{-PEO}}$ has a value of $\sim$ 2, $\sim$ 3 and $\sim$ 4, respectively. It is easy to understand that the aggregation number increases with the copolymer concentration because the copolymer chains have more chance to undergo interchain association before each of them can collapse into a single-chain globule and is stabilized by the grafted PEO chains.

Figures 49 and 50 show the temperature and concentration dependence of $\langle R_h \rangle$ and $R_{vv}(\theta)/KC$ of PNIPAM-*g*-PEO2 in water. Note that PNIPAM-*g*-

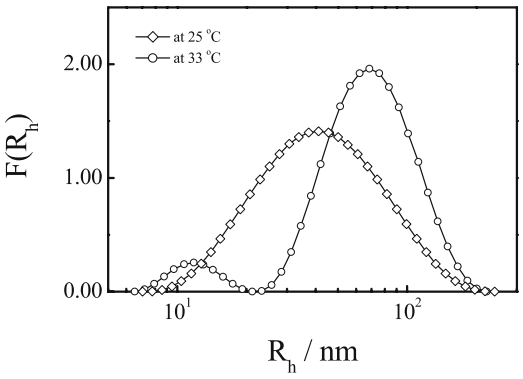

Fig. 49 Temperature and concentration dependence of the average hydrodynamic radius $\langle R_h \rangle$ of PNIPAM-*g*-PEO2 in deionized water [145]

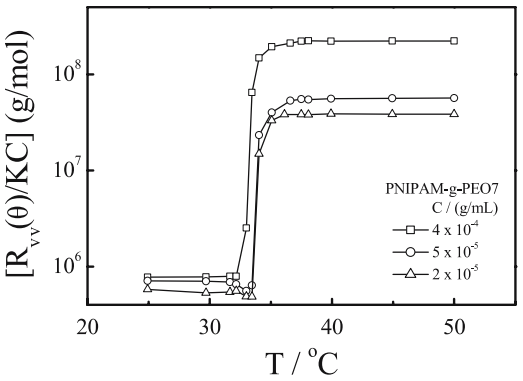

Fig. 50 Temperature and concentration dependence of the excess scattering intensity $R_{vv}(\theta)/KC$ of PNIPAM-*g*-PEO2 in deionized water [145]

PEO2 is 10 times shorter than PNIPAM-*g*-PEO1. Figure 49 reveals that short PNIPAM-*g*-PEO2 chains follow a different path; namely, after reaching a maximum at $\sim 33.5\,^{\circ}$C, $\langle R_h \rangle$ starts to decrease, while in the case of long PNIPAM-*g*-PEO1 chains (Fig. 47) $\langle R_h \rangle$ remains a constant after reaching the maximum value. However, there is no difference in the changing pattern of $R_{vv}(\theta)/KC$ between long and short chains (Figs. 48 and 50). Therefore, the decrease of $\langle R_h \rangle$ in Fig. 49 and the constant values of $R_{vv}(\theta)/KC$ in Fig. 50 lead to only one possibility, i.e., for short PNIPAM-*g*-PEO2 chains, interchain association is prior to intrachain "coil-to-globule" contraction. The average aggregation numbers of short chains inside each mesoglobule are ~ 80, ~ 90, and ~ 280, respectively, for $C = 2 \times 10^{-5}$, 5×10^{-5}, and 4×10^{-4} g/mL, which also reflect that interchain association is dominant in the case of short chains. A combination of Figs. 47–50 clearly shows that long chains aggregate much less than short chains.

6 Conclusion

In comparison with linear homopolymers, individual amphiphilic copolymer chains in dilute solutions, in which solvents are selectively good for only one of the comonomers, can fold into different single-chain core-shell nanostructures stabilized by a hydrophilic shell. The shell can be made of short hydrophilic chains grafted on the core or small hydrophilic (neutral or ionic) groups or loops (flower-petal) made of hydrophilic segments. The degree of amphiphilicity can strongly influence the folding of individual amphiphilic copolymer chains. For thermally sensitive copolymer chain backbones, the degree of amphiphilicity can be simply alternated by the solution temperature. The folding and unfolding of such thermally sensitive copolymer chains

can be switched on and off by a very small temperature change of 1–2 °C. It has been found that the chain folding greatly depends on both comonomer composition and distribution on the chain backbone.

The comonomer distribution can be alternated by controlling the synthesis conditions, such as the copolymerization at different reaction temperatures at which the thermally sensitive chain backbone has different conformations (extended coil or collapsed globule). In this way, hydrophilic comonomers can be incorporated into the thermally sensitive chain backbone in a more random or more segmented (protein-like) fashion. On the other hand, short segments made of hydrophobic comonomers can be inserted into a hydrophilic chain backbone by micelle polymerization. One of the most convenient ways to control and alternate the degree of amphiphilicity of a copolymer chain, i.e., the solubility difference of different comonomers in a selective solvent, is to use a thermally sensitive polymer as the chain backbone, such as poly(*N*-isopropylacrylamide) (PNIPAM) and Poly(*N*,*N*-diethylacrylamide) (PDEA). In this way, the incorporation of a hydrophilic or hydrophobic comonomer into a thermally sensitive chain backbone allows us to adjust the degree of amphiphilicity by a temperature variation.

Using this approach, hydrophilic (neutral or ionic) comonomers, such as end-captured short polyethylene oxide (PEO) chains (macromonomer), 1-vinyl-2-pyrrolidone (VP), acrylic acid (AA) and *N*,*N*-dimethylacrylamide (DMA), can be grafted and inserted on the thermally sensitive chain backbone by free radical copolymerization in aqueous solutions at different reaction temperatures higher or lower than its lower critical solution temperature (LCST). When the reaction temperature is higher than the LCST, the chain backbone becomes hydrophobic and collapses into a globular form during the polymerization, which acts as a template so that most of the hydrophilic comonomers are attached on its surface to form a core-shell structure. The dissolution of such a core-shell nanostructure leads to a protein-like heterogeneous distribution of hydrophilic comonomers on the chain backbone.

On the other hand, hydrophobic comonomers, such as 2′-methacryloylaminoethylene)-3α,7α,12α-trihydroxy-5β-cholanoamide (MACA) and styrene (St), can be incorporated into the thermally sensitive chain backbone by copolymerization of different comonomers in a common organic solvent, which results in a random distribution of hydrophobic comonomers on the chain backbone, or by micelle copolymerization in water with the help of surfactant micelles in which hydrophobic comonomer molecules are concentrated, which leads to evenly distributed short hydrophobic segments on the chain backbone.

For copolymers with some protein-like comonomer distributions, individual copolymer chains can “memorize” or “inherit” its parent globular state; namely, their folding back into the core-shell nanostructure is much easier, resulting in a smaller and denser single-chain particle in comparison with their counterparts, randomly distributed comonomers on the

chain backbone. On the other hand, for copolymers with evenly distributed short hydrophobic segments, individual random-coil chains can first fold to a novel "ordered" coil state before they collapse into their final single-chain flower-like globules. Conventional wisdom tells us that introducing hydrophobic segments will lead to chain association, resulting in phase separation. Surprisingly, it has been shown that the copolymerization of a few molar percent of hydrophobic comonomers into the hydrophilic chain backbone can actually stabilize the resultant single-chain core-shell globules and make the coil-to-globule transition much easier in extremely dilute solutions.

As the polymer concentration increases, interchain association inevitably occurs, but some amphiphilic chains can undergo a limited interchain association to form a stable mesoglobular phase that exists between microscopic single-chain globules and macroscopic precipitation. As expected, when the solvent quality changes from good to poor, intrachain contraction and interchain association occur simultaneously and there exists a competition between these two processes. Such a competition depends on the comonomer composition and distribution on the chain backbone and also depends on the rate of micro-phase separation. When intrachain contraction happens quickly and prior to interchain association, smaller mesoglobules are formed. A proper adjustment of the rates of intrachain contraction and interchain association can lead to polymeric colloidal particles with different sizes and structures.

Such chain folding and association in solutions can be effectively and accurately studied by a combination of static and dynamic laser light scattering (LLS). This is because LLS can directly measure the weight average molar mass (M_w), the average radius of gyration ($\langle R_g \rangle$) and average hydrodynamic radius ($\langle R_h \rangle$) of individual chains or interchain aggregates. On the basis of these measurable micro-parameters, one can further calculate the average aggregation number (N_{agg}), the average chain density ($\langle \rho \rangle$) and the average surface area occupied per "stabilizer" that can be ionic groups (as $-COO^-$ and $-SO_3^-$) or neutral hydrophilic moieties, such as short grafted hydrophilic chains, small hydrophilic loops and even tiny hydrophilic segments. In particular, the ratio of $\langle R_g \rangle / \langle R_h \rangle$ reflects the chain conformation and the chain density distribution inside interchain aggregates.

Considering the competition between intrachain contraction and interchain association, we have to discuss an overlooked viscoelastic effect in the formation of stable mesoglobules in dilute solutions. Otherwise, it would be difficult to understand why copolymer chains with a high content of hydrophobic comonomers could form smaller interchain aggregates. In the micro-phase separation, copolymer chains in solutions contract and associate. The collision between contracted and associated chains would not be effective if the collision (or contact) time (τ_c) is much shorter than the time (τ_e) needed to establish a permanent chain entanglement between two ap-

proaching aggregates. This is because when $\tau_c \ll \tau_e$, two colliding aggregates have no time to stick together and they behave just like two tiny elastic non-adhesive "glass" balls. Such an effect is a character of the viscoelasticity of long polymer chains. It has been shown that the local chain density inside the aggregate in the collapsed state could be as high as 30 wt % even though the overall concentration was very low ($\sim 10^{-6}$ g/mL). Therefore, the relaxation of long chains inside each aggregate is very slow.

Over the years, researchers always tried to make the periphery of aggregates hydrophilic to prevent inter-particle aggregation based on thermodynamics, which actually reduces τ_c, but overlooked that in polymer colloids we can easily increase τ_e to make $\tau_c \ll \tau_e$, i.e., *playing the viscoelastic effect on the stabilization of mesoglobular phase*. Following such a viscoelastic consideration, there are different ways to increase τ_e. For example, using long chains (larger N) should be very effective because long chains can reach the condition of $\tau_e > \tau_c$ much more easily in the initial stage of the micro-phase separation than short chains. As soon as the condition of $\tau_e > \tau_c$ is reached, further inter-particle association via chain entanglements become impossible in the experimental time scale. In other words, the viscoelastic effect "overwrites" thermodynamics and leads to a special metastable, but very stable, state in dilute solutions.

On the other hand, increasing the hydrophobic content promotes both interchain association and intrachain contraction. In dilute solutions, enhancing intrachain contraction increases τ_e because of a higher local chain density, and at the same time, decreases τ_c because strong intrachain contraction reduces the initial size of the aggregates, making the random movement of each particle much faster. In an actual process, during the micro-phase separation, hydrophilic moieties are forced to stay on the periphery, which reduces τ_c, and at the same time, hydrophobic intra- and inter-chain association prevents the relaxation of chains inside each aggregate so that τ_e increases. Such a cooperative effect leads to $\tau_e > \tau_c$.

In some sense, it might not be that crazy to claim that hydrophobic association can make polymer colloidal particles more stable in dispersion. Further, we might have to reconsider the stabilization mechanism of globular proteins. Normally, we consider that hydrophobic amino acid residuals in a protein chain can lead to the chain folding because of hydrophobic association. However, we might have overlooked the stabilization role of such hydrophobic association in preventing further aggregation of resultant protein structures. The current studies of the folding and association of amphiphilic copolymer chains in dilute solutions are only one small step forward in a long journey towards a better understanding of protein folding. It is our opinion that polymer research and polymer industries have to move toward the direction of synthesizing, characterizing and studying more sophisticated and tailored structural copolymers besides the much-studied random copolymers and block copolymers.

Acknowledgements The financial support from the Hong Kong Special Administration Region Earmarked Grants and the National Science Foundation of China over the last ten years is gratefully acknowledged. We are also indebted to many of our students, postdoctorals and collaborators, particularly to Professors Jiang M in Fudan University and Zhou SQ in the City University of New York, to Drs. Qiu XP, Wang XH, Li M, Hu TJ, Peng SF, and to Mr. Li W and Miss Siu MH.

References

1. Stryer L (1988) Biochemistry. Freeman WH, New York
2. Zhou YQ, Karplus M (1999) Nature 401:400
3. Nelson ED, Teneyck LF, Onuchic JN (1997) Phys Rev Lett 79:3534
4. Klimov DK, Thirumalai D (1996) Phys Rev Lett 76:4070
5. Camacho C, Thirumalai D (1993) Phys Rev Lett 71:2505
6. Khokhlov AR, Khalatur PG (1998) Physica A 249:253
7. Zheligovskaya EA, Khalatur PG, Khokhlov AR (1999) Phys Rev E 59:3071
8. Khokhlov AR, Khalatur PG (1999) Phys Rev Lett 82:3456
9. Timoshenko EG, Kuznetsov YA (2000) J Chem Phys 112:8163
10. Schild HG (1992) Prog Polym Sci 17:163
11. Fujishige S, Kubota K, Ando I (1989) J Phys Chem 93:3311
12. Kubota K, Fujishige S, Ando I (1990) J Phys Chem 94:5154
13. Meewes M, RickaJ, Nyffenegger R, Binkert T (1991) Macromolecules 24:5811
14. Zhou SQ, Wu C (1995) Macromolecules 28:5225
15. Tiktopulo EI, Bychkova VE, Ricka J, Ptitsyn OB (1994) Macromolecules 27:2879
16. Virtenen J, Baron C, Tenhu H (2000) Macromolecules 33:336
17. Stockmayer WH (1960) Makromol Chem 35:54
18. Flory PJ (1953) Principles of Polymer Chemistry. Cornell University Press, Ithaca, NY
19. Ptitsyn OB, Kron AK, Eizner YY (1968) J Polym Sci Part C 16:3509
20. Yamakawa H (1971) Modern Theory of Polymer Solutions. Harper & Row, New York, NY
21. Grosberg AY, Kuznetsov DV (1992) Macromolecules 25:1996
22. Yamakawa H (1993) Macromolecules 26:5061
23. Post CB, Zimm BH (1979) Biopolymers 18:1487 and (1982) 21:2123
24. Park IH, Wang QW, Chu B (1987) Macromolecules 20:1965
25. Chu B, Park IH, Wang QW, Wu C (1987) Macromolecules 20:2833
26. Chu B, Yu J, Wang ZL (1993) Prog Colloid Polym Sci 91:142
27. Tanaka F (1985) J Chem Phys 82:4707
28. Tanaka F, Ushiki H (1988) Macromolecules 21:1041
29. Grosberg AY, Kuznetsov DV (1993) Macromolecules 26:4249
30. Yu J, Wang ZL, Chu B (1992) Macromolecules 25:1618
31. Chu B, Ying QC, Grosberg AY (1995) Macromolecules 28:180
32. Wu C, Zhou SQ (1995) Macromolecules 28:5388, 8381
33. Wu C, Zhou SQ (1996) Macromolecules 29:1574
34. Wu C, Zhou SQ (1996) Phys Rev Lett 77:3053
35. Gao J, Wu C (1997) Macromolecules 30:6873
36. Hu TJ, Wu C (1999) Phys Rev Lett 83:4105
37. Wu C, Wang XH (1998) Phys Rev Lett 79:4092
38. Wang XH, Qiu XP, Wu C (1998) Macromolecules 31:2972
39. Wang XH, Wu C (1999) Macromolecules 32:4299

40. Zhang GZ, Wu C (2001) Phys Rev Lett 86:822
41. Zhang GZ, Wu C (2001) J Am Chem Soc 123:1376
42. Zhou SQ, Fan SY, Au-yeung SCF, Wu C (1995) Polymer 36:1341
43. Zimm BH (1948) J Chem Phys 16:1099
44. Wu C, Xia KQ (1994) Rev Sci Instrum 65:587
45. Chu B (1991) Laser Light Scattering. Academic Press, New York, NY
46. Berne B, Pecora R (1976) Dynamic Light Scattering. Plenum Press, New York, NY
47. Stockmayer WH, Schmidt M (1982) Pure Appl Chem 54:407
48. Wu C (1998) Polymer 39:4609
49. Yamamoto I, Iwasaki K, Hirotsu S (1989) J Phys Soc Jpn 58:210
50. de Gennes P-G (1975) J Phys Lett 36:L55
51. Sanchez IC (1979) Macromolecules 12:276
52. Okada Y, Tanaka F (2005) Macromolecules 38:4465
53. Baulin VA, Halperin A (2002) Macromolecules 35:6432
54. Marchetti M, Prager S, Cussler EL (1990) Macromolecules 23:3445
55. Birshtein TM, Pryamitsyn VA (1991) Macromolecules 24:1554
56. Siu MH, Zhang GZ, Wu C (2002) Macromolecules 35:2723
57. Zhang L, Eisenberg A (1995) Science 268:1728 and references therein
58. Antonietti M, Heinz S, Schmidt M (1994) Macromolecules 27:3276
59. Henselwood F, Liu G (1997) Macromolecules 30:488
60. Wu C, Akashi M, Chen MQ (1997) Macromolecules 30:2187
61. Li M, Jiang M, Zhu L, Wu C (1997) Macromolecules 30:2201
62. Berlinova IV, Amzil A, Tsvetkova S, Panayotov IMJ (1994) Polym Sci Polym Chem 32:1523
63. Kawaguchi S, Winnik MA, Ito K (1995) Macromolecules 28:1159
64. Gref R, Minamitake Y, Peracchia MT, Trubetskoy V, Torchilin V, Langer R (1994) Science 263:1600
65. Fessi H, Puisieux F, Devissaguet J Ph, Ammoury N, Benita S (1989) Int J Pharm 55:R1
66. Eckert AR, Webber SE (1996) Macromolecules 29:560
67. Wu C, Qiu XP (1998) Phys Rev Lett 80:620
68. Virtanen J, Tenhu H (2000) Macromolecules 33:5970
69. Chen HW, Li JF, Ding YW, Zhang GZ, Zhang QJ, Wu C (2005) Macromolecules 38:4403
70. Hu TJ, Wu C (2001) Macromolecules 34:6802
71. Ostrovsky B, Bar-Yam Y (1994) Europhys Lett 25:409
72. Cohen-Stua MA, Waajen FHWH, Cosgrove T, Vincent B, Crowley TL (1984) Macromolecules 17:1825
73. Wagner M, Brochard-Wyart F, Hervert H, de Gennes P-G (1993) Colloid Polym Sci 271:621
74. Cook RL, King HE Jr, Peiffer DG (1992) Phys Rev Lett 69:3072
75. Polik WF, Burchard W (1983) Macromolecules 16:978
76. Devanand K, Selser JC (1990) Nature 343:739
77. Tanford C (1980) The Hydrophobic Effect: Formation of Micelles and Biological Membranes. Wiley, New York, NY
78. Bekiranov S, Bruinsma R, Pincus P (1993) Europhys Lett 24:183
79. Martin JI, Wang Z-G (1995) J Phys Chem 99:2833
80. Milner ST (1991) Science 251:905
81. Auroy P, Auvray L, Leger L (1991) Phys Rev Lett 66:719
82. László K, Kosik K, Geissler E (2004) Macromolecules 37:10067
83. Ding YW, Ye XD, Zhang GZ (2005) Macromolecules 38:904

84. Glass JE (1989) Polymers in Aqueous Media: Performance through Association. American Chemical Society, Washington, DC
85. McCormick CL, Bock J, Schulz DN (1989) In: Mark HF, Bikales NM, Overberg CG, Menges G (eds) Encyclopedia of Polymer Science and Engineering. Wiley-Interscience, New York, NY, vol 17
86. Halperin A (1991) Macromolecules 24:1418; Borisov OV, Halperin A (1995) Langmuir 11:2911 and (1996) Macromolecules 29:2612
87. Urakami N, Takasu M (1996) J Phys Soc Jpn 65:2694; Urakami N, Takasu M (1997) Prog Theor Phys Suppl 126:329
88. Semenov AN, Joanny J-F, Khokhlov AR (1995) Macromolecules 28:1066
89. de Gennes P-G (1995) Isr J Chem 35:33
90. Halperin A (2000) In: Ciferri A (ed) Supramolecular Polymers. Marcel Dekker, New York, NY
91. Hu Y, Armentrout RS, McCormick CL (1997) Macromolecules 30:3538
92. Noda T, Morishima Y (1999) Macromolecules 32:4631
93. Kikuchi A, Nose T (1996) Macromolecules 29:6770
94. Zhang GZ, Winnik FM, Wu C (2003) Phys Rev Lett 90:35506
95. Biggs S, Hill A, Selb J, Candau F (1992) J Phys Chem 96:1505
96. Dowling KC, Thomas JK (1990) Macromolecules 23:1059
97. Cui SX, Liu CJ, Zhang WK, Zhang X, Wu C (2003) Macromolecules 36:3779
98. Hugel T, Seitz M (2001) Macromol Rapid Commun 22:989
99. Oesterhelt F, Rief M, Gaub HE (1999) New J Phys 1:61
100. Buchard W (1996) In: Brown W (ed) Light Scattering Principles and Development. Clarendon Press, Oxford
101. Qiu XP, Li M, Kwan CMS, Wu C (1998) J Polym Sci Polym Phys Ed 36:1501
102. Wu C, Chan KK, Woo KF, Qian R, Li X, Chen L, Napper DH, Tan G, Hill AJ (1995) Macromolecules 28:1592
103. Ricka J, Meewes M, Nyffenegger R, Binkert Th (1990) Phys Rev Lett 65:657
104. Meewes M, Ricka J, Nyffenegger R, Binkert Th (1991) Macromolecules 24:5811
105. Wu C (1994) Macromolecules 27:298
106. Antonietti M, Bremser W, Schmidt M (1990) Macromolecules 23:3796
107. Antonietti M, Heinz S, Schmidt M, Rosenauer C (1994) Macromolecules 27:3276
108. Wu C, Akashi M, Chen MQ (1997) Macromolecules 30:2187
109. Li M, Jiang M, Zhu L, Wu C (1997) Macromolecules 30:2201
110. Li M, Jiang M, Zhang YB, Wu C (1999) Macromolecules 31:6841
111. Gao J, Wu C (2000) Macromolecules 33:645
112. Gao J, Wu C (2005) Langmuir 21:782
113. Jordan DS, Green DW, Terry RE, Willhite GP (1982) J Soc Petrol Eng 8:463
114. Flory PJ, Osterheld JE (1954) J Phys Chem 58:653
115. Ohmine I, Tanaka T (1982) J Chem Phys 77:5725
116. Ben Jar PY, Wu YS (1997) Polymer 38:2557
117. Ikegami A, Imai N (1962) J Polym Sci 56:133
118. Dubin P, Bock J, Davies RM, Schulz DN, Thies C (1994) Macromolecular Complexes in Chemistry and Biology. Springer, Berlin Heidelberg New York
119. Narh KA, Keller A (1993) J Polym Sci Polym Phys 31:231
120. Michaeli I (1960) J Polym Sci 48:291
121. Family F, Landau DP (1984) Kinetics of Aggregation and Gelation. North-Holland, Amsterdam
122. Burns JL, Yan YD, Jameson GJ, Biggs S (1997) Langmuir 13:6413
123. Kolb M, Botet R, Jullien R (1983) Phys Rev Lett 51:1123

124. Meakin P (1983) Phys Rev Lett 51:1119
125. von Schulthess GK, Benedek GB, Deblois RW (1980) Macromolecules 13:939
126. Schaefer DW, Martin JE, Wiltzius P, Cannell DS (1984) Phys Rev Lett 52:2371
127. Jullien R, Kolb M (1984) J Phys A 17:L693
128. Brown WD, Ball RC (1985) J Phys A 18:L517
129. Ball RC, Weitz DA, Written TA, Leyvraz F (1987) Phys Rev Lett 58:274
130. Peng SF, Wu C (1999) Macromolecules 32:585
131. Ji HJ, Sun ZW, Zhan WX, Li ZH (1994) Acta Polym Sinica 11:559
132. Tanaka T, Nishio I, Ueno-Nishio ST (1982) Science 218:467
133. Yuko I, Michael B, Manfred S, Klaus H (1998) Macromolecules 31:728
134. Martin TA, Joost HJ, van Opheusden X (1996) Phys Rev E 53:5044
135. Lin MY, Lindsay HM, Weitz DA, Ball RC, Klein R, Meakin P (1990) Phys Rev A 41:2005
136. Timoshenko EG, Kuznetsov YA (2000) J Chem Phys 112:8163
137. Timoshenko EG, Basovsky R, Kuznetsov YA (2001) Coll Surf A 190:129
138. Timoshenko EG, Kuznetsov YA (2001) Europhys Lett 53:322
139. Siu MH, Liu HY, Zhu XX, Wu C (2003) Macromolecules 36:2103
140. Halsey TC (2000) Phys Today 53:36
141. Siu MH, Cheng H, Wu C (2003) Macromolecules 36:6588
142. Wu C, Li W, Zhu XX (2004) Macromolecules 37:4989
143. Picarra S, Martinho JMG (2001) Macromolecules 34:53
144. Tanaka H (1993) Phys Rev Lett 71:3158 (1992) Macromolecules 25:6377
145. Qiu X, Wu C (1997) Macromolecules 30:7921